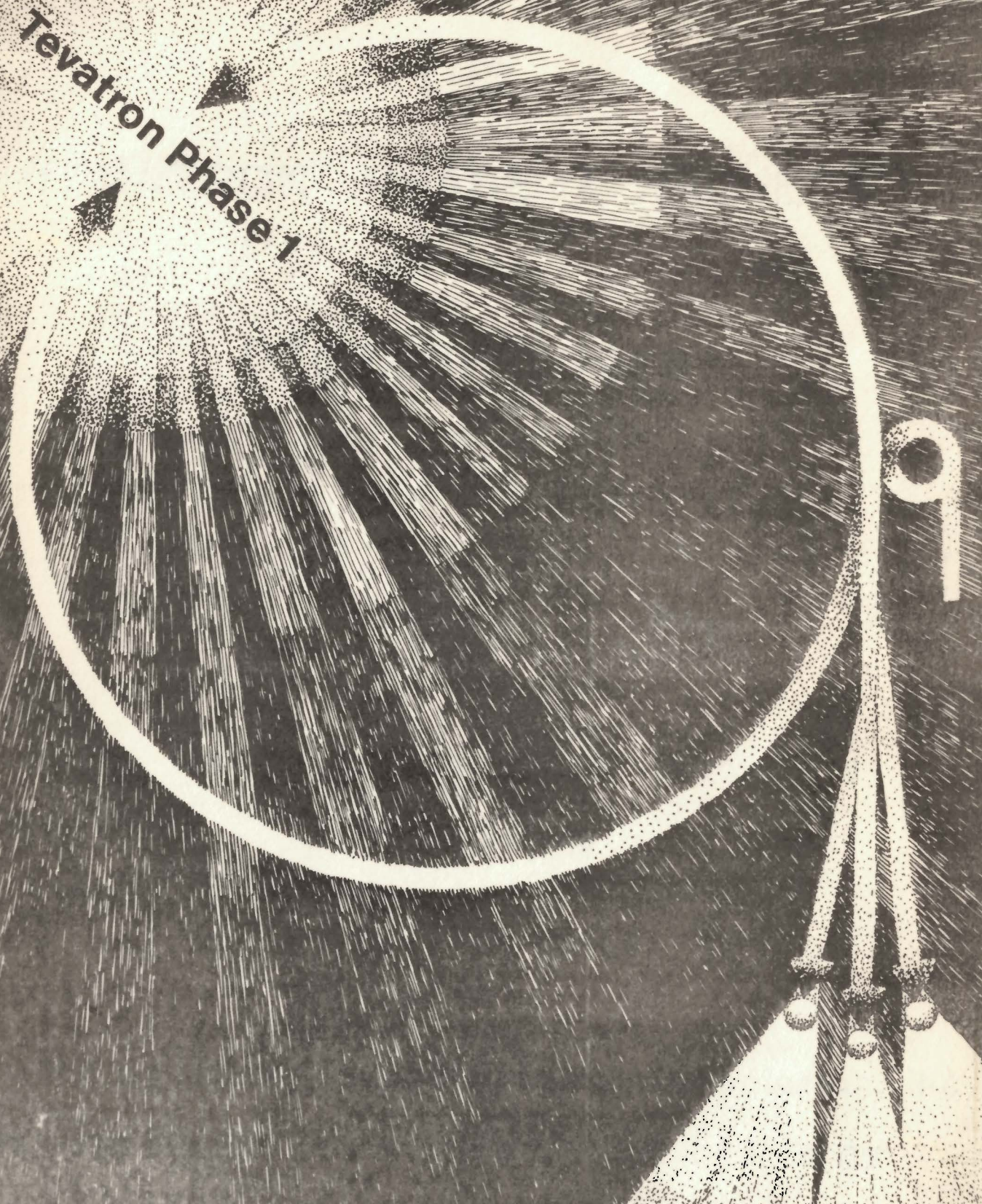


Fermilab Library
QC789.F3 F3 12/1979 010104 000
Fermi National Accelerator
Design report, tevatron phase



0 1159 0009452 1

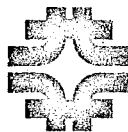
Tevatron Phase 1



9

THE
TEVATRON PHASE I PROJECT

DECEMBER, 1979



Fermi National Accelerator Laboratory

Batavia, Illinois

Operated by Universities Research Association, Inc.
for the United States Department of Energy

TABLE OF CONTENTS

	Page
A. Description of the Project	1
B. The Fermilab Collider: Physics Issues	5
1. Overview	5
2. Physics Opportunities and Where They Are in Phase Space	9
3. The Higgs Sector: What Can Be Done?	13
4. Cross-Sections	17
5. Decay Signatures	17
6. Subprocess Reconstruction: Methodology and Practicality	21
7. Conclusions	26
C. Antiproton Source	27
1. Introduction	27
2. System Performance	34
3. Antiproton Production and Transport	38
4. Stochastic Cooling and Deceleration in the Precooler	64
5. Precooler Ring Design	76
6. Acceleration and Storage in the Main Ring and Superconducting Ring	91
7. Shielding and Conventional Facilities	93
D. Superconducting Accelerator Systems	99
1. Acceleration System	99
2. Refrigeration	117
3. Special Devices	144
E. Experimental Areas	157
F. Costs and Schedules	163
1. Total Funding for Accelerator Colliding-Beam Project	163
2. Details of Construction Cost Estimates	165
3. Manpower Requirements	171
4. Schedules	171
Appendix: Schedule 44	

A. DESCRIPTION OF THE PROJECT

This report describes the "Tevatron Phase I" project at the Fermi National Accelerator Laboratory. The project follows research and development efforts and the earlier Energy Saver project. The R & D work has led to the development and fabrication of superconducting accelerator magnets and installation of a test string of magnets in A sector of the Main-Ring tunnel. The Energy Saver project, authorized in FY79 and now in progress, includes construction of a complete ring of superconducting magnets and their installation in the Main-Ring tunnel. The project includes refrigeration and rf equipment adequate for sustained operation of the ring at a peak energy of 500 GeV, making use of the existing experimental areas.

The Tevatron Phase I project has the goal of providing the capability of sustained operation of the superconducting magnet ring at 1 TeV (1000 GeV) and proton-antiproton colliding beams at up to 2 TeV in the center of mass with a luminosity of $10^{30} \text{ cm}^{-2} \text{ sec}^{-1}$. The project includes:

- (i) An antiproton source, including stochastic and electron cooling. In this report a design is presented that uses a precooler ring, about Booster length, to collect and stochastically momentum-cool antiprotons produced by 80-GeV protons from the Fermilab Main Ring. When the circulating beam has been sufficiently cooled, it is transferred to the Electron Cooling Ring for accumulation and further cooling. Stochastic momentum cooling is very

effective for high-energy, large momentum-spread beams, and electron cooling is most effective for relatively cool beams at low energy. Furthermore, electron cooling works equally well for transverse and longitudinal beam dimensions. The plan therefore exploits the relative advantages of both stochastic and electron cooling. A recent recognition that the stochastic-cooling process can be effectively iterated in steps separated by deceleration has resulted in placing modest demands on the Electron Cooling Ring and makes the attaining of the design goals substantially less dependent on large extrapolations of current experience. Approximately 5 hours of antiproton collection time are required to achieve the luminosity goal. A beam of 10^{11} antiprotons in collision with 10^{11} protons/bunch will produce a luminosity of more than 10^{30} cm^{-2} sec^{-1} .

- (ii) A complete rf system for acceleration to 1 TeV of protons and antiprotons simultaneously.
- (iii) Additional refrigeration for the superconducting accelerator adequate to give a sustained 1-TeV capability.
- (iv) Special devices, including low-beta interaction straight sections additional correction magnet elements for long-term coasting beam, and addition beam-sensing devices.
- (v) Conventional facilities for two colliding-beams

experimental areas to be built in straight sections B and D. Detectors are not within the project scope.

The physics justification and the design of these elements are described in the succeeding chapters of this report. Estimated costs and schedules are given and a Schedule 44 for the project is appended.

B. THE FERMILAB COLLIDER: PHYSICS ISSUES

1. Overview

The objective of the Fermilab colliding beams program is to obtain $\bar{p}p$ collisions in the energy doubler at a c.m. energy of 2 TeV, with a luminosity exceeding $10^{30} \text{ cm}^{-2} \text{ sec}^{-1}$. This energy corresponds to an equivalent laboratory momentum of $2 \times 10^{15} \text{ eV}/c$, and the luminosity permits the study of a wide range of new phenomena. We shall briefly describe how experiments at this extremely high energy will complement and extend Fermilab's 1 TeV/c fixed-target program. It is important to emphasize that 1 TeV represents a significant c.m. energy landmark for both strong and weak interactions. Thus the Fermilab Collider operating at 2 TeV will not merely duplicate the physics possibilities of the $\frac{1}{2}$ TeV CERN Collider, but will open new horizons.

The physics objectives of the Fermilab Collider are most easily, and perhaps most profoundly, explained in terms of the constituents of hadrons and the interactions among those constituents. We believe the strongly-interacting particles to be composed of quarks, structureless objects which define the properties of hadrons. The quarks appear to be permanently confined within hadrons by massless vector quanta known as gluons. The case for the probable existence of gluons is greatly strengthened by the recent results from the electron-positron storage ring PETRA. Just as photons couple to electric charge and the intermediate vector bosons couple to weak isospin and hypercharge, gluons couple to the strong or nuclear charge known as color. Thus a hadron may be viewed as a collection of quarks, antiquarks, and gluons bound together by their mutual strong interaction.

A monoenergetic beam of a single hadron species is therefore to be regarded as a mixed beam of quarks, antiquarks, and gluons. This unseparated beam of constituents is a broad-band beam, because each constituent carries a fraction of the energy of the complete hadron. Determination of the energy spectrum of the constituents of various hadrons has been an important part of the Fermilab fixed-target program. This will continue in the Tevatron era.

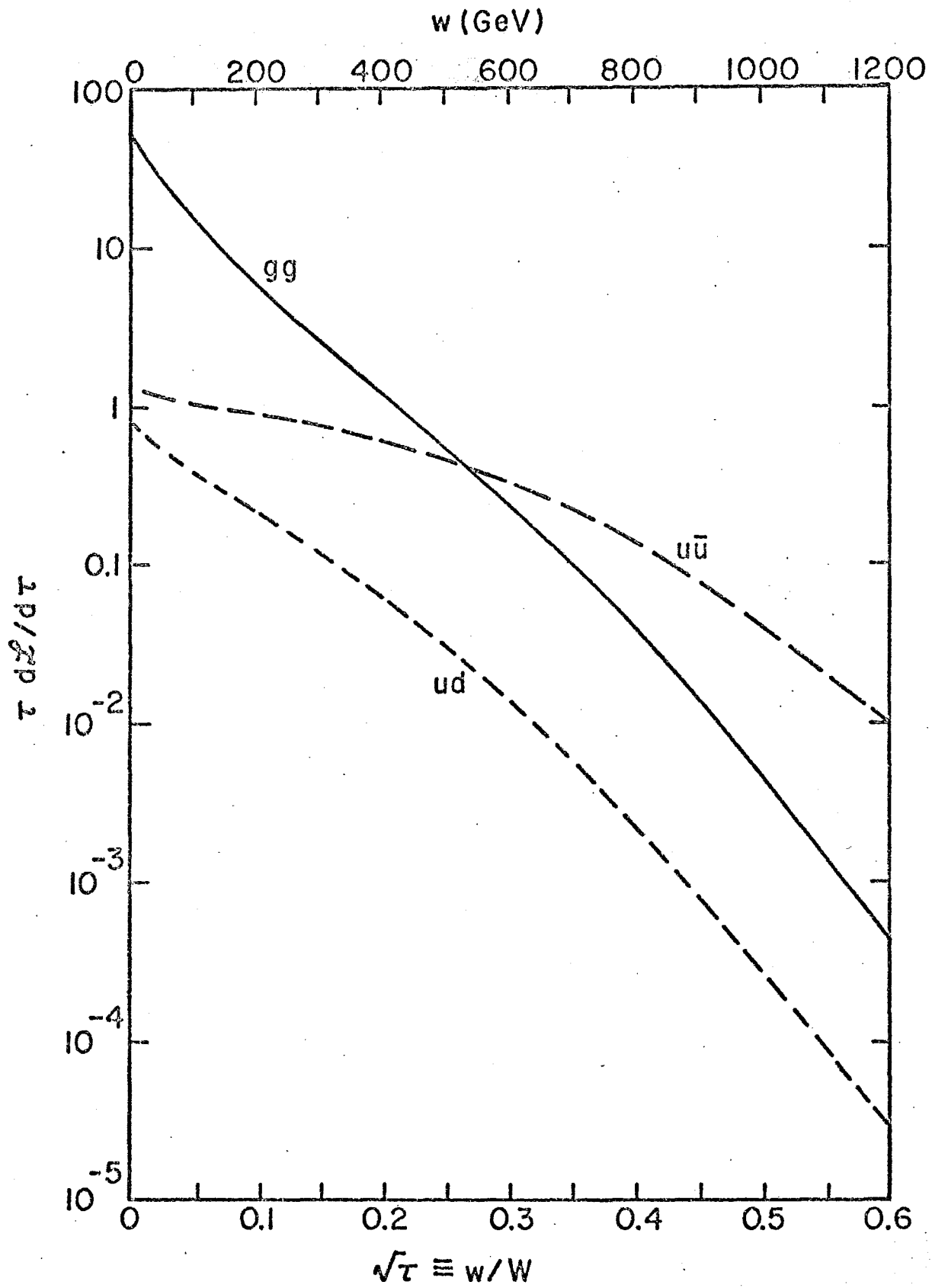


Fig. 1. Differential luminosity

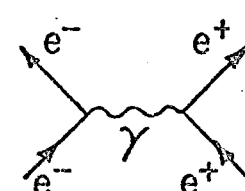
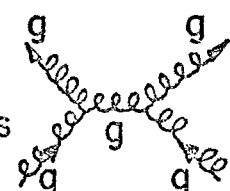
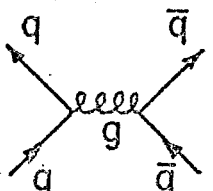
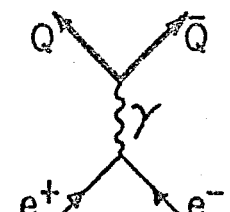
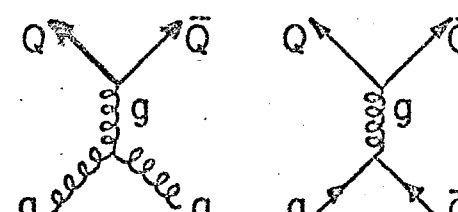
Violent collisions of hadrons may be understood in terms of an impulse approximation, in which a single constituent of the projectile hadron interacts with an individual constituent of the target hadron. This provides an opportunity to isolate and study the elementary interactions among the constituents. An important parameter for devices intended to study these elementary interactions is the differential luminosity $d\mathcal{L}$ of elementary collisions at c.m. energy w per hadron-hadron collision at c.m. energy W . This may be computed as a convolution of the energy spectra of the constituents. In Fig. 1 we plot a related quantity, $\tau d\mathcal{L}/d\tau$, which is more convenient for cross section calculations. The scaling variable τ is related to the fraction of hadron-hadron c.m. energy W which is represented in a collision of constituents:

$$\tau \equiv w^2/W^2.$$

As typical examples, we sketch in Fig. 1 the luminosities expected for up quark-down quark collisions, gluon-gluon collisions, and up quark-up antiquark collisions in the $\bar{p}p$ Collider.

With this information in hand, we may obtain a useful perspective on the physics potential of the collider by comparison with electron-positron colliding beams. This is done in Table I. At the constituent level, each basic e^+e^- process has its analog in gluon-gluon (gg), quark-quark (qq), quark-antiquark ($q\bar{q}$), or quark-gluon (qg) collisions. In particular, just as e^+e^- annihilation is a source of all charged objects, so also are $q\bar{q}$ and gg annihilation sources of all colored objects. The main difference is cross-section: in e^+e^- annihilation, production of new objects is proportional to $\alpha^2 = (1/137)^2$, while in $q\bar{q}$ or gg annihilation the analogous quantity is $\alpha_s^2 \sim (0.1 - 0.2)^2$, at least a factor 100 larger. However, while a new quark Q of mass $m_Q \lesssim 0.8E_{\text{beam}}$ can be observed in an e^+e^- collider, it is unreasonable to expect more than $\sim 25\%$ of the proton beam

Table I. Comparison of e^+e^- and $p\bar{p}$ Colliders

$e^+e^- \mathcal{L} \sim 10^{32} \text{ cm}^{-2} \text{ sec}^{-1}$	$p\bar{p} \mathcal{L} \sim 10^{30} \text{ cm}^{-2} \text{ sec}^{-1}$
e^+e^- makes new charged quanta	$q\bar{q}$ } make new gg } colored quanta
Bhabha scattering  Strength $\sim \left(\frac{1}{137}\right)^2$	gg } hard collisions  $q\bar{q}$ }  Strength $\sim \alpha_s^2 \sim \left(\frac{1}{6}\right)^2$
Annihilation into charged fermions  Strength $\sim \left(\frac{1}{137}\right)^2$	Annihilation into colored fermions  Strength $\sim \left(\frac{1}{6}\right)^2$
Threshold: $m_Q \lesssim 0.8 E_{\text{beam}}$ To match Tevatron, need $E_{\text{beam}} \sim 250 \text{ GeV}$ with $\mathcal{L} \lesssim 10^{32} \text{ cm}^{-2} \text{ sec}^{-1}$	Threshold: $m_Q \lesssim 0.8 E_g \lesssim 0.2 E_{\text{proton}}$ For Tevatron $m_Q \lesssim 200 \text{ GeV!}$
Clean initial state; possibility of direct channel resonances (eg Z^0)	Complex initial state direct channel resonances smeared by initial-state distribution

energy to be found in a single quark or gluon; hence the limit for $p\bar{p}$ or pp colliders is only $m_Q \lesssim 0.2E_{\text{beam}}$. Nevertheless, this still indicates that the Tevatron $p\bar{p}$ collider could pair-produce new colored quanta with masses of order 200 GeV. In general, a rule of thumb is that colored quanta can be produced in a $p\bar{p}$ collider of luminosity $\sim 10^{30} \text{ cm}^{-2} \text{ sec}^{-1}$ about as well as charged quanta can be produced in an e^+e^- collider of luminosity $\sim 10^{32} \text{ cm}^{-2} \text{ sec}^{-1}$, when the proton energy is ~ 5 times the corresponding electron beam energy.

The observability of the final state is easier in e^+e^- annihilation than in pp or $p\bar{p}$ colliders. However, the detectability of new phenomena becomes easier in the $p\bar{p}$ colliders as the mass scale increases far beyond what is characteristic for strong interactions, and appears not to be an insurmountable obstacle. This is discussed later on in more detail.

2. Physics Opportunities and Where They Are in Phase Space

Figure 2 illustrates the regions of longitudinal phase-space in which various collision processes of interest lie, along with the region covered reasonably well by the proposed detector. An important reason for exploring higher energies and probing shorter distances within hadrons is that we do not know what will be found. However, the first round of experiments will be guided by what we expect to find. If the physics is as we expect, the principal change from present experimentation will be the use of the intermediate boson Z^0 (as opposed to ψ and T) to calibrate detectors. A neutral intermediate boson coupled with typical strength to the light quarks will be produced with a cross section of approximately

$$\sigma_Z(M_Z = \sqrt{s}) \approx 2 \times 10^{-33} \text{ cm}^2 \times \tau \frac{d\mathcal{L}}{d\tau}(q\bar{q}),$$

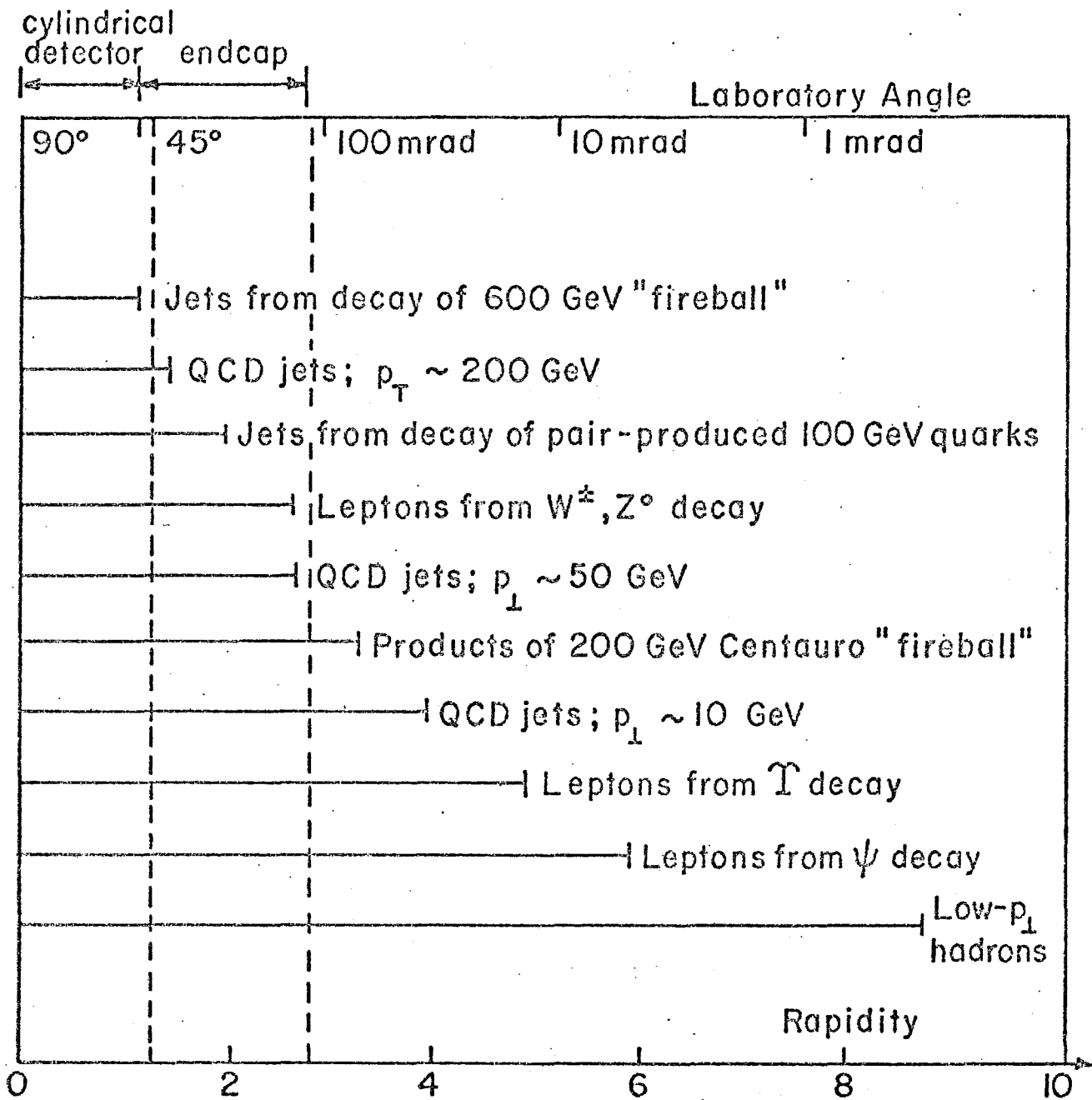


Fig. 2. Tevatron Collider Physics: Where It Is in Phase Space

which permits a meaningful search out to a mass of about $1 \text{ TeV}/c^2$. A similar range in masses can be searched for charged weak bosons, for which we expect

$$\sigma_{W^+}(M_W = \sqrt{\tau}W) = \sigma_{W^-}(M_W = \sqrt{\tau}W) \approx 6 \times 10^{-33} \text{ cm}^2 \times \tau \frac{d\mathcal{L}}{dt}(u\bar{d}).$$

Additional conventional physics for the collider includes:

- (i) search for new narrow states: $\psi, T \dots$
- (ii) study of dilepton production in the continuum
- (iii) large- p_{\perp} physics
- (iv) test of charge conjugation invariance
- (v) measurement of the total cross section
- (vi) "soft" collisions-multiple production of hadrons
- (vii) search for new quark flavors
- (viii) free quark search.

Why do we view 2 TeV as an important energy to reach? What distinguishes it from $\frac{1}{2}$ TeV? Obviously the energy scale in Fig. 1 must be divided by four at $\frac{1}{2}$ TeV, with a consequent loss of sensitivity for massive objects. This is a relative argument (and a good one!) but there are absolute arguments for the higher energy as well.

What, for example, of the strong interactions? At c.m. energies $W \approx 50 \text{ GeV}$, multiple production of hadrons is dominantly a short-range-correlation phenomenon. The rising total cross section and unitarity considerations suggest the onset of long-range correlations and a new event structure at much higher energies. In addition, cosmic ray experiments hint that a beam momentum of $\sim 10^{14} \text{ eV}/c$ is a possible threshold for new phenomena such as very high multiplicity ($\gg 100$ particles) events, penetrating showers, events free of neutral pions, multiple cores at high transverse momentum. At an equivalent momentum of $\sim 2 \times 10^{15} \text{ eV}/c$, the collider is well within this possible new regime.

Another example of the possible importance of 2 TeV physics is provided by the options open for the strength of weak interactions at high energies.

Option I. No intermediate bosons exist (the Collider having conducted a sensitive but fruitless search.) Lepton-lepton, lepton-quark, and quark-quark scattering by the weak interactions must then become strong at c.m. energies exceeding about 600 GeV. [The c.m. energy at which weak interactions become strong depends on the channel. For the weak process $ud \rightarrow du$, it is about 880 GeV.] The onset of weak jets and of C-violations may be useful as signals of "strong" weak interactions.

Option II. The intermediate bosons W^\pm, Z^0 exist, but do not have gauge couplings, i.e. are not as given by renormalizable theories. Then quark-quark (etc.) scattering will always remain weak, but WW scattering becomes strong at energies exceeding about 1 TeV.

Option III. (Present prejudice) Renormalizable gauge theories describe the weak and electromagnetic interactions. These imply, as discussed in the next section, the existence of new gauge particles known as Higgs scalars. If the mass of the (lightest) Higgs particle exceeds about $1 \text{ GeV}/c^2$, weak interactions among the gauge bosons must become strong at energies around 1 TeV. If the Higgs boson mass is far less than $1 \text{ TeV}/c^2$, weak interactions may always remain weak, unless superheavy quarks (masses $\geq \frac{1}{2} \text{ TeV}/c^2$) exist. An interesting intermediate case occurs for a Higgs boson mass below about $600 \text{ GeV}/c^2$ but above twice the intermediate boson mass. A spectacular signal of intermediate boson pair production would ensue.

With any of these options, we may expect new particles to discover and study or a qualitatively new kind of weak interaction. Hadron-hadron collisions at energies far exceeding $1/\sqrt{G_F} \approx 300 \text{ GeV}$ are required to make this exploration thinkable.

Let us now move on to speculations concerning production of colored states with mass large compared to the intermediate bosons. These are most naturally associated

with new quark degrees of freedom. Table II illustrates families of quarks and leptons, old and new. The top quark (assuming, for simplicity, its existence) is interesting to $p\bar{p}$ colliders provided it is too massive to be found at PEP or PETRA. And even if top is found, there might be another quark generation at still higher mass. In addition, there is some reason for speculating that there exist other families of quarks and leptons which possess another strong interaction analogous to QCD. This property has been dubbed technicolor. These "technifermions" would comprise a nontrivial technicolor multiplet and bind, in analogy to QCD, into technicolored singlets via technigluon exchange. All this is to happen at a distance scale small (a factor $\sim 10^3$?) compared to the characteristic distance-scale of QCD. Why such an extravagant speculation? The answer has to do with the central problem of the gauge theory of weak interactions-the so-called Higgs sector. In the following we sketch the problem and its relationship to the technicolor hypothesis, following work of Susskind, Farhi, and Dimopoulos.

3. The Higgs Sector: What Can Be Done?

The electromagnetic, strong, and weak forces are all supposed to be described by gauge theories. While the electromagnetic and strong forces are mediated by massless spin-one quanta (the photon and gluon respectively), the weak force is generally supposed to be mediated by massive intermediate bosons W^\pm and Z^0 . These differ from the photon (and QCD gluons) in having three, not two, polarization states. The existence of this third polarization state has profound consequences for electroweak theory-consequences best seen by imagining the electromagnetic coupling constant α and weak coupling constant $\alpha_{wk} = \alpha \csc^2 \theta_w$ temporarily set to zero. In that limit the intermediate-boson masses vanish, and the third (longitudinal) polarization state of each boson decouples from the transverse "gauge" degrees of freedom. According to the fundamental premises of electroweak gauge theory, these longitudinal degrees of freedom are to be identified

Table II. Fermion Families

	ν_e	e	uuu	ddd	
	ν_μ	μ	ccc	sss	
	$\nu_\tau?$	τ	$ttt??$	bbb	
	\vdots	\vdots	\vdots	\vdots	
Technicolor multiplet	{	N	E	UUU	DDD
		N	E	UUU	DDD
		\vdots	\vdots	\vdots	\vdots

as massless, spinless, bosons (h^\pm, h^0) which are collective modes of some new dynamical system with a spontaneously broken symmetry analogous to superconductivity or superfluidity. This is the Higgs-sector; it is an unavoidable element of electroweak gauge theory. The orthodox "minimal" theory and the technicolor models form two extreme views of this system. The orthodoxy is analogous to the Ginzburg-Landau theory of superconductivity, while the technicolor model is analogous to the Bardeen-Cooper-Schrieffer (BCS) theory.

In the "minimal" orthodoxy, the massless h^\pm and h^0 are accompanied by a single massive ($10 \text{ GeV}/c^2 < m_H < 10^3 \text{ GeV}/c^2$?) neutral spinless boson H^0 -the Higgs boson. These four bosons interact reasonably strongly with each other, but very weakly with quarks and leptons-unless there exist superheavy fermion degrees of freedom. The self-interactions of this Higgs system are ad hoc, and have nothing to do with any known gauge theory.

In the technicolor model, the Goldstone modes h^\pm, h^0 are 1S_0 $Q\bar{Q}$ bound states of the aforementioned techniquarks (via the technicolor force), and are directly analogous to the 1S_0 $q\bar{q}$ pion states of the ordinary strong interactions.

In addition to the three massless h^\pm and h^0 , there are many other 1S_0 "technipion" bound states which fall into various classes, as shown in Table III. The most interesting for $p\bar{p}$ colliders are colored technipions, with mass estimated in the 100-200 GeV region. (For e^+e^- collisions the colorless, but charged, bound states of the technileptons are estimated to have mass in the 10-50 GeV/c^2 range and should be readily observable.)

One need not take seriously either extreme view of the Higgs sector. What must be taken seriously is the existence of some kind of Higgs-sector, with mass scale not exceeding ~ 1 TeV. Thus in principle this Higgs system very likely is accessible to the Tevatron collider. The problem lies in whether the quanta can be produced with large enough cross-section and whether, once produced, they can be detected.

Table III. Properties of Technipions

State (subscript is color rep'n)	Comments
$(Q\bar{Q})_1 = \begin{cases} (U\bar{U})_1 \\ (U\bar{D})_1 \\ (D\bar{U})_1 \\ (D\bar{D})_1 \end{cases}$	<p>3 out of four are massless h^0, h^\pm "eaten" by W^\pm and Z^0. Fourth neutral member H^0 is neutral, has mass $\sim 500-1000$ GeV, and behaves like Higgs-boson of the orthodoxy.</p>
$(Q\bar{Q})_8 = \begin{cases} (U\bar{U})_8 \\ (U\bar{D})_8 \\ (D\bar{U})_8 \\ (D\bar{D})_8 \end{cases}$	<p>Mass $\sim 100-200$ GeV; color octet. Confined; pointlike on mass scale less than 500 GeV. Copiously produced in gg or $q\bar{q}$ collisions. Charged states decay into $W^\pm + g$ or $(L\bar{L})_1^\pm + g$. Neutral states decay into $g+g, Z^0+g, \gamma+g, (L\bar{L})_1+g, \dots$</p>
$(Q\bar{L})_3 = \begin{cases} (U\bar{E})_3 \\ (D\bar{E})_3 \\ (U\bar{N})_3 \\ (D\bar{N})_3 \end{cases}$	<p>Mass $\sim 100-200$ GeV?; color triplet; confined. Pointlike on mass scale less than 500 GeV. Copiously produced in gg collisions. Decay into $q + \bar{l}$ is induced by additional interactions of 10-100 GeV mass-scale ("extended technicolor").</p>
$(L\bar{L})_1 = \begin{cases} (E\bar{E})_1 \\ (E\bar{N})_1 \\ (N\bar{E})_1 \\ (N\bar{N})_1 \end{cases}$	<p>Mass $\sim 10-50$ GeV? Charged members $(E\bar{N})$ and $(N\bar{E})$ are especially accessible to e^+e^- colliders. Neutral members behave more or less like the ordinary Higgs boson and can be searched for in $\text{onium} \rightarrow H^0 + \gamma, Z^0 \rightarrow H^0 + \mu^+\mu^-, \text{ etc.}$</p>

4. Cross-Sections

The cross-section for pair-production of colored objects can be crudely estimated from the QCD-jet production via $q\bar{q}$ and gg elastic "Bhabha" scattering. The latter has been estimated, and is shown in Fig. 3. For e^+e^- annihilation, the ratio of $e^+e^- \rightarrow \gamma \rightarrow \mu^+\mu^-$ or $e^+e^- \rightarrow \gamma \rightarrow Q\bar{Q}$ is a factor ~ 10 below the 90° Bhabha cross-section. Here we take (conservatively??) the analogous processes $q\bar{q} \rightarrow g \rightarrow Q\bar{Q}$ and $gg \rightarrow g \rightarrow Q\bar{Q}$ to be a factor ~ 30 lower than the QCD Bhabha estimate, and crudely cut them off at low p in accordance with expectations from simple kinematics. (These are not very quantitative estimates; only rough guesses good to at best a factor $\sim 3-10$). We see that production of 100 GeV $Q\bar{Q}$ pairs may be of the order of a nanobarn. A similar order of magnitude and possibly larger may be expected for production of colored technihadrons.

5. Decay Signatures

The production of heavy colored states is reasonably well matched to the available luminosity of the $p\bar{p}$ collider provided one pays little penalty in observable branching ratios for the decays. For heavy quarks such as a 30 GeV top quark one may hope to see nonleptonic decay into 3 quark jets ($t \rightarrow q\bar{q}q$) much as one would have expected at PETRA easy observability of 30 GeV toponium into 3 gluon jets ($(t\bar{t}) \rightarrow ggg$).

The expected branching ratios for top decays are, roughly

$$t \rightarrow q\bar{q}q \quad \sim 67\% \text{ (nonleptonic)}$$

$$t \rightarrow q\bar{\ell}\nu \quad \sim 33\% \text{ (semileptonic)}.$$

Thus for $t\bar{t}$ pair-production in hadron collisions, one expects for the decay products

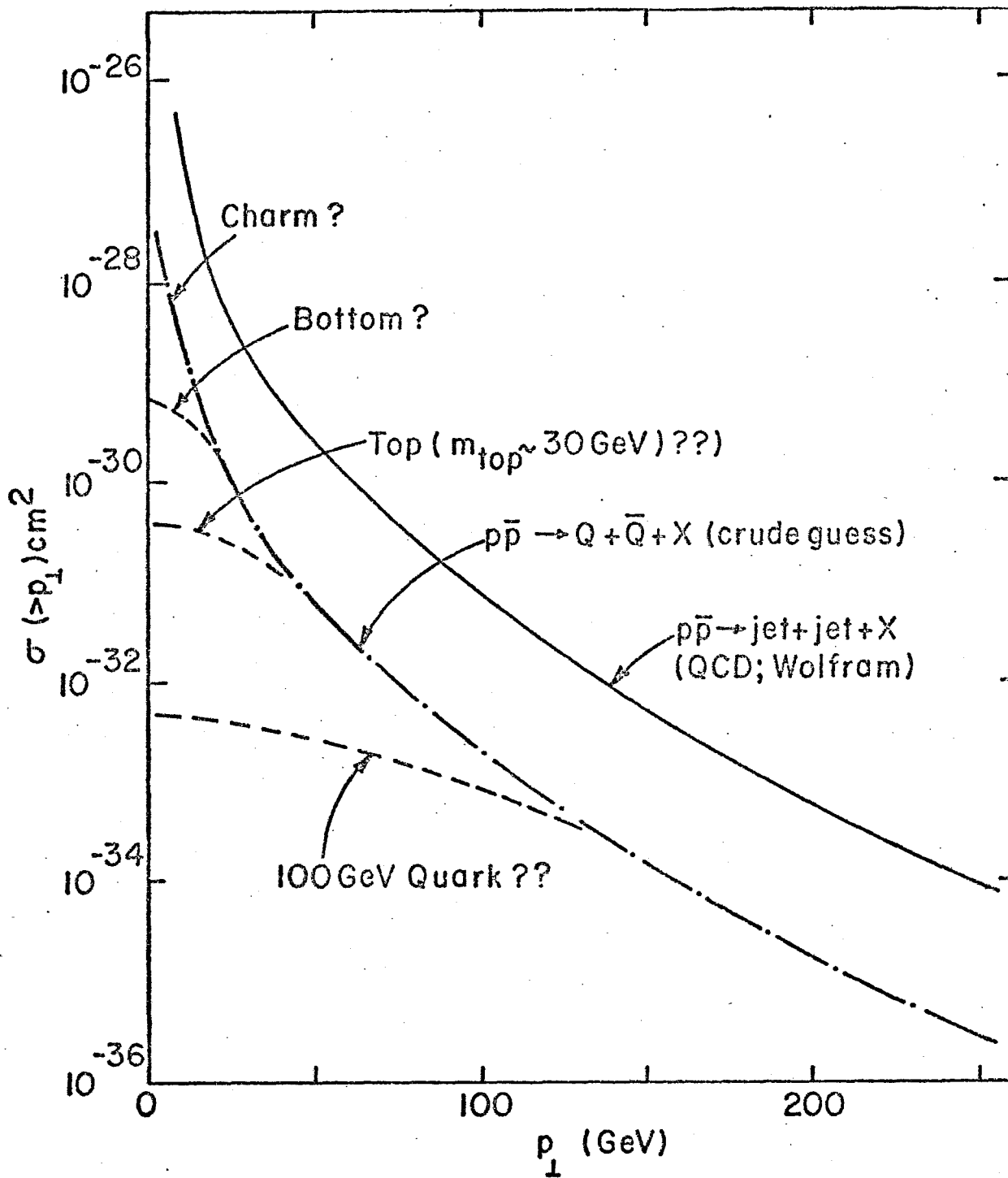


Fig. 3. Integral cross sections for production of high- p_{\perp} systems.

$$pp \rightarrow \begin{cases} 6 \text{ jets} + \dots & \sim 45\% \\ 4 \text{ jets} + 1 \text{ charged lepton} & \sim 45\% \\ 2 \text{ jets} + 2 \text{ charged leptons} & \sim 10\% \end{cases}$$

For superheavy quarks ($m_Q \gtrsim 100 \text{ GeV}$) the principal decay mode is

$$Q \rightarrow q + W \begin{cases} \rightarrow q\bar{q} \\ \rightarrow \ell\bar{\nu} \end{cases}$$

leading to similar final states as above. There is an extra constraint for the nonleptonic channel, inasmuch as two of the three jets must have an invariant mass equal to that of the intermediate boson W^\pm . This constraint should be useful for reducing background.

The signatures for technicolored particles, in particular the colored technipions, are spectacular. Some decay modes are tabulated in Table IV. Many involve W^\pm, Z^0 or γ in the final state. Colored technipions typically decay into at least one gluon. Production of technihadrons via $g\bar{g}$ or $q\bar{q}$ annihilation may be enhanced by intermediate direct-channel "technirho" resonances (mass $\sim 500\text{-}1000 \text{ GeV}/c^2$?). In any case, one may anticipate a significant amount of multiple production of intermediate-bosons. For example, consider

$$g + g \rightarrow (Q\bar{Q})_8^{J=1} \begin{cases} \downarrow \\ (Q\bar{Q})_8^{J=0} + (Q\bar{Q})_8^{J=0} \\ \downarrow \quad \downarrow \\ W^+ + g \quad W^- + g \\ \downarrow \quad \downarrow \\ q + \bar{q} \quad \ell + \bar{\nu} \end{cases}$$

Table IV. Observability of Quark and Gluon Jets

<u>e^+e^- collisions</u>	<u>pp and $p\bar{p}$ collisions</u>
<u>$E_{\text{CMS}} \sim 5 \text{ GeV}$ (SPEAR)</u> 2-jet structure barely discerned	<u>$p_{\perp}^{\text{visible}} \sim 2 \langle p_{\perp} \rangle^{\text{jet}} \lesssim 10 \text{ GeV}$ (FNAL)</u> 2-jet events barely discerned; some residual skepticism
<u>$E_{\text{CMS}} \sim 10 \text{ GeV}$ (DORIS)</u> 2-jet structure seen by eyeball 3-jet structure barely visible (T decay)	<u>$p_{\perp}^{\text{visible}} \gtrsim 20 \text{ GeV}$ (ISR)</u> 2-jet events easily seen.
<u>$E_{\text{CMS}} \sim 30 \text{ GeV}$ (PETRA)</u> 3-jet structure seen by eyeball	<u>$p_{\perp}^{\text{visible}}$ at TeVatron $\lesssim 400 \text{ GeV}$</u>

This example has again a 4-jet + lepton signature, as already discussed above for top-decay. However, here the mass-scale is much greater and detection problems should be less.

In all these cases, it is evident that it is necessary to measure momenta of quark and gluon jets with an accuracy sufficient to uncover the underlying kinematics of the process.

6. Subprocess Reconstruction: Methodology and Practicality

Observation of superheavy quark production or of technihadrons-or, for that matter, production of just about any system of colored states in the 100 GeV region-thus requires reconstruction of multijet final states; quarks and gluons are identified by the hadron jets into which they evolve. While this has been historically a very difficult business, there is nevertheless cause for optimism that this technique will work at Tevatron energies. Table IV summarizes the status of the observability of quark and/or gluon jets in e^+e^- annihilation and in hadron-hadron collisions. One sees that thus far it has taken roughly twice as much center-of-mass energy (of the subsystem of quarks and gluons) in hadron-hadron collisions as in e^+e^- collisions in order to cleanly see a given multi-jet phenomenon. Thus when the visible p_{\perp} exceeds ~ 50 GeV/c one may expect final states in pp collisions containing 3 high- p_{\perp} jets to be as clean as the 3-jet final states observed in e^+e^- collisions at 30 GeV (PETRA data). With visible p_{\perp} in excess of ~ 200 -400 GeV/c, the interesting 4-jet (and maybe more) final states we have discussed can therefore be expected to emerge rather clearly.

At a more quantitative level, we may consider how much phase-space a high- p_{\perp} jet occupies; i.e. how large a cone angle about a jet axis is needed to capture a given fraction of the parent quark momentum. An estimate (normalized to e^+e^- data in the T region) is shown in Fig. 4. The simple parton-model (e.g. Feynman-Field model) would

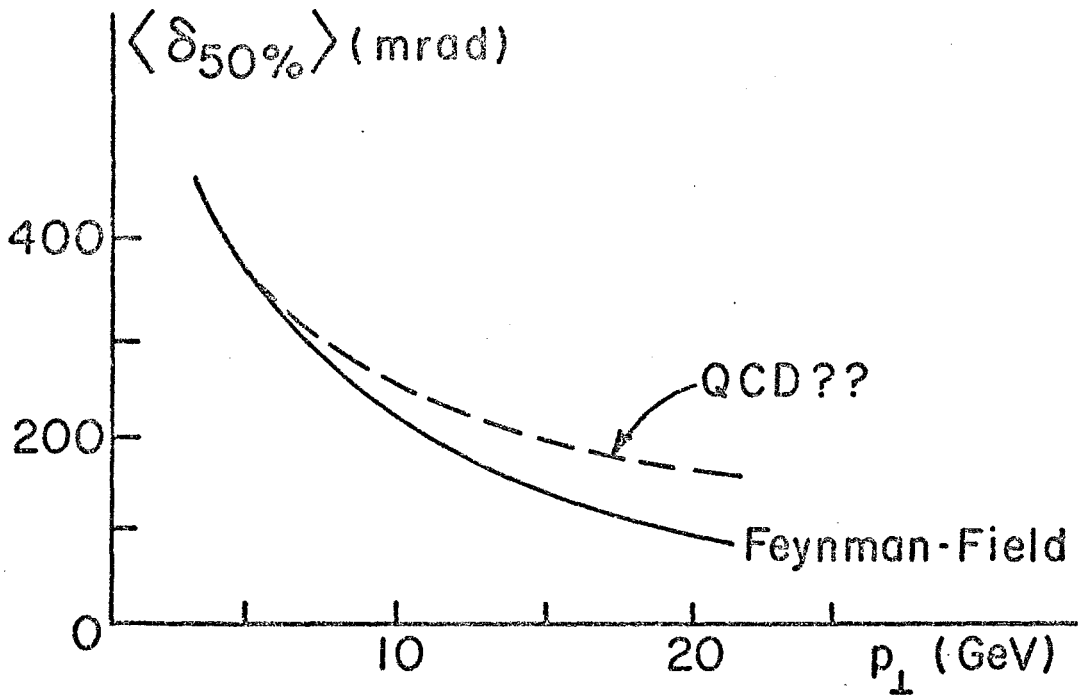
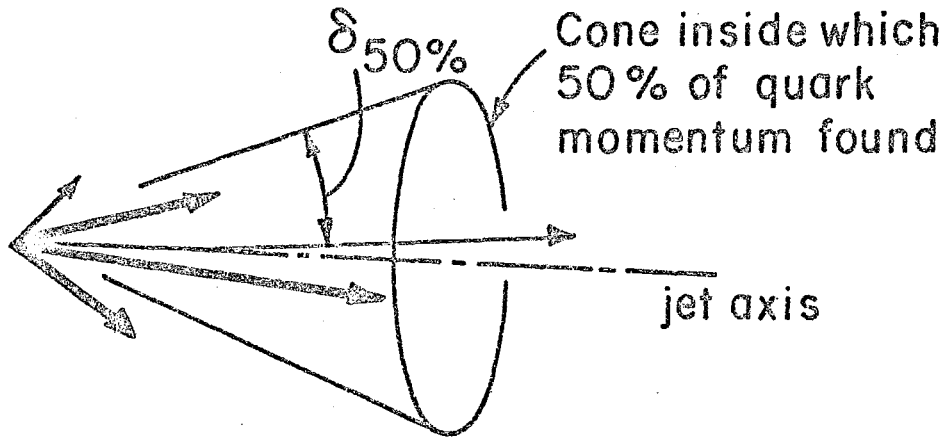


Fig. 4. Angular distribution of momentum in quark (or gluon ?) jets.

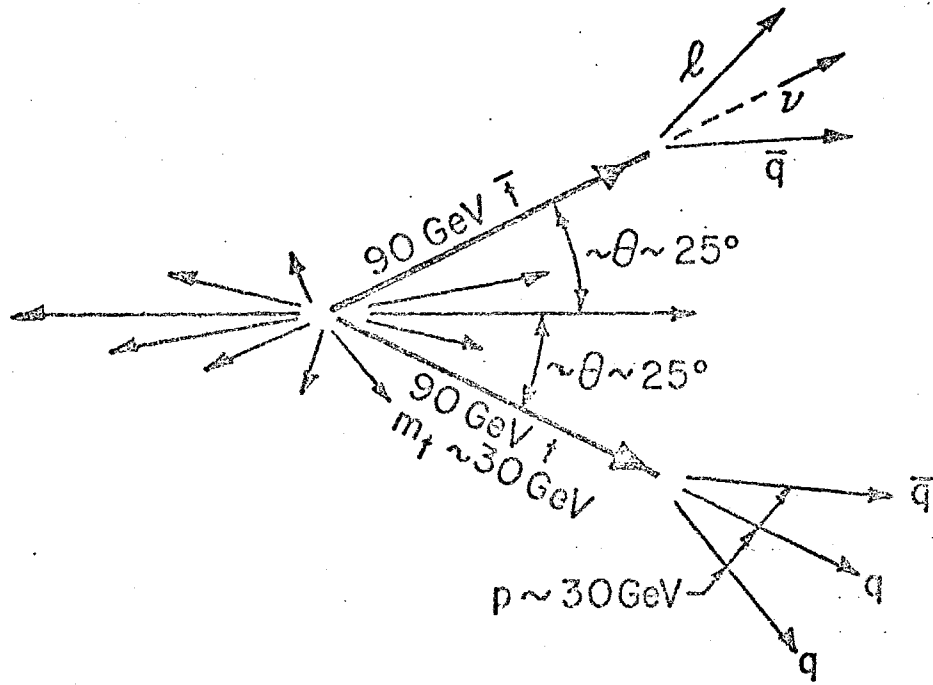
predict this cone angle would decrease inversely with the jet momentum, while QCD gluon emission would lead to a slower decrease (on average) but with a large amount of fluctuation (leading to a multicore structure reminiscent of what one sees for electromagnetic showers at a depth of a few radiation lengths).

The details of this jet structure are best learned empirically. The e^+e^- data from PEP and PETRA will give a sample of quark and gluon jets of momenta (or, better, p_{\perp}) up to $\sqrt{15}$ GeV. Already it is known that a large fraction of such jets are quite narrow, like Feynman-Field jets, while a large fraction of the remainder are broadened by what appears to be single-gluon emission. It remains to be seen whether quark and gluon jets are distinguishable; a year or two of e^+e^- experimentation may suffice in providing an answer.

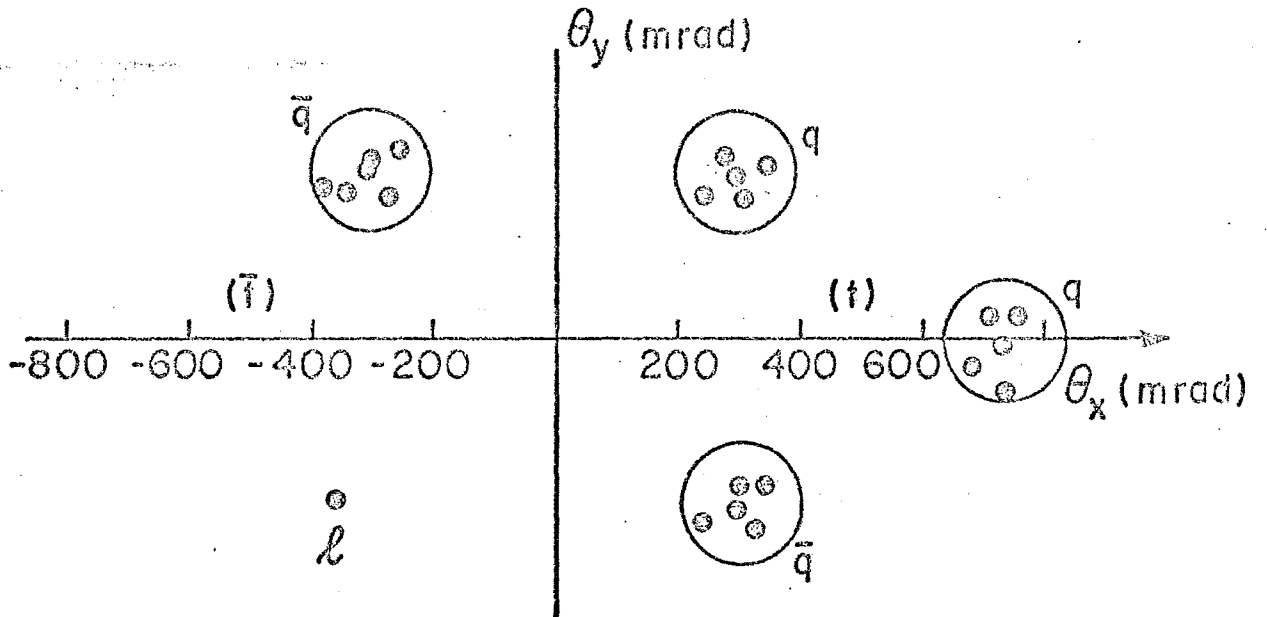
For jets with p_{\perp} large compared to 15 GeV/c, the "Bhabha" background in the $p\bar{p}$ collider itself may be used to define empirically (in the same apparatus) the structure of the quark and gluon jets. This knowledge can then be put to use in constructing an optimum algorithm for reconstructing the momenta and directions of quarks and gluons in multijet events.

While a detailed strategy should await more empirical information on e^+e^- jet phenomena (and perhaps more information from the present generation of experiments at CERN ISR), a rough sketch of the possibilities may still be useful for orientation purposes. As a test example we consider production of $t\bar{t}$ pairs, with a top-quark mass $\sqrt{30}$ GeV/c². While this is clearly a very relevant process to examine, it is probably as difficult a case to consider as any, owing to the relatively small mass scale. As mentioned previously, the final state of four jets plus a high- p_{\perp} lepton is probably the best signature. The strategy might be:

(1) Cut on visible $p_{\perp} \geq 50$ GeV/c. [According to Fig. 3, production of t with $p_{\perp} \geq 30$ GeV should not be greatly suppressed.] Most of this initial p_{\perp} should remain in the decay



(a) An ideal $t\bar{t}$ production event



(b) Jet cores (50% of parent momentum within the circles)

Fig. 5

products, which in fact add some more of its own. [However the QCD "Bhabha" background may be a factor $\sim 10^2 - 10^4$ larger than the signal at this point.]

(2) Cut on low "transverse thrust" and high "transverse sphericity" to eliminate QCD "Bhabha" events. ["Transverse thrust and sphericity" are 2-dimensional analogues of the quantities used in e^+e^- experiments.]

(3) Demand one high- p_{\perp} isolated lepton ($p_{\perp} > 5 \text{ GeV}/c$??). [This, along with (2), should kill most of the QCD background.]

(4) Demand \geq four high- p_{\perp} jet cores. [We return below on what this might entail.]

(5) Estimate the momenta and angles of these cores and reconstruct the masses m of triples of the four cores, searching for a peak at $m = m_{\text{top}}$.

Items (4) and (5) are the least straightforward, and will require Monte-Carlo simulations, as well as direct experience, to know what the attainable mass-resolution might be. To get a feeling for what is involved, consider an "ideal" $t\bar{t}$ production event as shown in Fig. 5. The p_{\perp} of the top quarks is taken as $\sim 40 \text{ GeV}/c$, and the p_{\parallel} are each $\sim 80 \text{ GeV}/c$. The decay plane of the t is taken as normal to its direction of motion, with each decay quark having equal laboratory momentum $\sim 30 \text{ GeV}/c$. To identify the four cores, we choose typical cone-angles inside which, on average, half the jet momentum is to be found. At this quark momentum (from Fig. 4) this half-angle is $\sim 100 \text{ mrad}$. Thus the major portion of the energy is indeed deposited in well-separated, identifiable cores. Therefore to categorize events by core structure (step (4)) seems not too formidable a task. To actually measure the momenta accurately is more problematical. To encompass 80-90% of the jet momentum requires expanding the radii by a factor $\sim 3-5$. Furthermore, one must keep in mind that this event is idealized; many $t\bar{t}$ events will have overlapping jets, or at least one jet near a beam direction. The importance of these effects can be evaluated by Monte-Carlo simulation. We must also keep in mind that $t\bar{t}$ production is the most difficult case, and the corresponding search for $100-200 \text{ GeV}/c^2$ quarks will be much easier.

7. Conclusions

The $p\bar{p}$ collider program will be rich in conventional physics, such as low- p_{\perp} particle production, dilepton production, high- p_{\perp} constituent scattering, and production of intermediate-bosons W^{\pm} and Z^0 . But there is also the potential for a quite new kind of physics involving subprocess center-of-mass energies large compared to M_W and M_Z , and approaching the 1 TeV center-of-mass energy which still characterizes the mass-scale at which the poorly understood aspects of electroweak theory (the Higgs sector) must manifest itself. We have illustrated this with scenarios for heavy quark production ($m_Q \sim 100-200$ GeV) and for conjectured colored technihadrons. While neither scenario is a compelling one theoretically, each remains as a prototype of what may happen if there exist any pointlike objects possessing color with masses in the 30-200 GeV range. The $p\bar{p}$ collider program should be able to detect and study such objects if they do happen to exist.

C. ANTIPROTON SOURCE

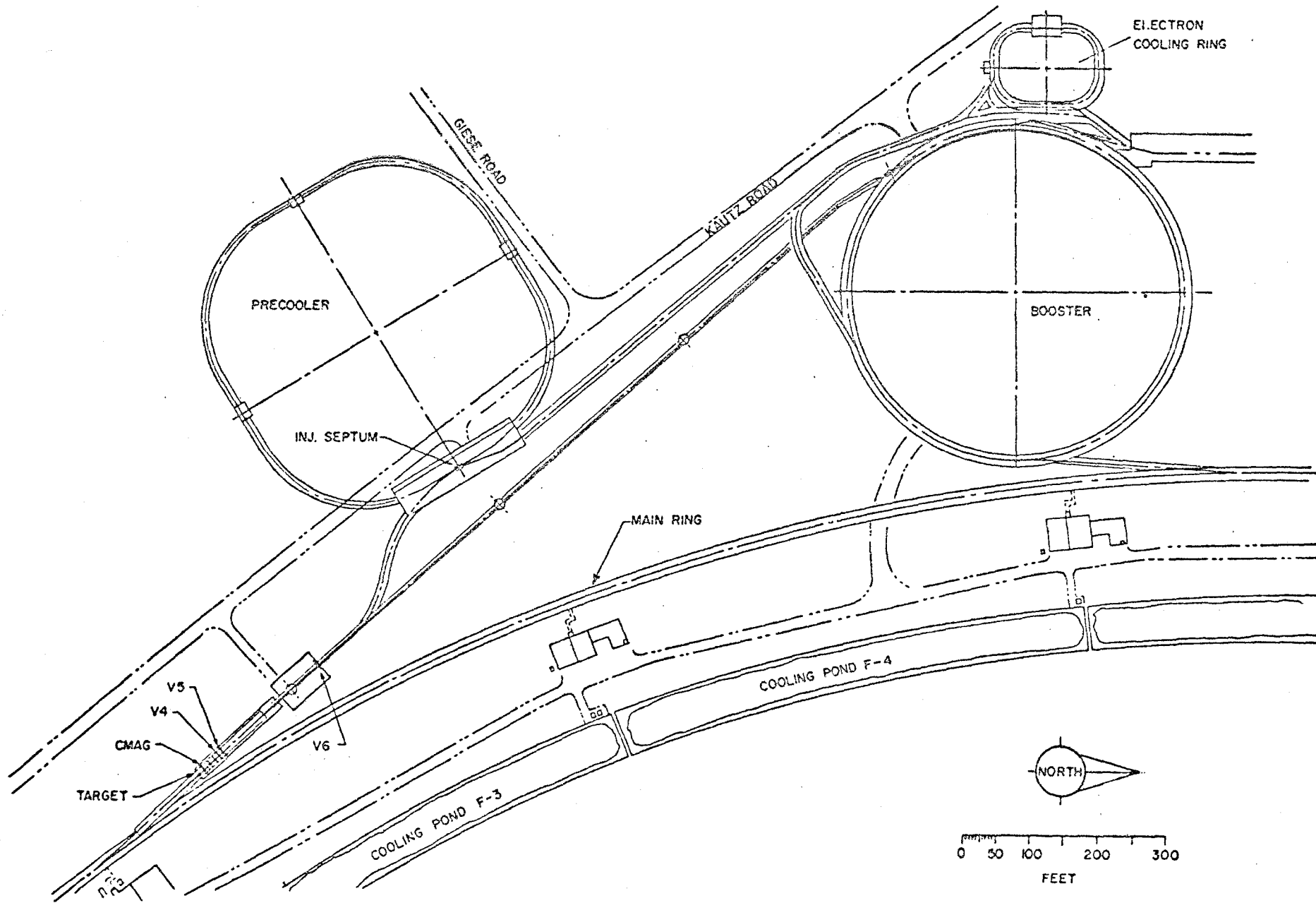
1. INTRODUCTION

1.1 Scope of the Work

This section of the report describes the design of a high-intensity antiproton source to be constructed at the Fermi National Accelerator Laboratory. The centerpiece of this source is a Precooler, a storage ring and accelerator for cooling antiprotons. The Precooler is approximately the size of the Fermilab Booster accelerator. With this Precooler, the antiproton source will yield antiproton intensities that will produce antiproton-proton luminosities greater than $10^{30} \text{ cm}^{-2} \text{ sec}^{-1}$ at 2 TeV in the center of mass in the Energy Saver-Doubler superconducting accelerator already under construction at this Laboratory. The existing Electron Cooling Ring, in a modified and improved form will be a part of the plan. A layout of the plan showing the location of the Precooler is shown in Fig. 1-1.

The Precooler design discussed in this report is a magnet ring of 75.47 m average radius with four long straight sections, which are dispersion-free. There are rf systems for deceleration and acceleration. It is to be installed in its own tunnel south of the Booster, by the intersection of Kautz and Giese Roads, and connected to the Main Ring and Electron Cooling Ring by beam-transport tunnels.

It is the current plan to leave the Electron Cooling Ring in its present configuration and location. It will, however, be necessary to improve the facility, to upgrade some power-supply systems, and to add some shielding for the stacking of a beam of 10^{11} 200-MeV antiprotons.



1-1 Layout of the High-Intensity Antiproton Source.

1.2 Concept of the Precooler

The concept of colliding-beam experiments with antiprotons and protons at Fermilab was first proposed by Cline, McIntyre, Mills and Rubbia¹ in 1976. The system envisaged initially used electron cooling exclusively and would, it was estimated, produce a luminosity of $5 \times 10^{28} \text{ cm}^{-2} \text{ sec}^{-1}$. The electron cooling was to be accomplished in a 200-MeV storage ring. A research and development effort began in 1977 to build a small ring for tests of electron cooling. This ring is now virtually complete.

Further study, including a workshop in 1978,² has led to the belief that it would be possible to produce a luminosity greater than $10^{30} \text{ cm}^{-2} \text{ sec}^{-1}$, far more useful for experiments. A general plan using a separate Precooler ring has several significant advantages. It now appears³ that it will be difficult to achieve the 50-msec cooling time in the existing Electron Cooling Ring needed to synchronize efficiently with the Booster cycle. It is possible to consider extending the straight sections of the Electron Cooling Ring to install more cooling and thus shorten the cooling time, but there are severe difficulties in the accelerator lattice of such an extension.⁴

What is discussed here is therefore a plan to utilize the Precooler to capture 4.5-GeV antiprotons and momentum-cool them stochastically in several steps⁵ as they are decelerated to 200 MeV. The 200-MeV beam is extracted then injected into the existing Electron Cooling Ring, where it is cooled further both in momentum and in betatron phase space. The sequence is

repeated, stacking the antiproton beam in the Cooling Ring until approximately 10^{11} have been accumulated. This beam is then transferred back to the Precooler, accelerated to 8 GeV and injected into the Main Ring and Superconducting Ring for acceleration to 1 TeV.

1.3 The Development Effort

In late 1978, an informal design study group began to meet regularly at Fermilab in order to develop a plan for producing high-luminosity $\bar{p}p$ collisions in the Energy Saver-Doubler. Participants in this design study are from Fermilab, ANL, LBL, and the University of Wisconsin. The study group has been part of the larger collaborative research and development effort among the above institutions, plus the Institute of Nuclear Physics, Novosibirsk to develop $\bar{p}p$ capabilities at Fermilab.

At first the group worked to establish a better understanding of appropriate accelerator physics and technology, including questions regarding fundamental limits of the performance of various systems. It has gone on to analyze quantitatively various suggested schemes from the standpoint of technical feasibility and practical performance.

This report describes a specific design. This design is regarded as a basis for proceeding with the more detailed design and construction of a high-luminosity $\bar{p}p$ colliding-beam system at Fermilab. Luminosity of greater than 10^{30} cm^{-2} sec^{-1} after a few hours of antiproton collection time should be possible with the scheme, provided that the performance of the techniques utilized can, in fact, be realized. Some of the important items are:

- (i) Electron Cooling Ring Performance. The experimental data from Novosibirsk on electron cooling are incomplete and do not quite address the problems of cooling large-emittance beams and of accumulation.⁶ Recently, CERN has accomplished electron and stochastic cooling and it appears that the predictions of the theory are borne out by the experiments.⁷
- (ii) Main-Ring performance. The plan presented here requires Main-Ring charge redistribution. Although a preliminary experiment has been conducted⁸ there is still work to be done in this area.
- (iii) Similarly, experiments will be undertaken to investigate the assumption that large bunch charge (of order 10^{11} p/bunch) can be produced and stored in the Superconducting Ring.
- (iv) p production targetry is a complicated part of the plan. Experiments need to be conducted to evaluate realizable proton beam quality and various target design options.

Currently a research and development program is being pursued to address these items. A major effort during 1980 will be directed toward experiments on the Electron Cooling Ring, both on electron cooling and stochastic cooling, on storing and rebunching proton beams in the Main Ring, and on the construction of an extraction and target system for 80-GeV protons. It is

also a goal to acquire experience in handling low-intensity \bar{p} -beams by decelerating them in the Booster accelerator to 200 MeV and transporting them to the Electron Cooling Ring for cooling and accumulation.

Obviously, the design will be refined as more detailed information is obtained, but the framework developed in the last year and described in this report is adequate to support the anticipated detailed development without fundamental changes in scope or concept.

References

- ¹D. Cline et al., Proposal for Fermilab Expt. 492, 1976.
D. Cline, P. McIntyre, F. Mills, and C. Rubbia, Collecting Antiprotons in the Fermilab Booster and Very High Energy \bar{p} Collisions. Fermilab Report TM-687, 1976.
- ²Proceedings of the Workshop on Producing High Luminosity, High Energy Proton-Antiproton Collisions, March 27-31, 1978. Fermilab and Lawrence Berkeley Laboratory Report LBL-7574.
- ³T. Ogino and A. G. Ruggiero, The Physics of Electron Cooling, Fermilab \bar{p} Note in preparation.
- ⁴D. E. Johnson, New Thoughts on the Extended Electron Cooling Ring Lattice, Fermilab \bar{p} Note 21, Aug. 1979.
D. E. Johnson, Fast Electron Cooling and an Expanded Electron Cooling Ring, Fermilab \bar{p} Note 41, Sept. 1979.
A. Ruggiero, On the Effects of Inserting Long Cooling Regions, Fermilab \bar{p} Note 49, Sept. 1979.
- ⁵W. P. Kells, Methods for Longitudinal Cooling by Large Factors

in a \bar{p} Precooler Ring, Fermilab \bar{p} Note 43, October 1979.

⁶V. V. Parchomchuk et al., IEEE Trans. Nucl. Sci., Vol. NS-26, No. 3, Jun. 1979, p.3487.

⁷M. Bell et al., Electron Cooling Experiment at CERN, CERN EP/79-96, 3 Sept. 1979.

⁸J. E. Griffin and F. E. Mills, Proc. of the 1979 Particle Accelerator Conference, IEEE Trans. Nucl. Sci., NS-26, No. 3, Jun. 1979, p. 3589.

2. SYSTEM PERFORMANCE

2.1 The Sequence of \bar{p} Collection

The sequence of steps to collect the required number of antiprotons is outlined here and presented in more detail in Section 3 of this report.

1. Approximately two-thirds of the Main-Ring circumference is loaded by the Booster for acceleration. The Main Ring accelerates 1.8×10^{13} protons to an energy of 80 GeV, then flat-tops.
2. The charge is redistributed in the Main Ring by rf manipulation to occupy approximately 1/13 the circumference (one Precooler length). All finer time structure is lost in this process.
3. The protons are extracted in a single turn and targeted on a \bar{p} production target.
4. Antiprotons are collected in a large-aperture Precooler ring, of approximately Booster circumference, at 4.5-GeV kinetic energy in a transverse emittance of 4.8π mm-mrad in each plane and momentum spread $\pm 2\%$. The beam is stochastically momentum cooled by a factor of about a hundred in several seconds.¹ Cooling takes place in three or four steps, each 1 to 2 seconds cooling followed by some deceleration to re-establish phase mixing.
5. The cooled beam is decelerated to 200 MeV. Depending on the stochastic cooling realized, the beam will be

bunched on either the first or second harmonic to reduce the bunch length down to the circumference of the Electron Cooling Ring, then transferred to that ring. If it is necessary, bunches will be transferred and cooled sequentially.

6. The antiprotons are bunched on a low harmonic

($h \approx 6$ to 12) in the Electron Cooling Ring, then individual bunches are transferred to the Precooler ring at harmonic number 21, accelerated to 8 GeV and injected into the Main Ring, accelerated, then transferred into the Superconducting Ring in the reverse direction.

7. Protons are accelerated in the conventional manner in the Main Ring and transferred into the Superconducting Ring. Both beams are simultaneously accelerated to collision energy.

2.2 System Parameters

Parameters of a system to carry out these indicated steps are summarized in Table 2-I.

Table 2-I System Performance Parameters

	<u>Antiproton Production</u>
Proton energy for production (E_p)	80 GeV
Protons per MR cycle	1.8×10^{13}
MR cycle time	8 sec
Protons/sec	2.2×10^{12}
Antiproton energy (at collection)	4.5 GeV
\bar{p} transverse acceptance at 4.5 GeV, horizontal	$4.8\pi \times 10^{-6}$ m-rad
\bar{p} transverse acceptance at 4.5 GeV, vertical	$4.8\pi \times 10^{-6}$ m-rad
\bar{p} momentum collection ($\Delta p/p$)	$\pm 2\%$
Invariant \bar{p} cross section ($Ed^3\sigma/dp^3$)	0.8 mb/GeV ²
Total absorption cross section (σ_0)	33 mb
Number of \bar{p} 's per proton ($N_{\bar{p}}/N_p$)	3.2×10^{-6}
$N_{\bar{p}}/\text{sec}$.	$7.0 \times 10^{+6}$
$N_{\bar{p}}/h$ (with 80% efficiency factor)	2.0×10^{10}

2.3 Luminosity of $\bar{p}p$ Collisions

A scheme to produce a luminosity of 5×10^{28} cm⁻² sec⁻¹ was developed some time ago.² Provided the present Main-Ring proton intensity can be rebunched to approximately 10^{11} p/bunch (10 times the present bunch density) the collision of one such bunch with a single bunch of 6×10^9 antiprotons will yield a luminosity of 5×10^{28} . Development of higher-luminosity schemes primarily depends upon the use of more bunches and more antiprotons. Table 2-II lists a comparison of collision parameters for the scheme presented here and of the CERN project now under construction.

Table 2-II Luminosity Comparison

	Fermilab	CERN
Energy (GeV)	1000	270
Number of Protons (N_p)	1.2×10^{12}	6×10^{11}
Number of antiprotons ($N_{\bar{p}}$)	10^{11} (5 h)	6×10^{11} (24 h)
Number of bunches	~ 12	6
Low beta at inter- action $\beta^* = \sqrt{\beta_x \beta_y}$ m)	1.5	2.2
Proton emittance, horizontal (m-rad)	$2.6\pi \times 10^{-8}$	$3.5\pi \times 10^{-8}$
Proton emittance, vertical (m-rad)	$2.6\pi \times 10^{-8}$	$3.5\pi \times 10^{-8}$
Antiproton emittance, horizontal (m-rad)	$1.0\pi \times 10^{-8}$	$3.8\pi \times 10^{-8}$
Antiproton emittance, vertical (m-rad)	$1.0\pi \times 10^{-8}$	$1.9\pi \times 10^{-8}$
Luminosity ($\text{cm}^{-2} \text{sec}^{-1}$)	$>10^{30}$	10^{30}
Bunch length (m)	1	-

In addition to collection of more antiprotons and more bunches, there are possible improvements to be gained in luminosity lifetimes and magnitude by utilization of high-energy electron-cooling techniques³ or transverse stochastic cooling. Such techniques are not, however, within the main thrust of this report.

References

- ¹W. Kells, Methods for Longitudinal Cooling by Large Factors in a \bar{p} Precooler Ring, Fermilab \bar{p} Note 43, Oct. 1979.
- ²F. E. Mills and D. E. Young, A Scenario to Achieve a Luminosity of Approximately $5 \times 10^{29} \text{ cm}^{-2} \text{ sec}^{-1}$ for $p\bar{p}$ Collisions in the Fermilab Energy Doubler, unpublished report, Nov. 1978.
- ³D. Cline et al., High Energy Electron Cooling to Improve the Luminosity and Lifetime in Colliding Beam Machines, SLAC Pub 2278, March 1979.

3. ANTIPROTON PRODUCTION AND TRANSPORT

3.1 Requirements and General Layout

Here we summarize some considerations and parameters involved in the production and collection of antiprotons. The overall goal is to maximize the antiproton yield by appropriate design of the extracted beam, the p beam line, the production target, and the \bar{p} beam line. The principal difficulties in achieving this goal arise from the very small spot size (< 1 mm diam.) that is needed to obtain high \bar{p} source brightness and the resulting stringent conditions on beam optics and target heating and from the necessity to produce an antiproton beam of length appropriate to fit in the Precooler.

The basic parameters affecting the yield are taken to have the values given in Table 3-I.

Table 3-I Antiproton Production Parameters

Proton energy	80 GeV
Antiproton energy	4.5 GeV
Antiproton emittance accepted by Precooler	$4.8\pi \times 4.8\pi$ mm-mrad
Proton beam emittance	0.15π mm mrad
Momentum Acceptance of Precooler	$\pm 2\%$

The 80-GeV proton beam will be rebunched in the Main Ring to fit in a total length corresponding to the Precooler circumference, extracted at F17 and transported to the antiproton production target located in the Target Vault. The 4.5-GeV antiproton beam will then be transported to the Precooler. An overall layout of the system was shown in Fig. 1-1.

3.2 Operation of the Main-Ring Beam for High-Intensity Extraction

In order to maximize the \bar{p} intensity in a Booster-size Precooler, it will be advantageous to do single-turn injection of \bar{p} 's. Maximum intensity will be obtained if the largest possible quantity of Main-Ring beam is placed on the \bar{p} target during a period slightly less than the revolution period in the Precooler. Because the Main-Ring beam is initially distributed uniformly around at least a large fraction of the ring, redistribution of the beam prior to extraction will be required.

Recent measurement of the longitudinal emittance of individual Main Ring bunches at 100 GeV indicate emittances of about 0.2 eV-sec with 10^{10} protons per bunch corresponding to 213 eV-sec for the entire ring. If this emittance is coalesced into a 1.6- μ sec time slot, the energy spread will be 133 MeV and the fractional energy (or momentum) spread at 80 GeV will be 1.66×10^{-3} , a momentum spread easily contained in the Main-Ring aperture.

The Main-Ring beam could be coalesced into the 1.6- μ sec time slot using a first-harmonic rf cavity operating at 47.7 kHz: the voltage required would be approximately 50 kV. Such a cavity is not beyond question, but it would be a large and expensive device. Instead we will utilize a procedure by which a large fraction of the Main-Ring beam can be coalesced into a small azimuthal region just prior to extraction using only the existing Main-Ring rf system (53 MHz, $h = 1113$).

In order to coalesce protons from a wide range of azimuthal locations into a smaller region, charge from various parts of the

ring must be advanced or retarded with respect to some location designated as synchronous. This can be accomplished if the central momentum of each bunch varies linearly with distance from this synchronous bunch. With such a distribution established and all rf buckets removed, the bunch distribution will coalesce to the azimuthal location of the synchronous bunch in a time that depends on the momentum deviation and the energy. Because of the momentum spread within each bunch, the synchronous bunch, as well as all the others, will debunch during this drift time, so the fraction of the ring into which beam can be coalesced depends on the individual-bunch momentum spread, as well as on the momentum deviation of the nonsynchronous bunches. The useful aperture of the Main Ring and the initial longitudinal beam emittance place limitations on the entire process.

Let the total energy spread within a single bunch just prior to removal of the rf constraint be ΔE_b . After removal of the rf, the bunch will spread during some drift time T_d into a time interval ΔT given by

$$\frac{\Delta T}{T_d} = \eta \frac{\Delta E_b}{E_s}, \quad (3.1)$$

where η is the momentum dispersion and E_s is the synchronous energy. If ΔT is a fraction F of a Main-Ring revolution period T_o , then the drift time T_d is

$$T_d = \frac{E_s F T_o}{\eta \Delta E_b}. \quad (3.2)$$

During the drift time (many turns), a synchronous bunch advances by an azimuthal angle θ given by

$$\theta = 2\pi \frac{T_d}{T_0} \quad (3.3)$$

A bunch with its centroid removed from the synchronous energy by an energy deviation ΔE_d will gain or lose in azimuthal position by

$$\frac{\Delta\theta}{\theta} = \eta \frac{\Delta E_d}{E_s} \quad (3.4)$$

Then the total azimuthal angle gained or lost by a non-synchronous bunch during the drift time T_d is

$$\Delta\theta = 2\pi F \frac{\Delta E_d}{\Delta E_b} \text{ or } \frac{\Delta E_d}{\Delta E_b} = \frac{\Delta\theta}{2\pi F} \quad (3-5)$$

If the goal is to coalesce beam from 70% of the ring into an azimuthal length equal to that of the Precooler circumference, then $\Delta\theta$ becomes $\pm 0.7\pi$ and F is $1/13.25$. This gives the required ratio of the deviation energy of those bunches farthest removed from the synchronous bunch to the internal energy spread of whichever bunch has the greatest spread

$$\frac{\Delta E_d}{\Delta E_b} = \frac{0.07\pi \times 13.25}{2\pi} = 4.64 \quad (3-6)$$

The procedure to relocate the beam is then as follows:

1. The Main Ring ($h = 1113$) is loaded with Booster batches ($h = 84$) in the normal manner and the beam is accelerated to 80 GeV, where the guide field is held constant for approximately 2 seconds. Only that fraction of the Main Ring that will be coalesced need be filled with Booster batches.
2. During the transition from ramp to constant field, the rf voltage is adjusted adiabatically to a level of 4 MV, yielding minimum bunch length and maximum momentum spread. This configuration is shown roughly to scale in Fig. 3-1a. The bucket height is 0.77 eV-sec or 257 MeV; the bunch width is initially 2.5 nsec.
3. The rf is switched to the unstable phase angle and the bunches are allowed to deform along the separatrix until the bunches have a (projected) bunch length of 3 nsec. The total bunch length in the bucket becomes 1 rad. This is shown in Fig. 3-1b.
4. The rf is switched back to the stable stationary-bucket phase angle and the bunches are allowed to rotate approximately one-quarter of a synchrotron oscillation, as shown in Fig. 3-1c. The synchrotron period is 4.2×10^{-3} sec, so this operation requires only a few milliseconds.
5. The rf is switched to one harmonic number higher than the original frequency in a time short compared with a synchrotron period. During normal acceleration, the rf system is tuned over a frequency range of 290 kHz, so a

frequency jump of one revolution frequency, 47.7 kHz, is well within the normal tuning range. The $(h + 1)$ rf voltage is

$$V(t) = V_0 \sin (h + 1) \Omega_0 t, \quad (3-7)$$

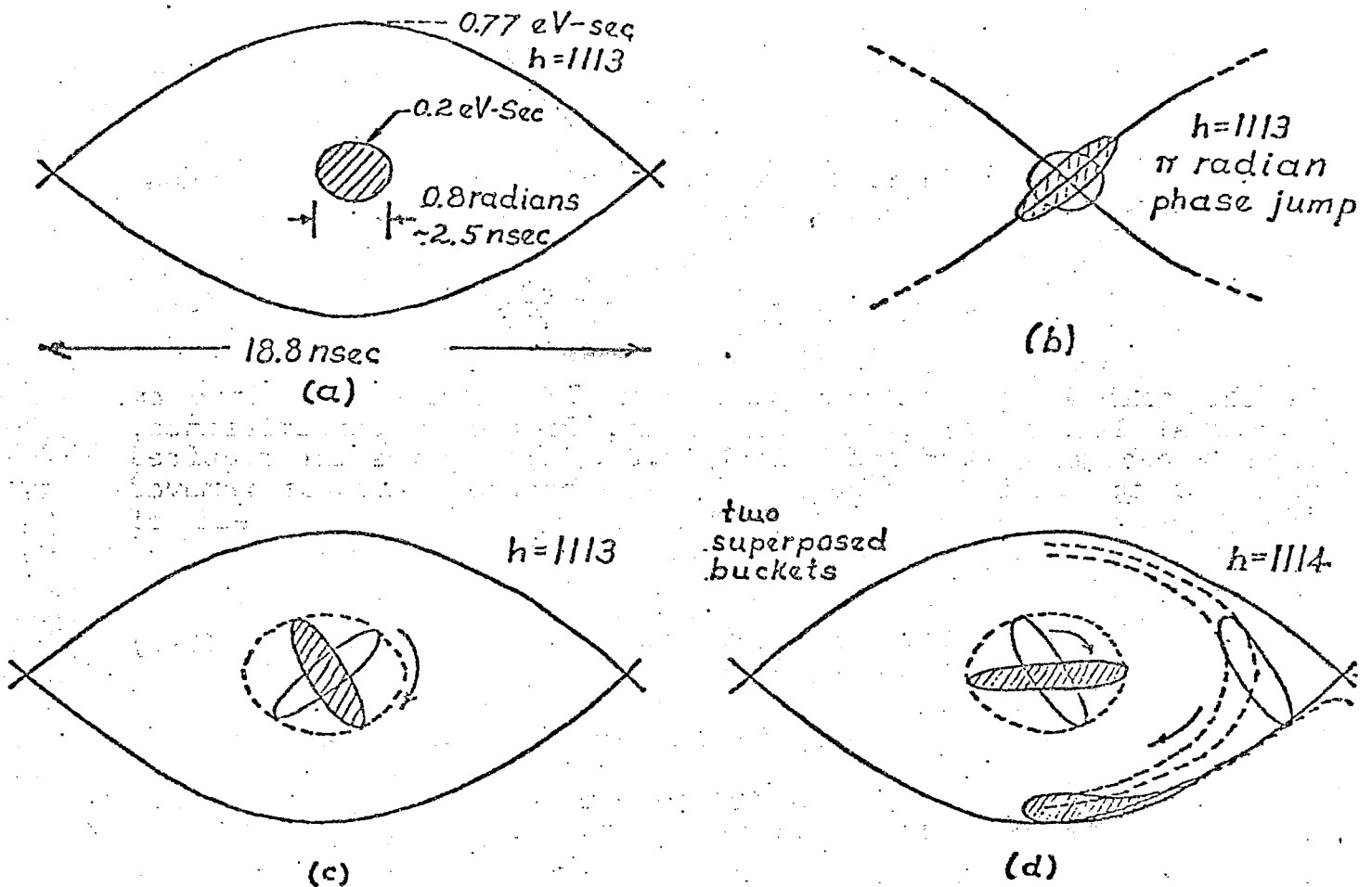


Fig. 3 - 1.a) 4 MV, $h = 1113$ bucket containing a matched bunch with emittance 0.2 eV-sec and bunch width 2.5 nsec. b) The same bucket as part (a) switched to the unstable phase angle. The bunch is allowed to distort along the separatrix until its width is 3 nsec. (3) The bucket switched back to stable position and the distorted bunch allowed to rotate about one quarter turn. (d) Superposition of two $h = 1114$, 4 MV buckets, one containing a centered bunch, the other containing a bunch displaced within the bucket to 0.7π radians. During the allowed drift time the bunches rotate to the positions shown.

where h is the original harmonic number and Ω_0 is the synchronous angular revolution frequency. The time of arrival of the k -th bunch at the effective accelerating gap location is then

$$t_k = k/f_{rf} = \frac{k}{h} T_0,$$

so the voltage seen by the k -th bunch immediately following reapplication of the rf voltage is

$$V_k = V_0 \sin \frac{2\pi k}{h}. \quad (3-8)$$

Since k ranges from zero to h , the voltage applied to the h bunch locations initially has the appearance of a voltage applied on the first harmonic. The important distinction between this ring voltage and a voltage at $h = 1$ is that the bunches are constrained to remain within a phase space defined by new buckets which have the same phase extent as the original buckets to within 0.1%.

Because of the one-unit difference between the number of buckets established at $(h + 1)$ and the original number of bunch locations, one bunch will be centered in the new bucket and bunches to either side of the centered bunch will be progressively displaced within the buckets. The center of the k -th bunch is displaced from the center of its bucket by an angle S

= $2\pi k/h$ rf radians, ($- 556 < k < 556$). With the application of the $(h + 1)$ rf voltage, the bunches begin to execute coherent synchrotron oscillations from these initial positions. The synchrotron motion is allowed to continue until bunches with small displacements have executed approximately $3/8$ of one oscillation. This allows bunches with larger initial phase displacement, but lower synchrotron frequency to reach a high momentum deviation. This motion is shown in Fig. 3-1d for the centered bunch and for a bunch displaced from the center of the bucket by 2.2 rad (0.7π). The centered bunch rotates on the phase contour shown to a horizontal position with total momentum spread of 0.148 eV-sec (49.4 MeV). The centroid of the bunch with initial displacement of 0.7π radians moves approximately one-fourth of a turn to a displacement of 0.686 eV-sec (220 MeV). The lower edge of the displaced bunch moves on a contour very close to the separatrix, while the innermost boundary of the bunch moves along the contour shown to a displacement of 0.63 eV-sec (210 MeV). The momentum spread of the displaced bunch then becomes 0.14 eV-sec, about the same as that of the centered bunch. The ratio of bunch displacement to momentum spread is 4.64 , which is just that which is required by Eq. (3-6). The momentum deviation distribution of bunches around the ring at the end of this short period of phase oscillation is shown in Fig. 3-2.

6. When the bunches reach the displacements described in Step 5, the rf is removed and the bunches are allowed to debunch and coalesce. The drift time given by Eq. (3-2) for this example is 0.93 sec.

Results of the first attempt at a relocation experiment are shown in Fig. 3-3, where two Bocster batches separated by 180° in

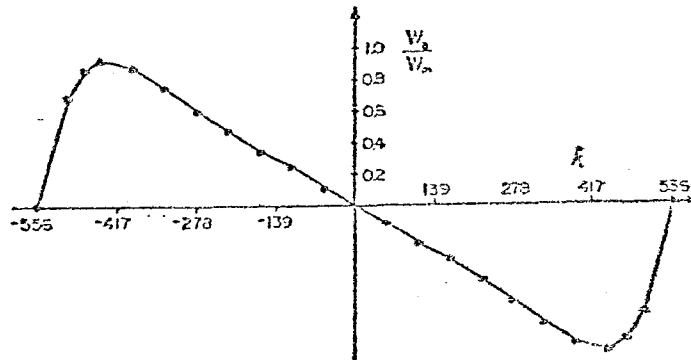


Fig. 3-2 Momentum deviation of bunches as a function of azimuthal position after $3/8$ synchrotron period in buckets with harmonic number $h + 1$.

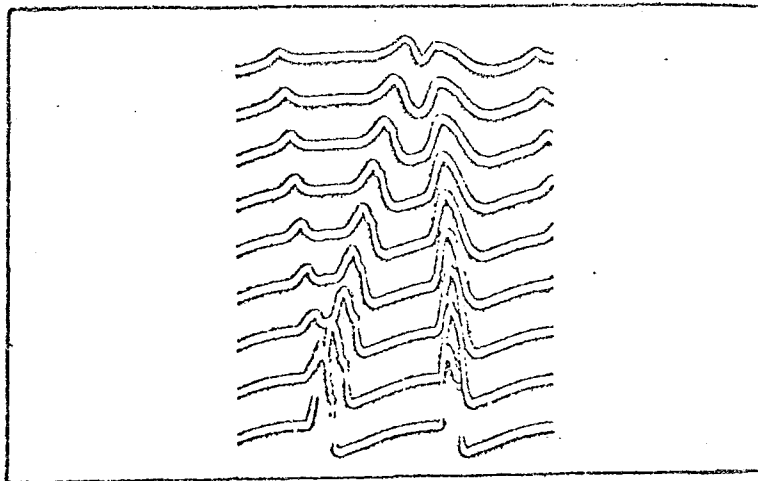


Fig. 3-3 Coalescence of two Booster batches originally separated by 180° . Time proceeds upward, traces separated by 0.2 sec.

the Main Ring are shown coalescing to about one-eighth the azimuth in a period of approximately 2 sec. In this experiment the rf voltages and the bunch widths were not optimized.

3.3 Proton-Beam Transport System to the Target

The extracted 80-GeV proton beam element layout and beam transport system are shown in Fig. 3-4. Extraction takes place in straight section F17 where a septum magnet will be placed. A kicker magnet is located at C48, an odd number of quarter wavelengths upstream. Extraction will be in the vertical direction because less angular deflection is required to miss the following dipole than for horizontal extraction. The nearest Main-Ring dipole must have a special coil so that the beam pipe can pass next to the magnet steel, under the end loop.

The extracted beam is pitched flat 19 in. above normal orbit height by two EPB (External Proton Beam) dipoles. The beam is then kept within the Main-Ring tunnel wall and made to follow the accelerator orbit closely, as seen in Fig. 3-4, by distributing horizontal bends evenly over positions F21 and F23 so that beam elements will not block the Main-Ring tunnel and impede normal maintenance activities. Finally, a counterclockwise bend near F25 brings the beam out through a penetration in the corner of an existing alcove at F25. Providing a tunnel penetration at any other point would require a long slot in the tunnel wall because of the small angles involved and the consequent weakening of the wall would be unacceptable.

The space around the F25 outward bend is very tight, and an EPB dipole cannot be placed in the alcove. This means the last

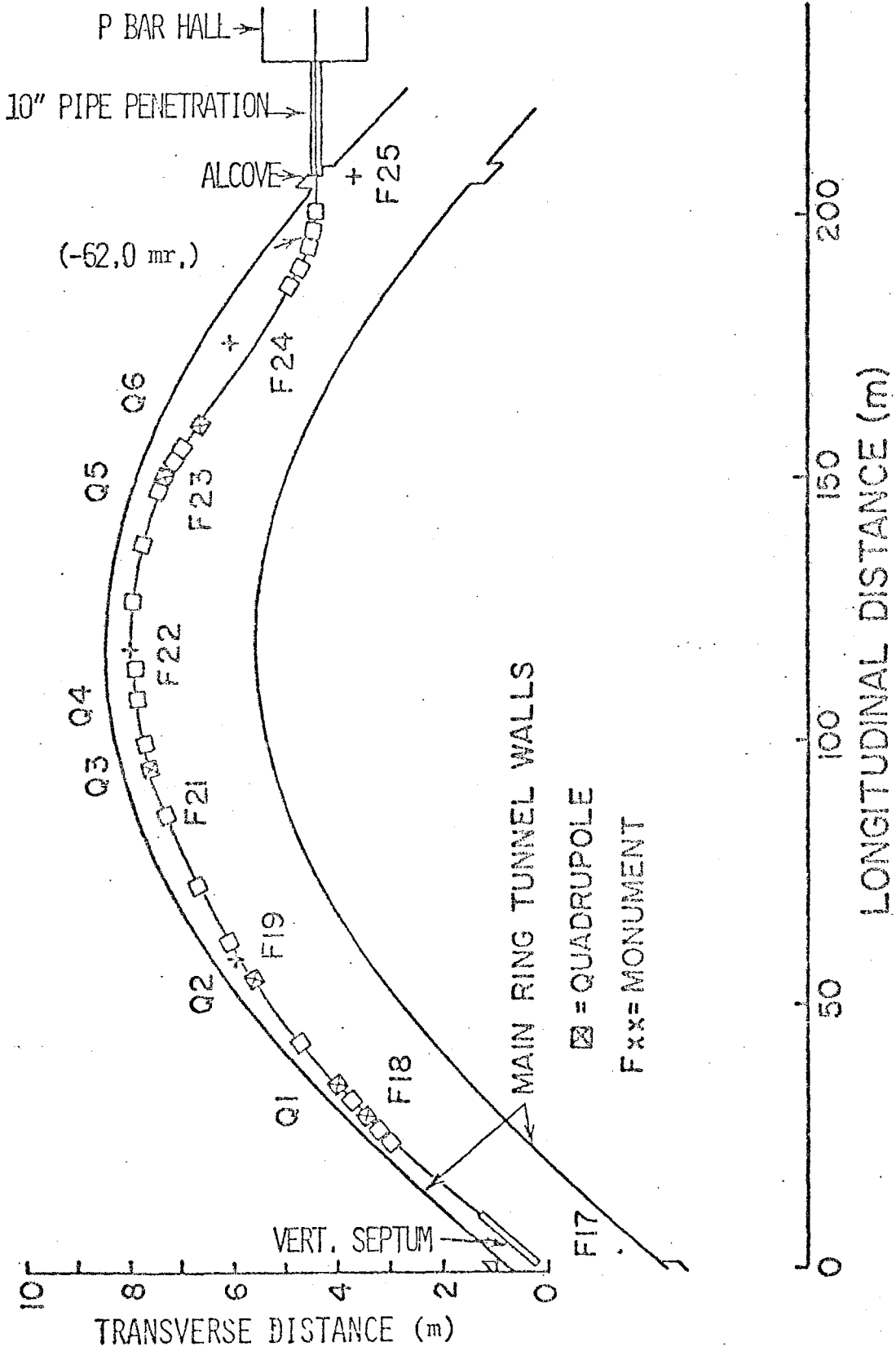


Fig. 3-4 Extracted-proton beam-transport layout.

bend, needing a total of five 10-ft EPB dipoles, encroaches upon tunnel space more than may be considered desirable. This can only be avoided by using special dipoles tailored to fit in the alcove, which must also house an Energy Doubler-Saver cold box down nearer the floor.

The extracted proton beam then enters a length of 10-in. pipe buried in the ground, which serves as a permanent radiation barrier for the next enclosure. In analogy with other Fermilab external-beam enclosures, we call the latter " \bar{p} Hall". It contains the quadrupoles required to produce a highly focused beam spot on the production target in the next enclosure, the Target Vault. \bar{p} Hall is accessible through a labyrinth, so that the elements there may be serviced in situ and the actual target may be reached by remote-handling devices. We note that it also contains four quadrupoles needed for the reverse-injection beam.

The Target Vault will be a high-radiation area, so that \bar{p} Hall will be protected from residual activity and gas activation by a wall between it and the Target Vault. The 130-ft Target Vault immediately follows \bar{p} Hall, with the target position as close as possible to the separating wall, as shown in Fig. 3-5. It will be possible to extract the target through the separating wall on a railway cart and store it in a lead pit in \bar{p} Hall. The target itself is normally in a magnetic field, which bends the 80-GeV proton beam downward by 5 mrad. This ensures that radiation from the beam dump beyond the target will be directed into the ground and will not fill the following tunnel with radiation.

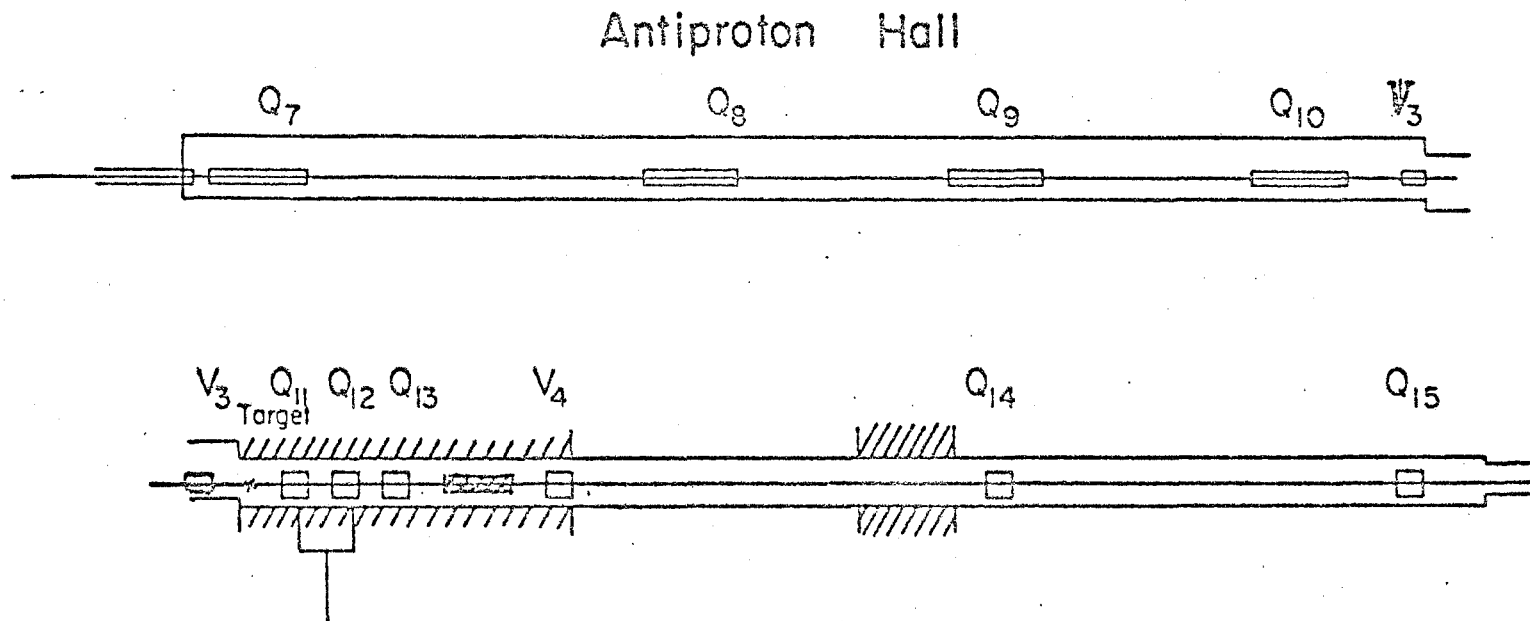


Fig. 3-5 \bar{p} Hall and Target Vault

3.4 Spot Size and Divergence Angle

At any point along the length of the target, the antiprotons are produced from a spot the size of the proton beam at that point (if that size is smaller than the target size) with a divergence cone angle given roughly by the Cocconi angle $(0.3 \text{ GeV}/c)/p$. For the systems considered here, the solid angle of acceptance of the antiproton cone is only about 2% of the total cone of antiprotons produced and the distribution of \bar{p} 's within the acceptance cone is therefore approximately uniform.

To maximize the number of \bar{p} 's collected from a given point along the target, the transverse dimensions of the incident p-beam at that point must be sufficiently small. This means that the depth of focus of the \bar{p} collection system will also be small.

3.5 Antiproton Production Cross Section

Using existing experimental data, it is possible to estimate to $\pm 50\%$ accuracy¹ the \bar{p} production cross section of 0° production of 4.5-GeV antiprotons with 80-GeV protons bombarding a heavy target.

Two conclusions that can be reached from this data are:

- (i) The antiproton production cross section $d^2\sigma/dp d\Omega$ (at $X_F = 0$) for 80-GeV pp collisions is greater factor of 4 to 6 than for 26 GeV-pp collisions.
- (ii) The antiproton momentum for maximum yield from 80-GeV protons hitting heavy nuclei is between 3 and 6 GeV/c. The yield equation we use is²

$$\frac{d^2 N_{\bar{p}}}{dp d\Omega} = \frac{1}{\sigma_0} E \frac{d^3 \sigma}{dp^3} p_{\bar{p}} x_{\text{abs}} I_p, \quad (3-9)$$

where $\sigma_0 = 33$ mb is the pp inelastic cross section, $(E d^3 \sigma / dp^3) = 0.8$ mb/GeV² is the estimated pp \rightarrow \bar{p} invariant cross section for 80-GeV pp collisions, I_p is the number of protons hitting the target, and x_{abs} is the effective number of mean free paths of target. If the protons and antiprotons have an absorption m.f.p. of λ and L is the length of the target, then we have

$$x_{\text{abs}} = \frac{L}{\lambda} e^{-L/\lambda}. \quad (3-10)$$

This never exceeds 0.4 and is 0.3 for a target whose actual length is $\lambda/2$.

3.6 Transverse Matching

The target efficiency is further decreased by the requirement discussed above that a very small proton-beam spot size is required to obtain a bright source of antiprotons. The real two-dimensional \bar{p} yield into a fixed one-dimensional phase acceptance $\bar{\epsilon}$ can be written

$$Y \frac{d\bar{n}}{d\ell} \ell_{\text{eff}} \frac{\bar{\epsilon}}{\beta}, \quad (3-11)$$

where β is the envelope function of the antiprotons, ℓ_{eff} is the effective length of the target due to limited depth of focus of

the \bar{p} collection system, and $(d\bar{n}/d\ell)$ is the linear density of \bar{p} production.

The effective length ℓ_{eff} (i.e. the equivalent depth of focus) is given by¹

$$\ell_{\text{eff}} = 2 \int_0^{L/2} \frac{\beta_0 \bar{\beta}_0}{\beta \bar{\beta}} d\ell, \quad (3-12)$$

where β (or $\bar{\beta}$) is the betatron amplitude function for the protons (or antiprotons), and $\beta_0, \bar{\beta}_0$ are $\beta, \bar{\beta}$ evaluated at the focus at $\ell = 0$.

With no focusing field at the target, the integral in Eq. (3-12) can be evaluated to be $\ell_{\text{eff}} = 0.38 L$.

3.7 Focusing Within the Target

By passing a longitudinal current along the target rod, an azimuthal magnetic field that focuses antiprotons (and unfortunately defocuses protons) can be used as a field-immersion lens to increase the depth of field.³ Described in another way, this field allows one to confine the antiprotons from the upstream part of the target so that they appear to be emitted by the downstream part of the target, thus increasing the brightness of the target. Since substantial engineering problems would be involved in pulsing large currents through a target wire, we have not included this feature in the present target design.

3.8 Target Design

To arrive at a practical target design, one must add to the foregoing factors such practical considerations as energy deposition in the target material. The emphasis on high-

brightness production leads to peak instantaneous thermal energy density of the order of 15 kJ/cm^3 . For this reason, we are giving serious consideration to a target of liquid mercury that will not explode during a beam spill and recover between spills.

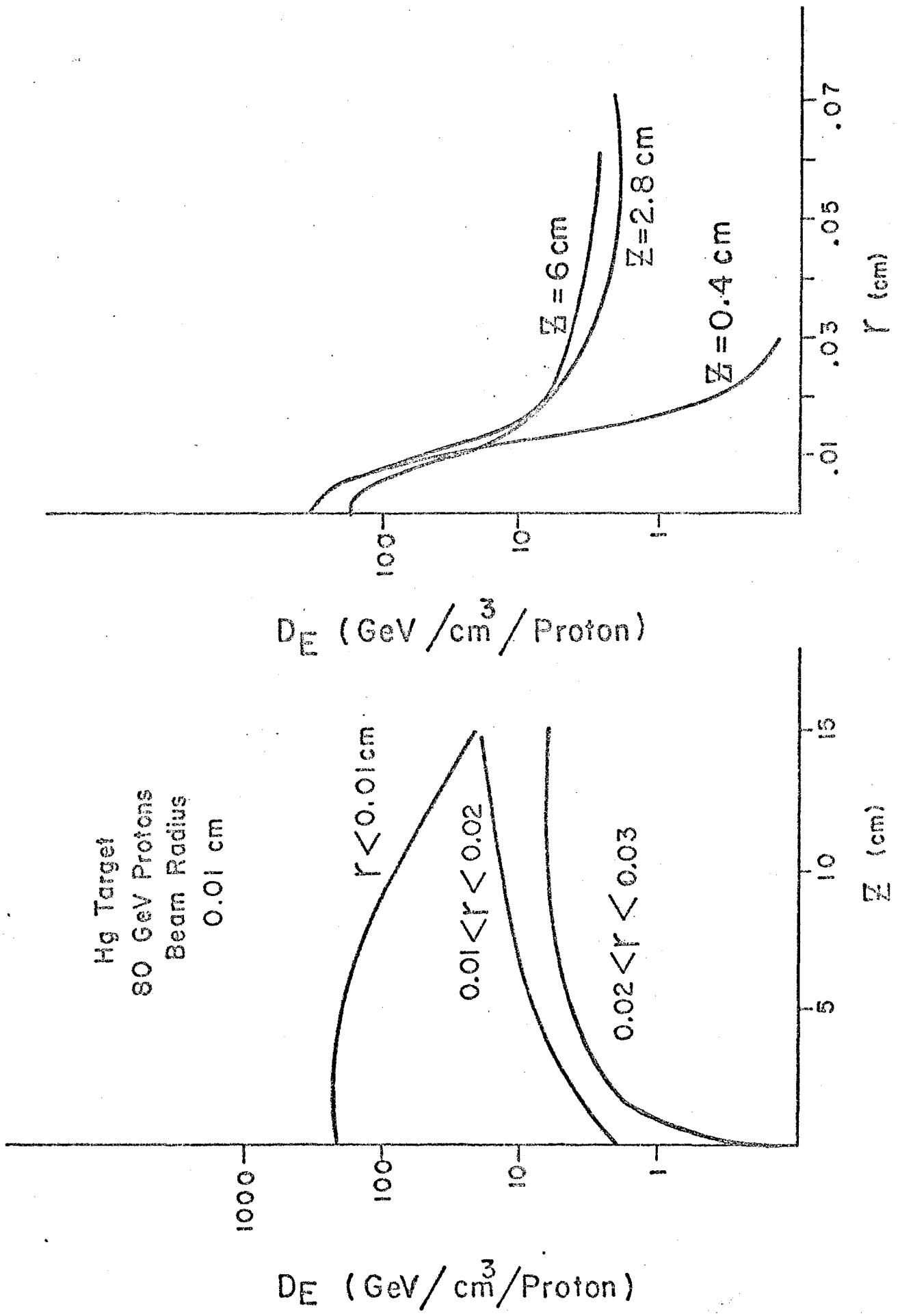
Some additional design considerations are:

- (i) The target assembly must fit the limited space that is available between the proton beam and the antiproton beam.
- (ii) The target container must be large enough to reduce the pressure and temperature bump produced by the vaporization of the target material.
- (iii) The container will have to handle:
 - a. time-dependent loading;
 - b. thermal shock;
 - c. stress due to differential heating;
 - d. creep stress due to constant pressure;
- (iv) Liquid-metal embrittlement may occur unless a judicious choice is made of container material.
- (v) Creep resistance becomes an increasingly important consideration at elevated temperatures, becoming the dominating design consideration for temperatures greater than half the melting temperature.
- (vi) Wall thickness should be reduced to a minimum to lessen the tendency to fracture under shock.
- (vii) The gas used around the vessel must be inert with the chosen vessel material.
- (viii) Good heat conduction must be provided.

(ix) Radiological and chemical toxicity must be contained.

We have carried through a schematic design of target and container that aims towards optimization with respect to the above constraints. Compatibility between items (i) and (ii) has not been achieved in this design. The volume restriction for the target container, in conjunction with the permissible clearance between the primary and secondary beams, will require a change of the vessel cross section from circular to elliptical or a change in the beam transport. The choice among these alternatives can be made when other features of the targetry are more firmly established. The choice of optimum vessel thickness is established by a balance between rupture resistance on the one hand and fracture and differential heating on the other (items (iii c) and (vi)). The thickness chosen is appropriate for steel, which is a good choice for avoiding embrittlement caused by the mercury.

The energy deposition in the mercury target has been estimated using information from a detailed calculation. The magnitude of the thermal and mechanical transients has then been calculated. Figure 3-6 shows longitudinal and radial distributions of energy density per incident proton for a beam of 0.1-mm radius. The energy deposited is 3.1 kJ per spill, of which 860 J goes into heat of vaporization and 2240 J goes into instantaneous (i.e. constant-volume) heating of the vapor. The pressure and temperature after expansion into the vessel volume are approximately 30 psi and 180°C. Even if these estimates are somewhat low, they suggest that there is no major problem in this



respect. The critical consideration is the local instantaneous pressure and temperature at the beam windows.

Both the radiological and chemical toxicity of the target are matters of concern. The design incorporates reasonable shielding, redundant sealed containment, and maintenance-free installation. The only manipulation required for an activated target will be an infrequent total replacement. The target has no support requirements other than a closed-loop cooling system. The concerns of radiation-safety specialists have been included in the criteria that have resulted in the schematic design presented. A prototype target will be fabricated and tested in the coming months.

Table 3-II summarizes the target design parameters.

Table 3-II Target Design Parameters

Target Length, L		6 cm
\bar{r}_0		1 cm
Spot radius $r_{\bar{p}}$		0.2 mm
Production angle		24 mrad
Target material		Hg
\bar{p} energy		4.5 GeV
$\Delta p/p$	=	$\pm 2\%$
Solid angle (eff)	=	10^{-3} ster*
Absorption length	=	12 cm
Eff. no. of abs. lengths	=	0.30
$F_{\text{geom}} = \lambda_{\text{eff}}/L$	=	0.38

*In principle this number could be as large as 1.8×10^{-3} ster for the indicated production parameters. The smaller value was chosen to reflect the fact that the vertical admittance of the Electron Cooling Ring is about half the horizontal.

Then we can estimate the yield as

$$\begin{aligned} N_{\bar{p}}/N_p &= \frac{1}{\sigma_0} E \frac{d^3 \sigma}{dp^3} p_{\bar{p}} \Delta_{\bar{p}} \Delta \Omega x_{\text{abs}} F_{\text{geom}} \\ &= \left(\frac{1}{33}\right) (0.8) (5.4) (0.22) (10^{-3}) (0.30) (0.38) \\ &= 3.2 \times 10^{-6} \end{aligned}$$

This value for $N_{\bar{p}}/N_p$ is consistent with that calculated by Chadwick⁴ using a rather different procedure. It is smaller than the (scaled) yield obtained by Pondrom⁵ apparently mainly because F_{geom} was taken to be unity in Pondrom's calculation.

3.9 Beam Transport from \bar{p} target to Precooler

This transport line carries a beam of 4.5-GeV antiprotons to the Precooler. The solid-angle acceptance of the system is defined by the \bar{p} -collection quadrupole triplet at approximately $\pi \times (24 \times 10^{-3})^2$ or 1.8×10^{-3} sr (semicone acceptance angle of 24 mrad). Since the admittance of the Precooler is 4.8×10^{-6} m-rad in each plane at 4.5 GeV, the primary-beam focus should be less than 0.37 mm in radius. An achromatic match to the Precooler is required for the $\Delta p/p = \pm 2\%$ \bar{p} beam, and therefore a substantial portion of the transport must consist of a chromatic-correction section.

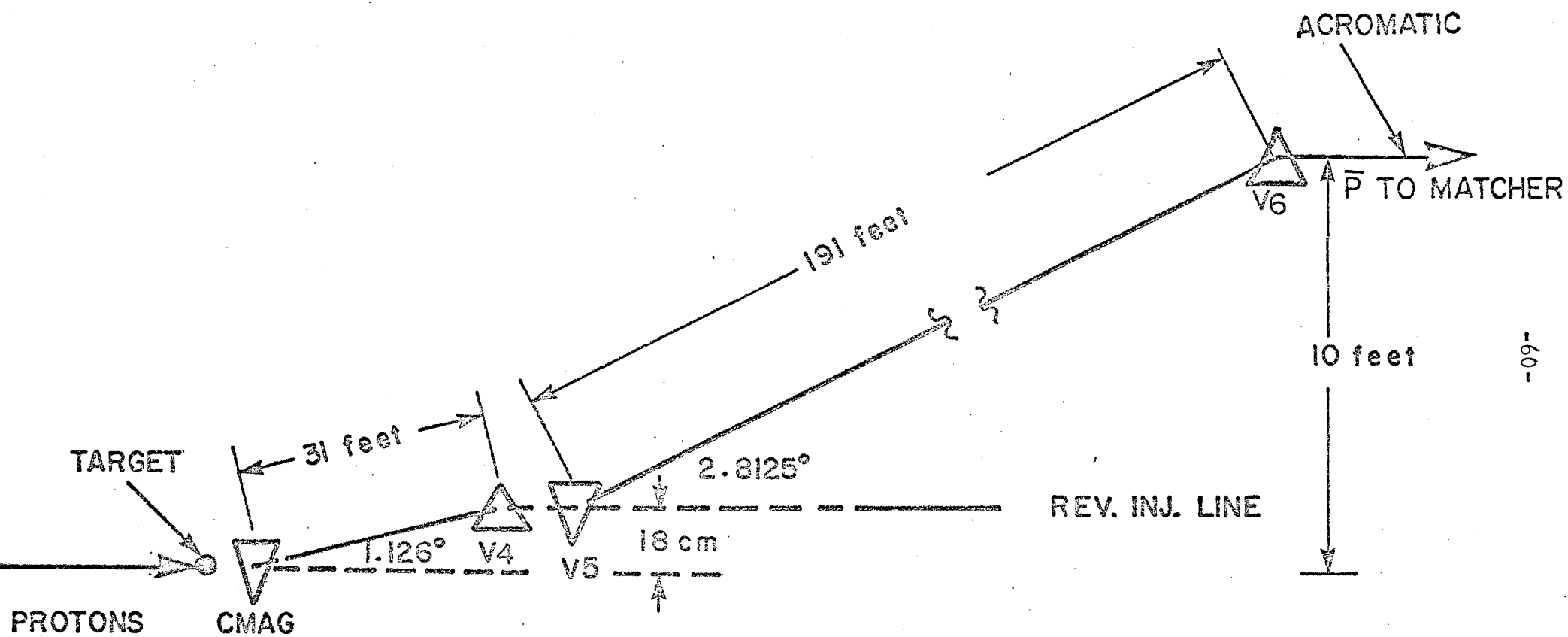
The design is subject to the following physical constraints:

- (i) the \bar{p} beam rises in elevation by 0.1874 m from the target to the center of dipole V4;

- (ii) The distance from \bar{p} target to Precooler must be less than 175 m;
- (iii) the Precooler is sited 10 ft (3.048 m) in elevation above the \bar{p} target.

The vertical translation of the system is sketched in Fig. 3-7. A vertical dipole (V5) is powered to kick the 4.5-GeV \bar{p} beam up by 2.8125° . It rises to Precooler elevation and is brought flat and made achromatic by the dipole V6. This rise occupies 191 ft (58.2 m) and is a conventional translation system. Quadrupole focusing is of course required to maintain reasonable beam size. V6 is followed by transport in the horizontal plane to the injection point into the Precooler; the elements of this beam transport are shown in Fig. 3-8.

It is planned to inject the \bar{p} beam into a dispersion-free straight section of the Precooler where the beam characteristics are $\beta_x = 16.48$ m, $\beta_y = 26.52$ m, and $\alpha_x = 1.19$ and $\alpha_y = 0.34$. Furthermore the beams should be achromatic. That is, the phase-space ellipses for all $\Delta p/p$ should be nearly identical. Thus it will be necessary to correct for the quadrupole chromatic aberrations by using sextupole magnets suitably placed in a periodic channel, such as suggested by Brown.⁶ We assume the same periodic structure as used in the Precooler design, i.e., a cell length of 9.119 m and a phase shift of 90° per period. The correction section is chosen to be made up of 8 cells with total phase shift of 4π . Bending magnets are placed midway between F and D quadrupoles, with one missing at the midpoint, so that 16 dipoles are required. The system will first bend to the left in the first 4 cells and then bend back an equal amount in the final



-09-

ELEVATION VIEW

Antiproton Vertical Translation Systems

Fig. 3-7 Vertical translation of the \bar{p} beam.

four cells, such as is shown in Fig. 3-8. We do not specify the bends precisely at this time, but it is reasonable to assume a bend of 40° per 2π section or 5.0° per magnet.

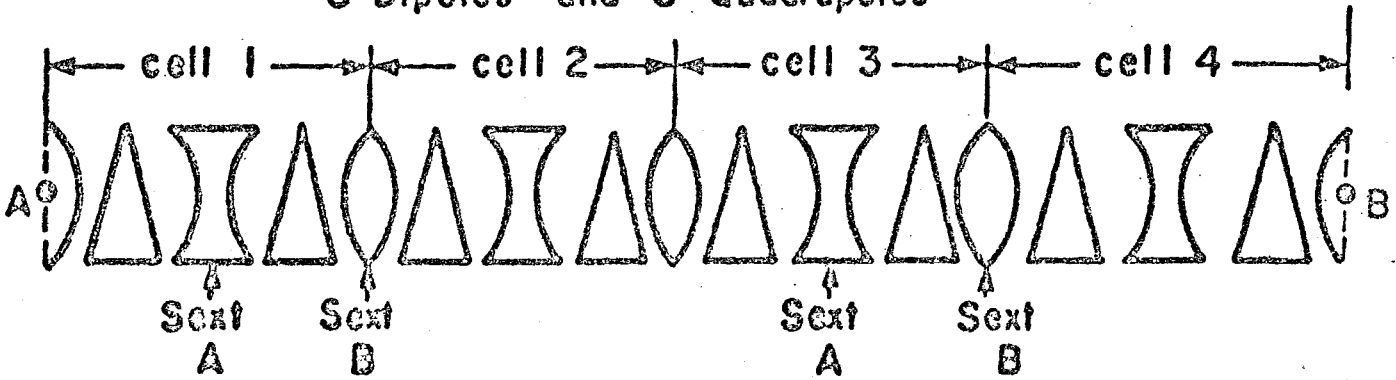
It is necessary to construct a matching section from V6 to the point A of the chromatic corrector. At point A the lattice parameters are $\beta_x = 15.231$ m, $\beta_y = 2.7255$ m, $\alpha_x = \alpha_y = 0$ and the beam is achromatic. Point B represents the transition between the two 120-ft correctors. At point C, the beam enters the final matching section (at QFA) and is transported to the injection septum at point D in Fig. 3-8. This matching section is identical to that in the lattice, except that the dipoles are missing.

We believe that four sextupole families are required to achieve the achromatic beam conditions at point D. The two identical members of a family are spaced by π phase shift to cancel the geometric aberrations. A possible configuration for locating the sextupole families is also indicated in Fig. 3-8. The sextupole windings are included in the quadrupoles.

This design is discussed in more detail in Ref. 7.

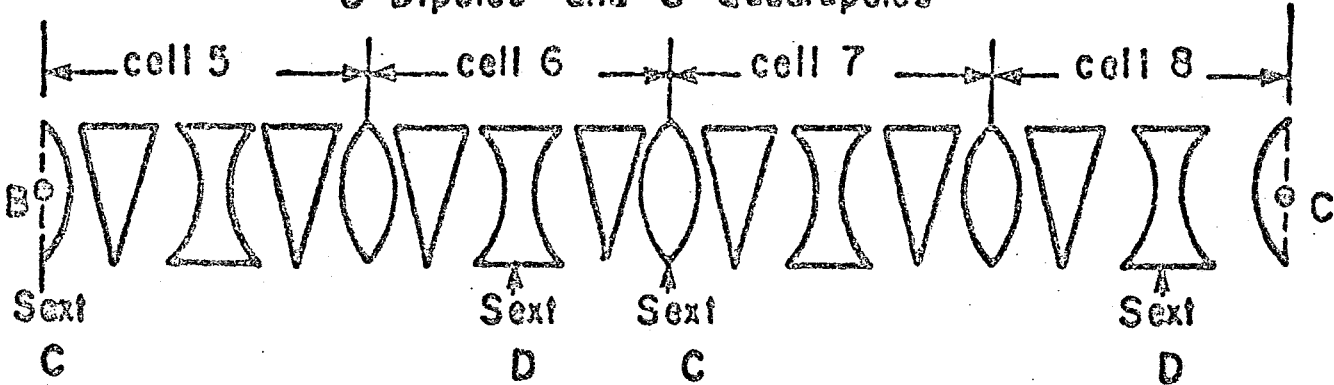
BEND TO LEFT

8 Dipoles and 8 Quadrupoles



BEND TO RIGHT

8 Dipoles and 8 Quadrupoles



MATCH AND INJECT INTO PRECOOLER

8 Quadrupoles



Fig. 3-8 Optics of the \bar{p} beam.

References

- ¹J. W. Cronin, 1977 Fermilab Summer Study, Vol. 1, p. 269.
- ²D. Cline, P. McIntyre, F. Mills and C. Rubbia, Collecting Antiprotons in the Fermilab Booster and Very High Energy $p\bar{p}$ Collisions, Fermilab Internal Report TM-689, 1976.
- ³D. Cline and F. Mills, Exploding Wire Lens For Increased- p Yield, Fermilab p Note 7, Jan. 1979.
L. C. Teng, Study of Current-Carrying p Production Target, Fermilab p Note, Feb. 1979.
- ⁴G. Chadwick, Considerations on the Antiproton Production Beam, Fermilab Note, Aug. 1977.
- ⁵L. G. Pondrom, 1977 Fermilab Summer Study, Vol. 1, p. 259.
- ⁶K. L. Brown, private communication.
- ⁷E. Colton, Optics Design From p Target to Precooler, Fermilab p Note 46, Oct. 1979.

4. STOCHASTIC COOLING AND DECELERATION IN THE PRECOOLER

4.1 Introduction

An unbunched pulse of antiprotons is to be injected into the Precooler with a kinetic energy of 4.5 GeV, a momentum spread of $\pm 2\%$, and betatron emittance of $4.8 \pi \times 10^{-6}$ mrad in each plane. For the Booster-circumference Precooler ring envisioned, this corresponds to a longitudinal phase-space area of 340 eV-sec. Because of the limitations imposed by the electron-cooling process, the Electron Cooling Ring requires something between 1 and 3 eV-sec. This section describes the stochastic cooling and rf decelerating processes utilized in the Precooler to effect the necessary phase-space area and energy reductions.

4.2 Stochastic Cooling Theory

Following the invention by van der Meer¹, the theory of stochastic cooling has been developed in various levels of detail, and with different approaches in a number of papers.²⁻⁴ At present, one feature of the technique is that momentum cooling using notch-filter methods appears to be much faster than transverse cooling. The antiproton collection scheme presented in this report recognizes this fact and incorporates only momentum cooling. Should techniques eventually be developed to speed up transverse stochastic cooling appreciably, the collection scheme could advantageously add it, but is not now part of the system.

Our knowledge of stochastic momentum cooling has greatly improved during the last year through analytical and computer investigations⁵⁻⁸ the point where we believe we have a workable

cooling-system design. Our calculations predict adequate performance and appear to be consistent with calculations and experiments conducted by CERN.

In the notch-filter method used, information regarding a particle's momentum is obtained through its relationship with its revolution frequency. A filter system in the pickup-kicker chain appropriately conditions signals to accelerate or decelerate particles toward a specific rotation frequency (i.e., momentum). A useful filter element for this purpose is a shorted transmission line whose length corresponds to half the rotation period. Such an element exhibits "zeroes" in its input impedance at all harmonics of the rotation frequency. The resultant transfer function of such an element, when used in a voltage-divider configuration, appears as a series of notches, hence the term "notch filter".

Figure 4-1 shows the results of a typical computer simulation. The choice of the dispersion $\eta = 0.02$ is particularly significant. It provides for operation of the Precooler between 200 MeV and 8 GeV without crossing transition γ , and provides proper phase mixing, as will be described in the following sections.

Fokker-Planck Simulation of $\Delta p/p$ Cooling

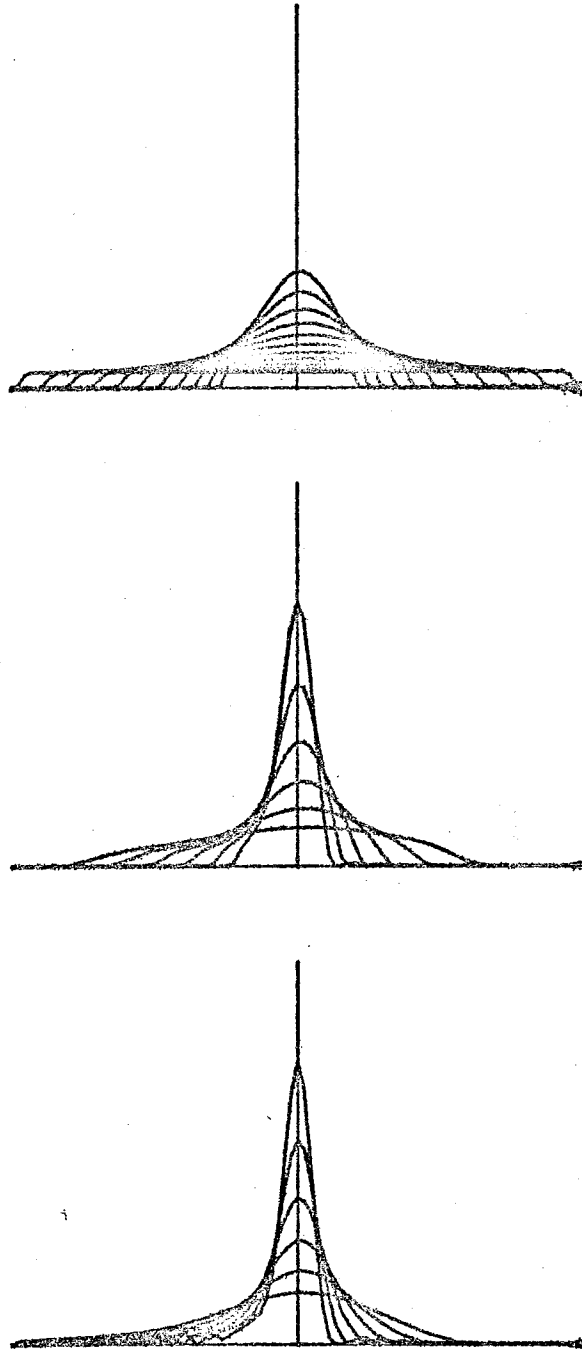


Fig. 4-1. Computer simulation of stochastic momentum cooling at (a) 4.5 GeV, (b) 2.6 GeV, and (c) 1.3 GeV. In each case, the scales are changed so that the final distribution at one energy is the initial distribution at the next lower energy.

4.3 Cooling Sequence

4.3.1. Choice of Optimum Cooling Steps. The essential ingredient in stochastic momentum cooling with the notch-filter technique is the revolution-frequency spread. A requirement for optimal cooling is that the notch at the highest harmonic in the feedback-system bandpass be filled with beam signals. As cooling proceeds, the frequency spread decreases and the notch gaps are less and less filled, until a situation is reached where the cooling is greatly reduced. By decelerating a cooled beam, the required frequency spread can be restored to make rapid cooling possible again.

The criterion that the width of the highest Schottky band at frequency $h\omega$ equal the notch width may be written as

$$h\Delta\omega = \text{const.} \quad (4.1)$$

But

$$\frac{\Delta\omega}{\omega} = \eta \frac{\Delta p}{p} \quad (4.2)$$

and it follows that

$$\frac{\eta}{\beta} \frac{\Delta p}{p} = \text{const.} \quad (4.3)$$

Eq. (4.3) can then be used to calculate the energy required to restore the initial mixing.

The cooling scheme we have developed will reduce the momentum spread by a factor 5 in 2 seconds or less at 4.5 GeV. After the beam has been cooled, it will be bunched at some harmonic number h and decelerated. One can stop the deceleration at 2.6 GeV and re-apply stochastic cooling with the same technique (but a slightly altered filter) to achieve a further reduction of $\Delta p/p$ by a factor 5 in 2 seconds. Obviously the deceleration ramp should first be flattened and the beam adiabatically debunched to avoid too-large dilution. After cooling, the beam will again be adiabatically rebunched and further decelerated.

The frequency-spread condition of Eq. (4.3) for stochastic cooling will again be met at a kinetic energy of 1.3 GeV. The beam will again be adiabatically debunched at constant field, cooled once more in 2 seconds with one more reduction of $\Delta p/p$ by a factor 5, adiabatically rebunched and decelerated finally to 200 MeV. Figure 4-2 is a schematic representation of the cooling process. Table 4-I gives the \bar{p} -beam momentum spread at the end of each cooling and decelerating step, together with other parameters, such as the total beam phase-space area S . The momentum spreads are for fully adiabatically debunched beams. No dilution has been included for deceleration and the debunching-rebunching processes. As shown in the Table, the final momentum spread (debunched) at 200 MeV is $\pm 0.133\%$ after three cooling steps. It is possible to perform a fourth period of cooling at 530 MeV; in this case $\Delta p/p = \pm 0.0266\%$ at 200 MeV. We might well find that stochastic cooling is more effective than we believe and that three steps of cooling will be adequate to achieve a

PRECOOLER CYCLE TIME

Deceleration rate = 8 GeV/sec

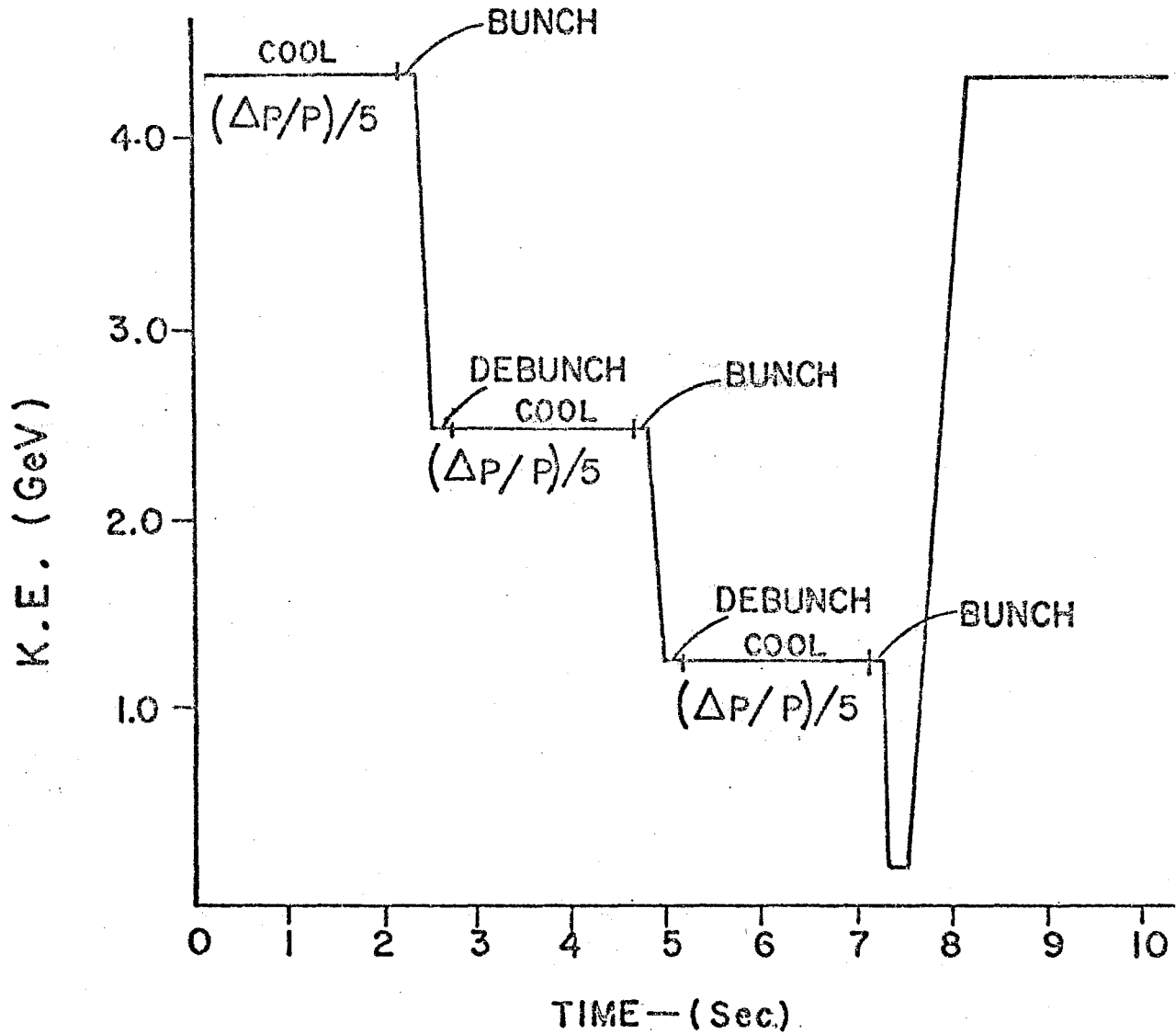


Fig. 4-2. Schematic plan of the cooling process.

momentum spread that can be accommodated in the present Electron Cooling Ring. Otherwise we can utilize four steps of cooling. The scheme we have outline for the Precooler is flexible enough to allow such variation in tactics.

Table 4-I Parameters for Stepped Stochastic Cooling

<u>Kinetic Energy</u> T(GeV)	<u>Momentum</u> p(GeV/c)	<u>Momentum Spread</u> $\Delta p/p(\pm\%)$	<u>Phase- Space</u> <u>Area</u> S(eV-sec)
4.5	5.36	2.0	340
	after stoch cool (1)	0.4	68
2.6	3.41	0.63	68
	after stoch cool (2)	0.13	14
1.3	2.03	0.21	14
	after stoch cool (3)	0.042	2.7
0.2	0.644	0.133	2.7
or			
0.53	1.13	0.075	2.7 optional
	after stoch cool (4)	0.015	0.54 4th step
0.2	0.644	0.027	0.54

4.3.2 Hardware Requirements. The same pickup, amplifier, and kicker system can be used for all cooling steps, although either separate notch filters (high-quality long transmission lines) or a tunable system are required because of the variation of β , and consequently of the revolution frequency, during deceleration. Because of this same variation of β , the delay between pickups and kickers must also be adjusted. Relatively fast switches can connect the preamplifier stages to the several notch filters and delay lines.

4.3.3 Requirement of Deceleration It is not desirable to accelerate at a high rate in the Precooler because a high rate would increase the rf system requirements with minimal gain in

the cycle time. Thus a metallic vacuum chamber can be used without appreciable chamber heating or induced sextupole fields from the eddy currents.

The most stringent requirements for the rf deceleration system will be encountered during the first step of deceleration from 4.5 GeV down to 2.6 GeV. In this step, the beam has the largest energy and phase-space area. If the deceleration occurs in a period of 0.2 sec, the energy loss per turn is

$$\Delta E = eV \sin\psi_s = 8.0 \text{ keV/turn.}$$

The rf voltage required to supply a bucket with an area at least equal to the beam bunch area ($68/h$ eV-sec) is

$$\frac{V}{h} = 65 \text{ kV.}$$

The smallest rf bucket area occurs at 2.6 GeV and is approximately equal to the bunch area. The voltage requirement through the deceleration cycle is shown in Table 4-II. V_{ad} is the voltage required to create stationary buckets with the same bunch area. V_{max} is the maximum voltage required for bucket area at the end of each deceleration step. The number in parentheses is the ratio of the bucket area to the bunch area corresponding to V_{max} and to decelerating at a constant rate of 8 keV/turn.

We observe that the harmonic number is still a free parameter that one may choose in the most convenient way. One choice would be $h = 1$. There are therefore the following

requirements for the rf system: it should provide a total of 65 kV and operate in the frequency range from 357.93 kHz to 622.72 kHz. The system can be accommodated in one of the four 20-m long dispersion-free straight sections.

Table 4-II Voltage Requirement Normalized to Harmonic Number h

<u>Kinetic Energy</u> GeV	<u>S</u> <u>V-sec</u>	<u>V_{ad}/h</u> <u>kV</u>	<u>V_{max}/h</u> <u>kV</u>	
4.5 2.6	68	6.5 34	65	(1)
2.6 1.3	14	1.35 6.6	26	(2)
1.3 0.2	2.7	0.3 1.7	26	(3)
1.3 0.53	2.7	0.3 1.3	26	(2.4)
0.53 0.2	0.54	0.053 0.068	10	(1.2)

4.3.4 Adiabatic Capture and Debunching. The beam should be adiabatically debunched before a cooling step and adiabatically recaptured at the end to avoid excessive phase-space area dilution. The rule we follow here is to turn the rf voltage on or off slowly according to a prescribed curve in a time that is approximately one phase-oscillation period at the voltage V_{ad} given in Table 4-II. The phase-oscillation period is approximately constant at a value of 25 msec. This time therefore gives negligible contribution to the total cycle time of the Precooler. The total cycle time is then as follows:

(3 or 4) × 2 sec (for stochastic cooling)

+

1 sec for deceleration

+

1 sec to ramp to original field

=

8-10 seconds.

In conclusion, every 8-10 seconds a beam of 6×10^7 p with a transverse emittance of $4.8 \pi \times 10^{-6}$ m-rad in each plane and longitudinal emittance of 0.55 eV-sec at 200 MeV is transferred to the Electron Cooling Ring.

There is an apparent bottleneck at 200 MeV, at the end of the Precooler cycle. When the 200-MeV beam is bunched to Electron Cooling Ring length, the momentum spread in the given bucket area becomes too large for the Electron Cooling Ring to cool in a reasonable time. This bottleneck can be avoided in any of several possible ways:

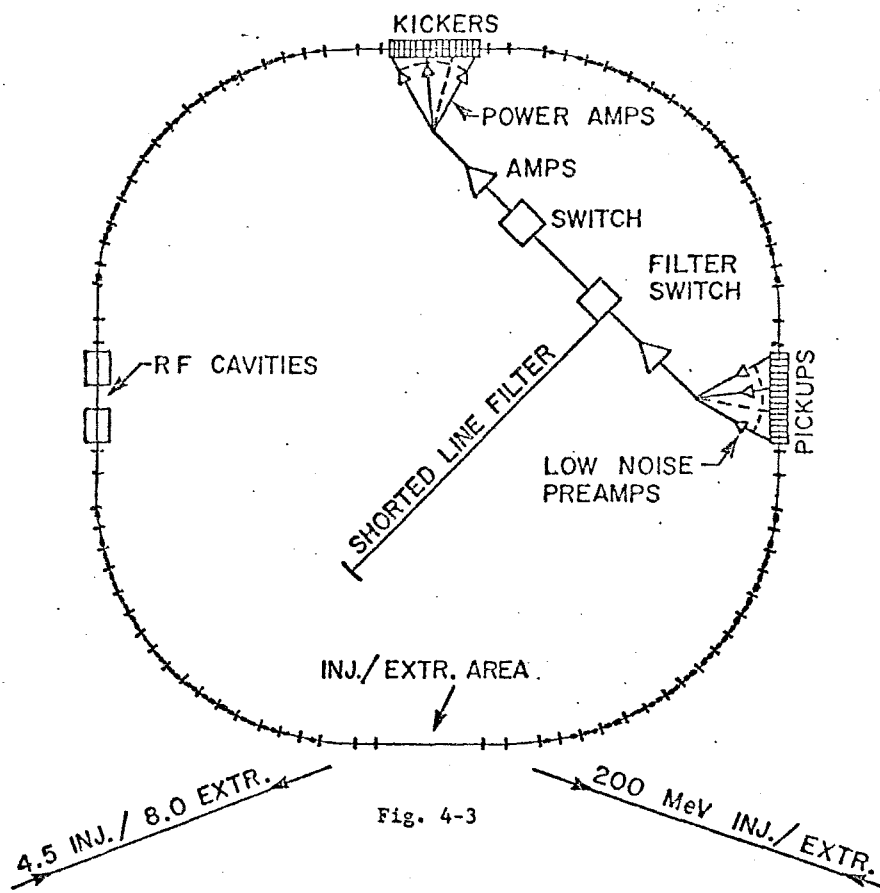
- (i) Rebunch on the 2nd harmonic in the Precooler and inject and cool the two bunches sequentially. This could lengthen the total cycle time to 10 seconds.
- (ii) Do the fourth cooling step. This will reduce the momentum spread, but will lengthen the total cycle to 10 seconds.
- (iii) Achieve more cooling per step.

There are uncertainties in the estimates of stochastic cooling and of dilution in the rebunching process and it may well be that the three-step cooling and first-harmonic bunching will

produce an acceptable momentum spread. With this uncertainty in mind, we are designing the rf system with enough frequency capability to cover (i).

It may be possible to avoid debunching and recapture of the beam by applying stochastic cooling to a long bunch trapped by a stationary rf bucket. Since the required cooling time is much larger than a phase-oscillation period, there is some incompatibility between cooling and mixing when they are influenced by phase oscillations. The cooling of bunched beams needs further analysis and evaluation before it is included in the design.

Figure 4-3 is a conceptual layout of the momentum-cooling system for the Precooler.



CONCEPTUAL LAYOUT OF
PRECOOLING SYSTEM

References

- ¹S. van der Meer, Stochastic Cooling of Betatron Oscillations in the ISR. CERN-ISR-PO/72/31 (1972).
- ²F. Sacherer, Stochastic Cooling Theory, CERN Report IST/TH 78-11 (1978).
- ³G. Carron and L. Thorndahl, Stochastic Cooling of Momentum Spread by Filter Techniques, CERN Report 2RF/78-12 (1978).
- ⁴D. Mohl, Stochastic Cooling, CERN Report PS/D7/78-75 (1978).
- ⁵A. Ruggiero, Computer Simulation of Momentum Stochastic Cooling, Fermilab \bar{p} Note 10, Jan. 1979.
- ⁶A. Ruggiero, Program ST COO to Simulate Stochastic Cooling, Fermilab \bar{p} Note 15, Jan 1979.
- ⁷E. Crosbie, Fermilab \bar{p} Note 13, July 1979.
- ⁸J. Simpson, Deceleration in the Precooler, Fermilab \bar{p} Note 20, Aug. 1979.

5. PRECOOLER RING DESIGN

5.1 Design Considerations

The requirements placed on the Precooler design by the antiproton collection scheme can be summarized as follows:

(i)	average radius	75 m
(ii)	momentum dispersion function (at 4.5 GeV)	0.02
(iii)	momentum acceptance	$\pm 2\%$
(iv)	transverse acceptance (with $\Delta p/p = \pm 0.13\%$)	$40 \pi \times 10^{-6}$ m-rad
(v)	dispersion-free straight section length	> 20 m
(vi)	peak operating energy	8.0 GeV
(vii)	transition energy	> 8 GeV
(viii)	highest practical superperiodicity	
(ix)	acceleration and deceleration rate up to	8 GeV/sec
(x)	deceleration from 4.5 GeV to 200 MeV	
(xi)	acceleration from 200 MeV to 8 GeV	

A study was made of the feasibility of using the recently decommissioned Argonne ZGS magnet ring as a basis for a Precooler and the results were presented in draft form in a study report in July, 1979. There were a number of drawbacks in use of the ZGS magnets, notably a necessarily low γ_t , low periodicity, large and expensive hardware (vacuum system, quadrupoles, etc), and a large containment structure and shield. A more suitable design, using new magnets, has been developed; it will meet all the require-

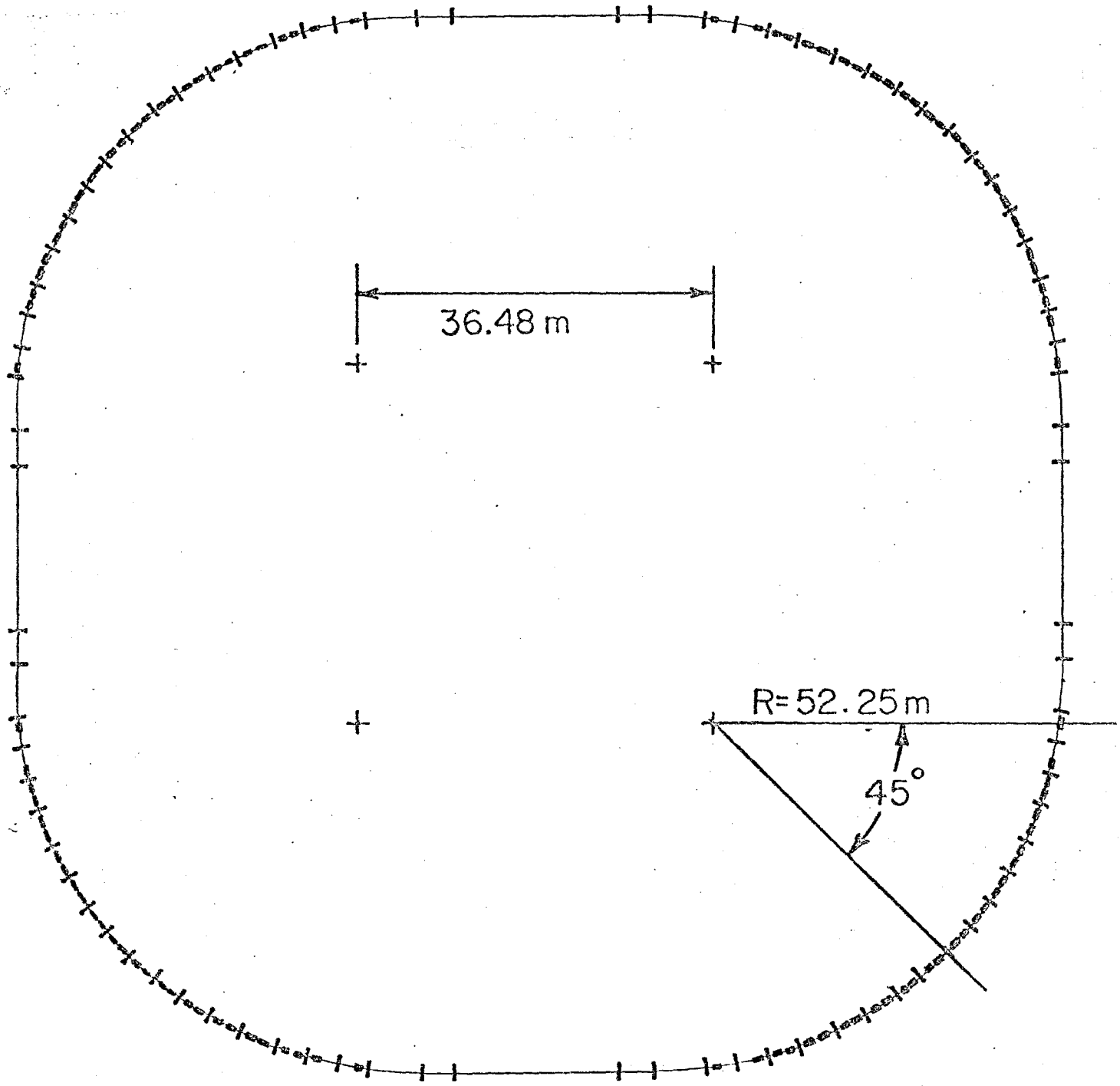
ments at a cost no more than that associated with the use of the ZGS magnets.

5.2 Lattice

These specifications have been met in a strong-focusing FODO design with 4 matched long straight sections and missing-magnet dispersion matching. A layout of the Precooler ring is shown in Fig. 5-1 and parameters are collected in Table 5-I. The lattice sequence and orbit functions are shown in Fig. 5-2. The horizontal magnet aperture is determined by the momentum spread at 4.5 GeV; the vertical aperture is set by the transverse emittance at 200 MeV. The majority of the quads are 2 ft long with a 4.8-cm pole-tip radius. In the matched straight sections, a large-aperture doublet is needed at both ends of the long drift space. These quads are 4 ft long and have a 7-cm pole-tip radius.

5.3 Injection and Extraction

It must be possible to inject at 4.5 GeV, to extract at 200 MeV, inject again at 200 MeV and finally to extract at 8.0 GeV. The necessary injection and extraction hardware consists of a low-energy set and a high-energy set. Each set can serve both functions because the directions of the beam circulation in the Precooler are opposite for the deceleration and acceleration processes. Both high-energy and low-energy systems are located in a single dispersion-free drift space. Both systems are horizontal full-aperture kickers and magnetic septa separated by 90° of betatron phase. The 200-MeV kicker is near one end of the



Precooler Layout

Fig. 5-1

- Dipole magnet
- | Quadrupole magnet

20m / inch

ORBIT FUNCTIONS FOR ONE OCTANT OF THE PRECOOLER

Fig. 5-2

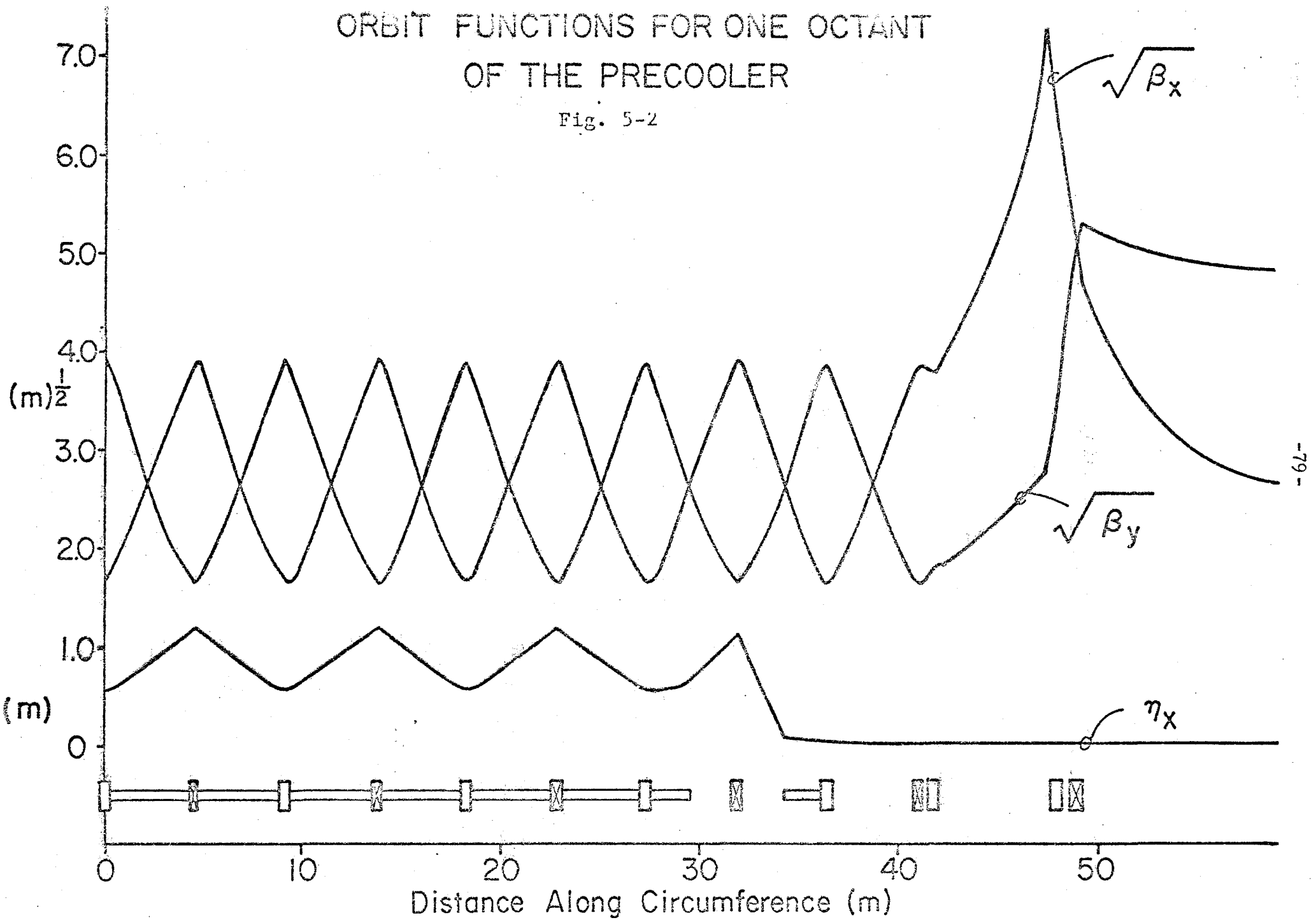


Table 5-I Precooler Parameters

Superperiodicity		4
Long drift sections, dispersion free		
length		20.2 m
number		4
Drift sections, dispersion matching		
length		2.3 m
number		16
Average radius		75.47 m
Betatron tunes		
ν_x		10.7
ν_y		11.7
Phase advance per normal cell		90°
Transition γ		9.63
Revolution period (at 4.5 GeV)		1.6 μ s
Dispersion $\eta = (\Delta t/t)/(\Delta p/p)$ @ 4.5 GeV		0.02
Orbit functions, maximum values		
$\hat{\beta}_x$		53.5 m
$\hat{\beta}_y$		28.1 m
x_p		1.1 m
Lattice structure		
Half cells	DF: QD O B OO B O QF	
	FD: QF O B OO B O QD	
Normal cell	C: DF FD	
Dispersion matching all	CXP: QD O1 B O2 QF O2 B O1 QD	
Half straight sections	SS: QFA O0 QDA QDA O3	
	QFB O4 QDB LL	
Octant	OCT: C C C CXP DF SS	
Ring	RING: 4 (OCT OCT)	
Lattice components		
bending magnet B		
field at 8 GeV		9.35 kG
length		1.52 m
gap height		6.0 cm
gap width between coils		16.0 cm
copper weight (raw material)		200 kg
iron weight (raw material)		1500 kg
number used		128
normal quadrupoles 2QF, 2QD, 2QDA		
gradient at 8 GeV		<160 kG/m
length		.61 m
pole-tip radius		4.8 cm
pole-tip field		<7.8 kG
copper weight (raw material)		100 kg
iron weight (raw material)		1100 kg
number used		80
special matching quads QFB, QDB		
gradient		<137 kG/m
length		.91 m
pole-tip radius		7.0 cm
pole-tip field		<9.6 kG
number used		16

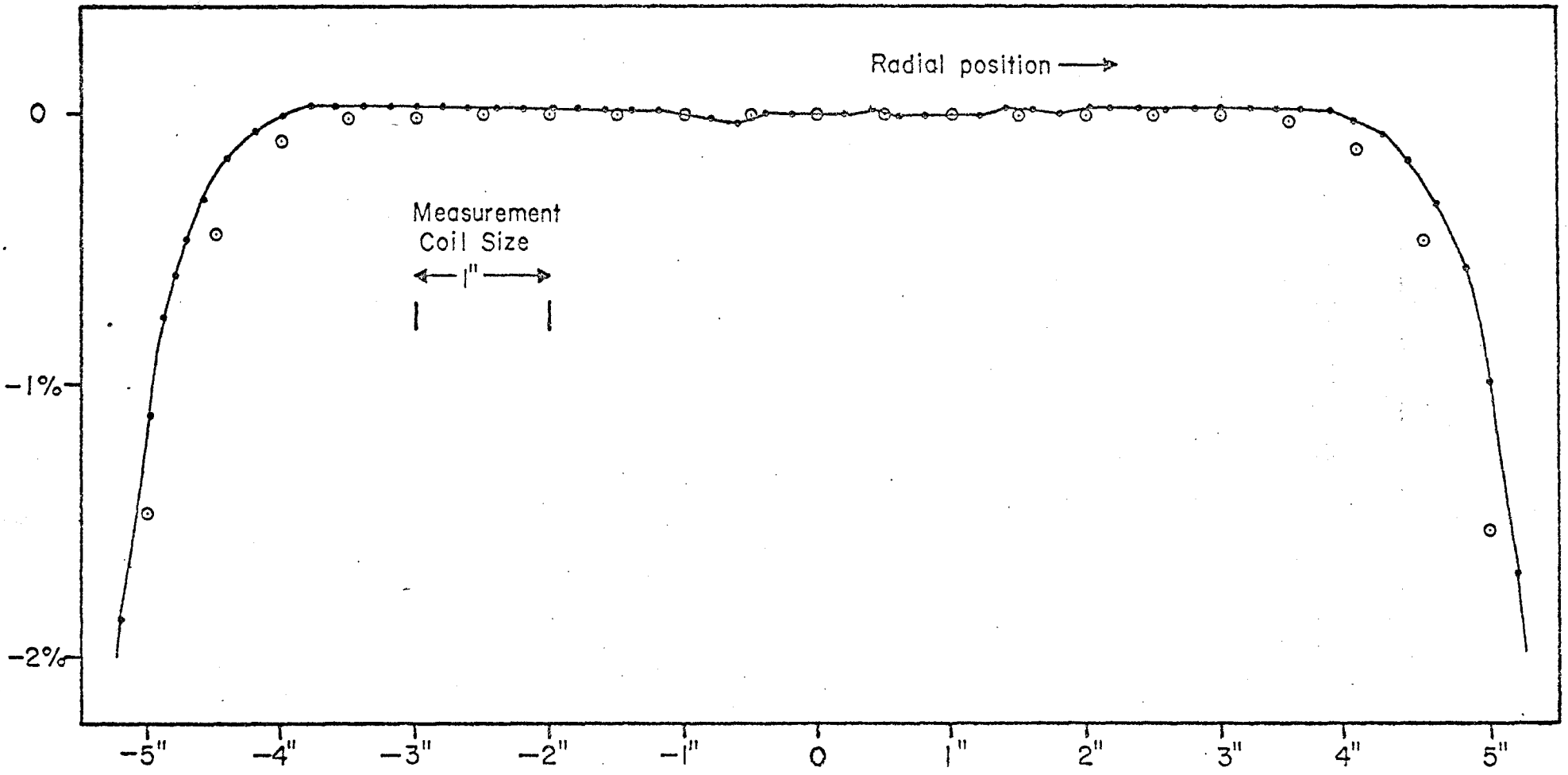
drift space and the septum is close to the other end. The high-energy system has its kicker near the 200 MeV septum. Both systems require rise and fall times of approximately 200 nsec for 90% filling of the ring. The bunch-by-bunch extraction of the 8-GeV beam discussed in Sec. 5.7.2 requires a rise time of approximately 70 nsec. For a horizontal emittance of 10^{-6} m-rad at 8 GeV, a 1.5-m, 200-G kicker will provide the displacement needed to clear a 1-cm magnetic septum. There is adequate space for all these components in the drift space.

We will not discuss the 200-MeV transport between the Precooler and Electron Cooling Ring in any detail. It is a simple, straightforward system.

5.4 Magnet Design

The magnet system designed and constructed for the Fermilab Electron Cooling Experiment Ring has successfully achieved the designed field values and stringent tolerances. Figures 5-3 and 5-4 indicate the measured dipole and quadrupole fields as evidence of their quality.

Although these particular magnets are not suitable for the Precooler, they are an indication of the capability of the design, which has been adapted for the Precooler magnets. The peak dipole field required (8 GeV in the Precooler) is 9.4 kG. A dipole magnet design capable of meeting this and the aperture requirements is shown in cross section in Fig. 5-5. A corresponding quadrupole design is shown in Fig. 5-6. Parameters of the magnets are given in Table 5-I.



Variation of $\int B dl$ in Dipole

- Measured Field in Magnet Center (Magnet 1002)
- ○ ○ Measured Integral (Magnet 1005)

Fig. 5-3 Field quality in Electron Cooling Ring dipole.

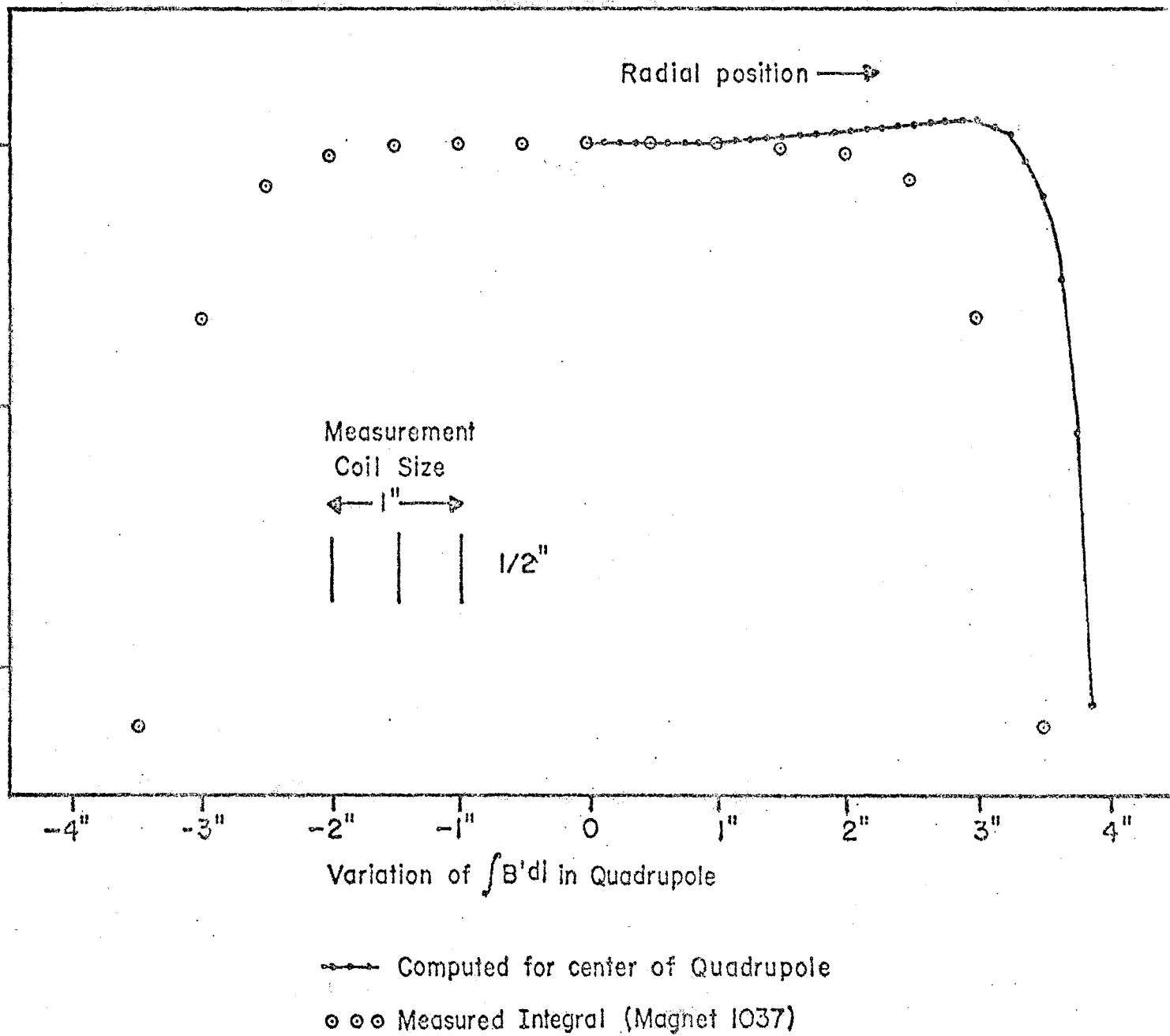


Fig. 5-4 Field quality in Electron Cooling Ring quadrupole.

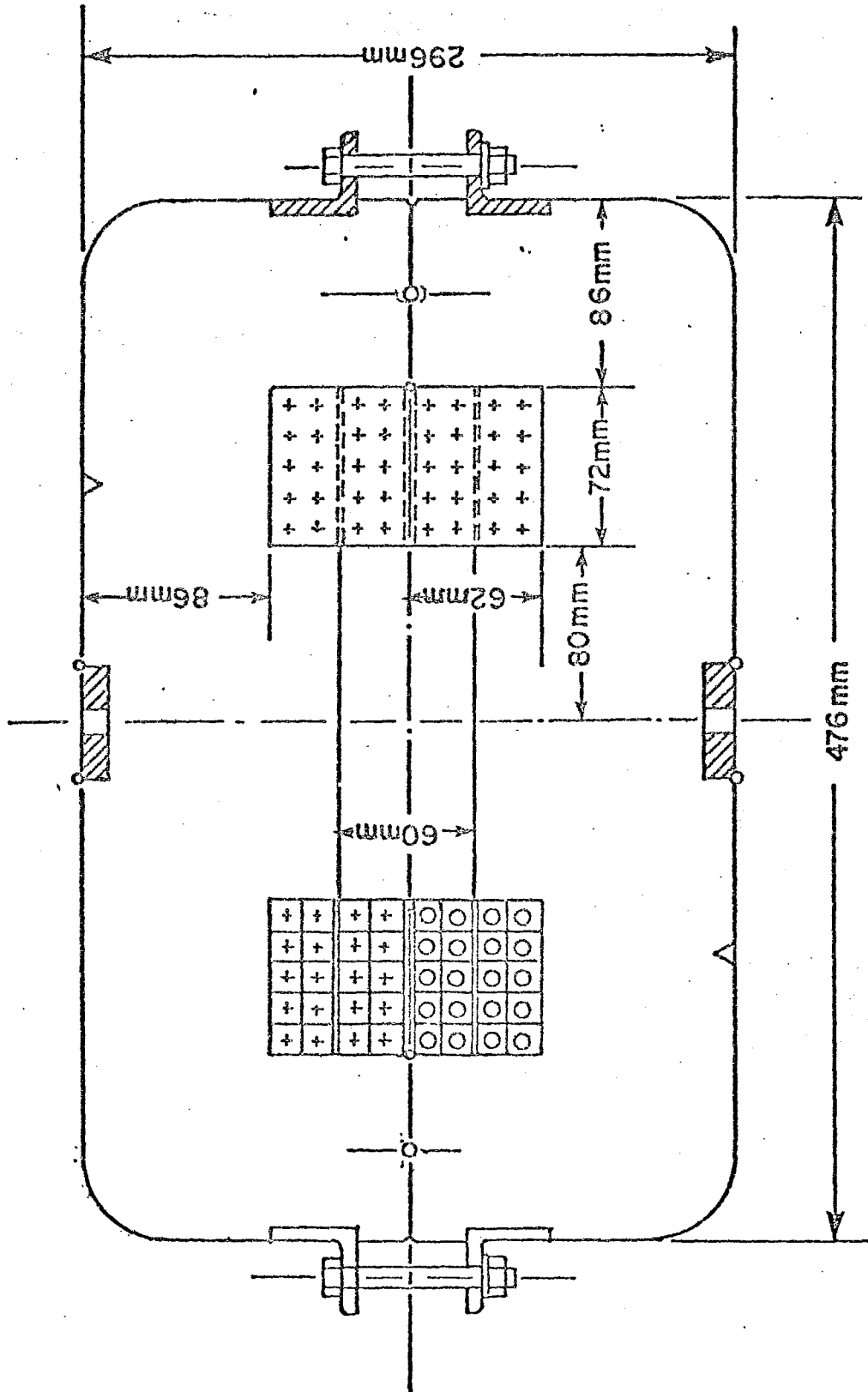


Fig. 5-5 Pre-cooler dipoles.

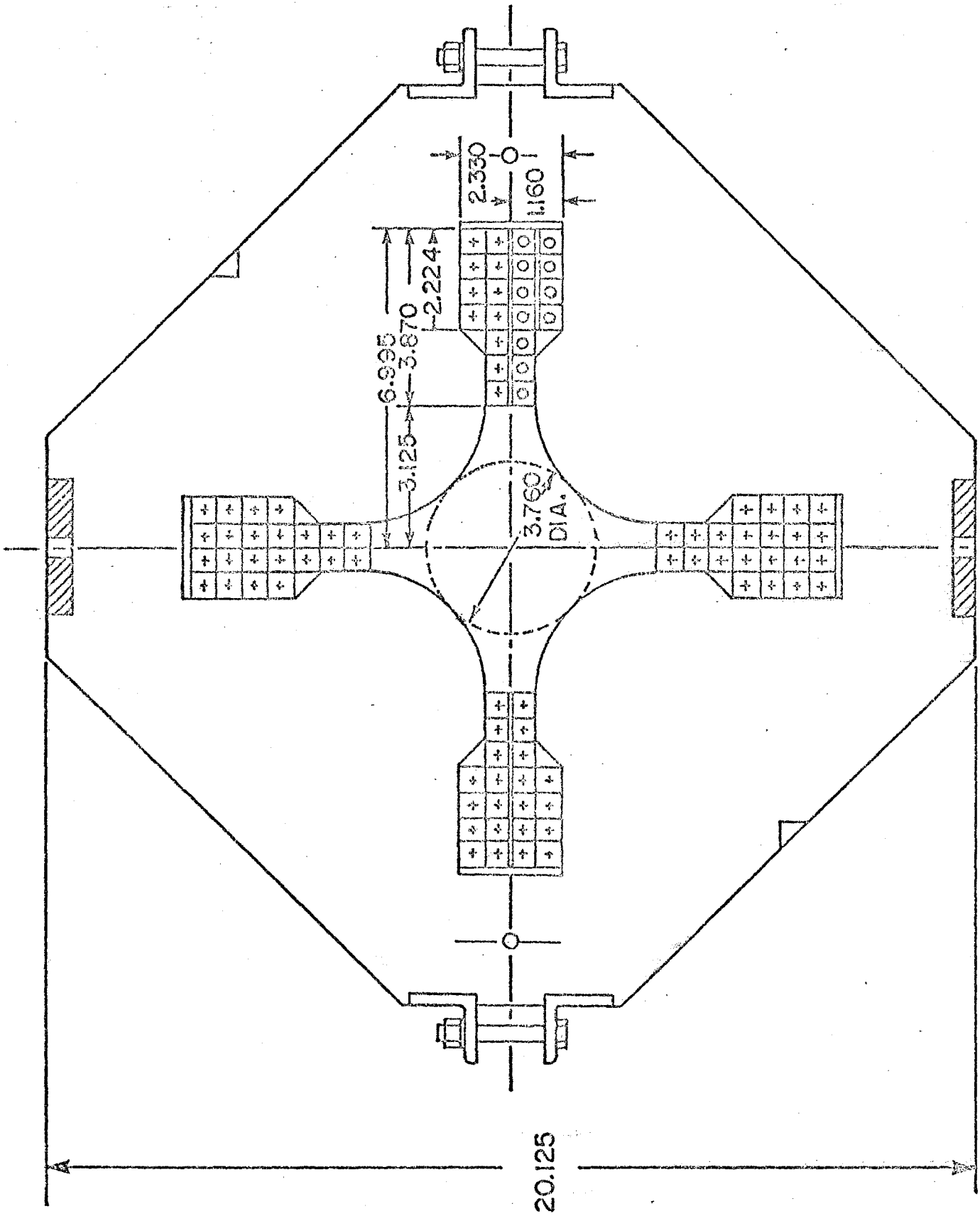


Fig. 5-6 Precooler quadrupole.

5.5 Vacuum System

The Precooler vacuum system design is based on a suitable modification of the existing Electron Cooling Ring system. Because of the magnetic cycle of the bending magnets, distributed ion pumping is not applicable. Thus the design is based on lumped commercial ion pumps in an all-metal, stainless-steel, welded system. Since the suggested average pressure of 2×10^{-9} Torr is higher than in the Electron Cooling Ring (10^{-10} T), pumping and baking requirements are relaxed. Two hundred 60 μ /sec ion pumps distributed around the ring with a nominal spacing of 2 meters will provide sufficient pumping capacity. A bake temperature of 200°C should provide a factor of 20 decrease in pressure (4×10^{-8} Torr unbaked to 2×10^{-9} Torr baked). The chambers are to be standard stainless tubing approximately 5-in. diameter for quadrupole and straight sections. The dipole chambers are rectangular in cross section and welded along the sides.

Basic degreasing followed by a 900°C , 10^{-5} Torr vacuum degas of chamber components is required prior to welding and assembly.

5.6 Controls and Diagnostics

The Precooler will employ normal Fermilab control hardware and software. Consoles employ keyboard and knob control, with an alphanumeric scope and storage scope for graphics. The consoles are serviced by Xerox 530 computers, which communicate with the equipment via Lockheed MAC-16 minicomputers and serial CAMAC. 1-MHz and 10-MHz clocks are synchronized with clocks in the whole facility. As the Fermilab control system is upgraded in the future, this system will also be upgraded.

The Precooler requires both routine and exotic beam-diagnostic equipment. The routine equipment for tuneup can utilize infrequent pulses of protons from the Electron Cooling Ring and can therefore be of low sensitivity. This includes 16 horizontal and 16 vertical position electrodes. Tune measurement can be by these same electrodes, which can also be used to tune out injection steering errors. A fast Q-electrode can be used for measurement of momentum spread, synchrotron frequency and injection phase error. Profile monitors can probably employ residual gas, in view of the modest vacuum requirements of the ring, although atomic jets, similar to the one developed for the Electron Cooling Ring might also be used.

More sophisticated diagnostics are associated with the stochastic cooling system. These diagnostics will be developed along with that system, but it is clear that they will certainly include high-gain wideband position and current probes.

5.7 RF Systems

The requirements for antiproton cooling and deceleration and for later acceleration of the cooled antiproton beams are different enough that separate rf systems have been designed for these two functions.

5.7.1 Precooler Decelerating System. Deceleration in the Precooler will be done at $h = 1$, with a required frequency range of 385-628 kHz. The maximum voltage requirement, 65 kV, occurs at the end of the first deceleration period, where a 67.3 eV-sec beam is barely contained within a 72.9 eV-sec bucket. A higher

upper-frequency requirement is set to accommodate injection into the Electron Cooling Ring at $h = 2$ if necessary. At this point, the system must be capable of generating 15 kV at 716 kHz.

The system can be composed of five separate cells of ferrite rings, each containing 44 rings, 18 cm i.d. \times 45 cm o.d. \times 2.5 cm thickness. An acceleration gap at the center of each cell will be driven push-pull by a pair of 10-kW tubes each capable of delivering an rf voltage swing of ± 7 kV. The total ferrite volume per cell will be 1.47×10^5 cm³ and the ferrite will be operated at an average rf flux level of 250 G (0.025 W/m²). At this flux level at 600 kHz, the dissipation will be about 100 mW/cc or 14.7 kW. The two driver tubes, operating below 50% efficiency, will dissipate another 16 kW, making the total power per cell 30 kW. Each pair of tubes will be driven by a transformer-coupled solid-state driver.

The ferrite rings proposed are produced by TDK and are similar to those presently being tested for the ISABELLE rf accelerating system.

5.7.2 Precooler Acceleration System. We assume that the momentum spread ($\Delta p/p$) of the stacked beam in the Electron Cooling Ring can be maintained at about 10^{-4} . The energy spread is 73 keV and the longitudinal emittance is 0.06 eV-sec. The cooled stacked beam is to be bunched adiabatically at harmonic number 12, 15.032 MHz. The rf period is 66.5 μ sec and if the beam is bunched to a bunch length of 35 μ sec, then a period of 31 μ sec will exist between bunches to allow for kicker rise and fall times. Because of the very small

initial momentum spread, allowance is made for a factor of two emittance blow-up, resulting in an emittance of 0.01 eV-sec per bunch. An rf voltage of about 2 kV will provide the required bunching. This voltage can be provided easily by the surplus PPA rf cavity presently installed in the Electron Cooling Ring.

After bunching the bunches will be extracted individually into stationary buckets in the Precooler ring. The accelerating rf system in the Precooler will operate at harmonic number 21 so the rf frequency at 200 MeV will be 7.516 MHz, exactly half that of the Electron Cooling Ring. In order for the Precooler bucket shape to match the extracted bunches the required rf voltage in the Precooler will be 12.3 kV. The Precooler stationary bucket area at this voltage will be 0.076 eV-sec and the bucket to bunch area ratio is 7.6. Acceleration to 8 GeV in 5 seconds requires an initial accelerating voltage of 4.36 kV per turn, which can be generated by a synchronous phase angle of 25.8° . If the beam is moved to this phase angle without increasing the rf voltage, the bucket area is reduced to 0.027 eV-sec and the beam will occupy about 37% of the bucket area. As the beam is accelerated, the rf voltage requirements will diminish, so the 10 to 15 kV required at the beginning of acceleration will be the maximum requirement anywhere. During the subsequent acceleration to 8 GeV, the Precooler frequency must be increased from 7.516 MHz to 13.193 MHz. The modest rf voltage requirement and frequency range are very well matched to the capabilities of a second existing surplus PPA rf cavity.

The Precooler harmonic number, 21, is an integral factor of the Main-Ring harmonic number, $1113 = (21 \times 53)$, so that the

Precooler frequency can be phase-locked to the Main-Ring injection frequency at 8 GeV. The Main-Ring frequency is precisely four times the Precooler frequency, so that the center of every fourth Main-Ring bucket can be made to overlap a Precooler bucket. If an additional factor of three longitudinal emittance blowup occurs during acceleration, so that each bunch has phase area 0.03 eV-sec, operation of the Precooler at 10 kV will result in a bunch length of 3.4 nsec. Bunches of this shape are well matched to stationary Main-Ring buckets with area 0.65 eV-sec. The required Main-Ring buckets are generated with a ring voltage of 1.2 MV, which is the normal injection voltage.

After appropriate bunching and phase-locking, bunches will be extracted from the Precooler and placed in the Main-Ring buckets at the desired locations. One Precooler acceleration cycle will be required for each of the twelve p bunches.

6. ACCELERATION AND STORAGE IN THE MAIN RING AND SUPERCONDUCTING RING

6.1. Bunch Reconfiguration in the Main Ring

In order to achieve the desired luminosity with antiproton-proton colliding beams, it is necessary to rebunch the proton beam in the Main Ring to approximately 12 bunches, concentrating more protons per bunch.

The plan is to debunch the beam from the usual harmonic $h = 1113$ by reducing the rf voltage adiabatically, then turning on a low-harmonic cavity to relocate bunches in phase space. After one-fourth of a phase oscillation, the bunches will have roughly clustered in phase at the lower harmonic, with an increase in total energy spread. The bunches are then recaptured in $h = 1113$ buckets by turning on the ordinary rf system.

Recent storage studies in the Main Ring have indicated, at an intensity of 2×10^{13} protons in approximately 1066 of the 1113 buckets, some 90% of the beam is contained within bunches 3 nsec long and appear to be matched to stationary buckets of 1.25 MV/turn. This corresponds to a bunch length $\Delta\phi$ of 0.5 radians and a bunch area of 0.19 eV-sec per bucket.

If the rf voltage is reduced until the bucket area has shrunk to the bunch area, then turned off, dilution by a factor $\pi/2$ will occur, so that the debunched emittance will be 0.3 eV-sec per bunch, corresponding to an energy spread of ± 7.8 MeV or a phase-space density of 5.7×10^{10} protons/eV-sec. In order to create bunches containing 10^{11} protons, a charge bunch occupying area 1.75 eV-sec must be captured. To compensate for losses in extraction, injection, and acceleration, we take this area to be 2 eV-sec.

The voltage to create a 150-GeV, 2-eV-sec bucket at $h = 1113$ is 226 kV, so that recapture will create no problems. The maximum energy spread corresponding to a 2-eV-sec bucket is ± 83 MeV, well within the observed useful momentum aperture at 150 GeV.

The low-harmonic cavity should keep the center of charge stationary with respect to $h = 1113$ buckets while rotating a set of bunches. Its harmonic number must therefore be a factor of 1113. Consider, for example, $h = 21$, corresponding to a frequency of 1.0019 MHz. This bucket covers the azimuthal region occupied by 53 bunches. Approximately 26 bunches can be rotated into a vertical strip 19 nsec long using a voltage of 12.7 kV. The synchrotron period is 0.6 sec, so rotation will require 150 msec.

If the same exercise is carried out at $h = 53$, $f = 2.53$ MHz, each bucket will encompass 21 of the original bunches. The required voltage is 32 kV, a little high. The problem of aligning the $h = 1113$ bunches vertically in this phase space also appears to be more difficult than at $h = 21$, because of synchrotron tune spread, so the $h = 53$ option looks less favorable.

There are some questions as to how beam lifetime, instability, and emittance growth are affected in such an operating mode. CERN has recently reported¹ successful operation of the SPS at densities of 10^{11} /bunch, and instability was indeed noted. It may be necessary to include a high-frequency Landau-cavity system to maintain stability of such bunches.

Following this bunch reconfiguration the beam will be transferred to the superconducting ring in the normal direction.

7. SHIELDING AND CONVENTIONAL FACILITIES

7.1 Shielding

There are two points along the sequence of the antiproton source that determine the shielding. The largest possible losses will occur either in the initial production of antiprotons in the Target Vault or in the acceleration of the accumulated antiproton beam to 8 GeV in the Precooler.

7.1.1 Target Vault. The production target is somewhat like the target areas in Fermilab external beams and will be shielded like them. The beam and target are 18 ft below grade. Components in the Target Vault will be radiation-hardened and provision will be made for removal of defective components by means of removable steel shielding. Estimates using a cascade Monte Carlo program, indicate that π^- and K^- are produced in the target in the broad momentum and angular range of interest at a ratio of 200 to 1 compared with the desired antiprotons. The negative secondaries not in the desired longitudinal and transverse phase-space interval will be selected out in the antiproton transport line to the Precooler (Sec. 3.9) and collimation will be provided to absorb the separated particles.

The π 's and K's in the desired phase space will be injected into the Precooler together with the antiprotons and will decay while circulating. Approximately 90% of these particles are pions, which decay into leptons that do not interact strongly. The kaons are only 10% of the total and their decay products are at lower energy, so the shielding provided for 8-GeV antiprotons will be ample.

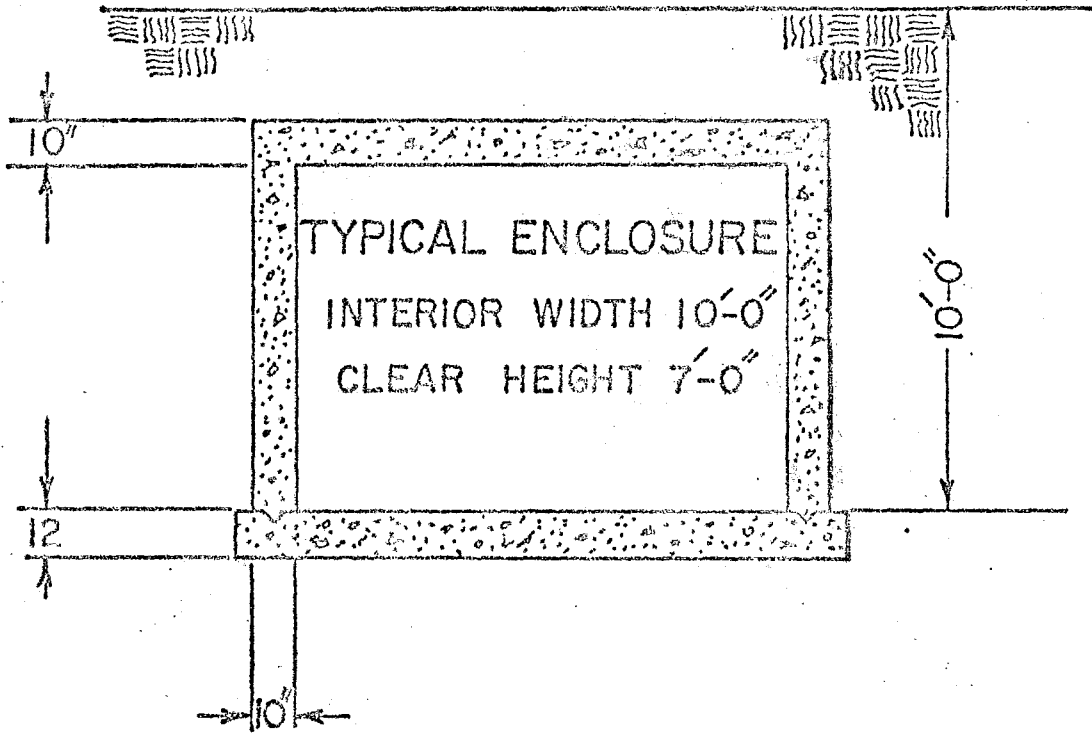
7.1.2 Precooler Ring. The circulating intensity of the accumulated 8 GeV beam of 10^{11} antiprotons in the Precooler is an order of magnitude less than the circulating proton intensity in the Booster. In addition, the average rate is much lower, because the Precooler has the beam only once in 5 hrs, rather than 15 times per second, as in the Booster. Shielding of 1 ft of concrete plus 2 ft of earth, compared with 5 ft in the Booster, is adequate for distributed losses. A rough simulation shows that it is also adequate for loss in a single magnet. The simulation gives an integrated dose of 20 mrem at the surface if 10^{11} antiprotons are lost in a single magnet.

7.2 Conventional Facilities

Antiproton Hall and the Target Vault were discussed in Sec. 3.3. Here we confine our discussion to the Precooler buildings.

7.2.1 Tunnel. A tunnel section is shown in Fig. 7-1. A clear space of 10 ft horizontally and 7 ft vertically is planned. Beam center line will be 3 ft above floor level and 18 in. in from the outer-radius wall. It is expected that the tunnel will be made of precast sections on a slab, a form that Fermilab has used successfully in several recent applications. Reinforcing will be supplied where Kautz Road is to be rebuilt over the tunnel. Ventilation will be provided by fans.

7.2.2 Service Buildings. At the north, west, and south long straight sections, there will be 200 sq. ft service buildings at grade level with penetrations for electronic cabling. These buildings will be of conventional concrete-block construction,



RING SECTION

Fig. 7-1

with conventional Fermilab coloring. Electrical service will be provided underground.

7.2.3 Main Building. The south long straight section will be covered by a 200 ft by 30 ft building for assembly, installation, injection and extraction. This building will be largely below grade level and reinforced concrete construction is appropriate and economical. Local shielding will be utilized as needed.

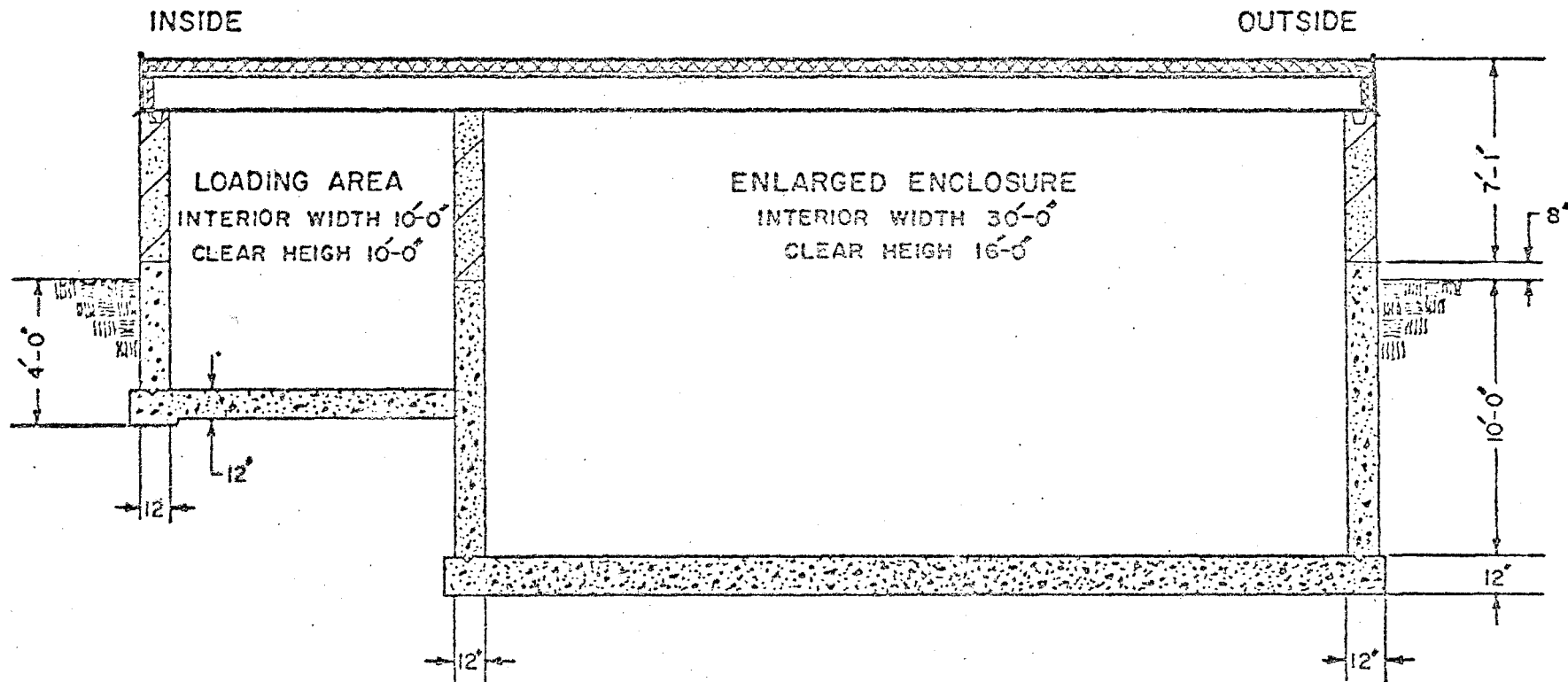
There will be a 10 ft covered loading area running the length of the building at grade level. Power supplies will be located in this area.

These facilities are shown in cross section in Fig. 7-2.

7.2.4 Utilities.

Electrical Service. There is enough spare capacity in the linac electrical system and an empty feeder running through the Booster pond to a point close to the Precooler site. Heating will be electric to avoid bringing gas service to the site.

Cooling Water. There is enough spare capacity in the Central Utility Building and an 8 in. pipeline close to the Precooler site.



MAIN BUILDING SECTION

Fig. 7-2

D. SUPERCONDUCTING ACCELERATOR SYSTEMS

1. ACCELERATION SYSTEM

1.1 Requirements

The first requirement on the system is that it be capable of accelerating a proton beam and an antiproton beam simultaneously. It must also provide enough bucket area to contain this beam. Measurements at 400 GeV and 2.5×10^{13} find a longitudinal emittance of approximately 0.3 eV-s, four times that measured at 8 GeV. We will make the conservative assumption that the beam emittance at 150 GeV, the injection energy, will have this larger value, 0.3 eV-s.

The rf voltage and power requirements for proton acceleration of two possible beam intensities are summarized in Table 1-I.

Table 1-I. RF Requirements for Protons.

Beam intensity	2.5×10^{13}	10^{14}	ppp
Average beam current	0.191	0.765	A
Beam power	0.3	1.2	MW
Ramp slope	75	75	GeV/s
Synchronous voltage	1.58	1.58	MV/turn
Bucket area (150 GeV @ 75 GeV/s)	0.9	0.9	eV-s
Synchronous phase	47	47	deg
Peak rf voltage	2.16	2.16	MV/turn
No. cavities	6	6	
Peak cavity voltage	360	360	kV
Total cavity dissipation/station	64	64	kW
Total power per station	126	290	kW
(Beam/total power)/station	0.4	0.7	

There are also special requirements arising from antiproton acceleration. When the ring is to be used only for unilateral acceleration of protons in either direction, the location and spacing of rf cavities is not dictated by any consideration other than available space. For simultaneous

bilateral acceleration and subsequent storage of protons and antiprotons, however, some restrictions must be imposed upon cavity spacing. By appropriate spacing and phasing of the rf fields in individual cavities, some aspects of bilateral operation can be optimized. The requirements for $\bar{p}p$ operation are:

(i) The rf system must create sufficient bucket area for simultaneous bilateral acceleration and storage of protons and antiprotons. Because the total number and longitudinal emittance of protons and antiprotons will almost certainly be quite different, the required bucket areas will not necessarily be the same.

(ii) The rf system should provide the capability for moving the bunch collision point azimuthally over some reasonable range (of order 20 m).

(iii) The system may be required to allow for independent control of the phase and amplitude (bucket location and size) of the proton and anti-proton buckets.

If requirement (iii) is satisfied, then (ii) is automatically, but it is possible that (ii) may be satisfied in a system that does not meet (iii).

1.2 Cavity Spacing

It is necessary to consider cavity spacing in order to satisfy the requirements listed above for bilateral acceleration. The basic unit is two adjacent cavities placed such that their effective gaps are $3\lambda/4$ apart, where λ is the rf wavelength. A particle moving downstream arrives at the second gap at a time phase $3\pi/2$ radians later than its arrival at the upstream gap.

If the downstream-cavity gap voltage leads the upstream voltage by $\pi/2$, a particle moving downstream will see the gap voltages exactly in phase (modulo 2π), and consequently the two cavities provide maximum voltage and bucket area for such a particle. But a particle moving upstream will see the gap voltages exactly out of phase and, if the gap voltages are equal, will see no net voltage. An additional similarly spaced doublet, with opposite relative phasing, can be placed arbitrarily close to the first pair. There is good reason to space the gaps of the nearest neighbors of adjacent doublets $\lambda/2$ so a pair of doublets (four cavities) will occupy a space of approximately 2.5λ . All three requirements above can be satisfied through the use of such doublets. Upstream and downstream doublets can be driven from separate rf sources and operated at different amplitudes and phases.

As an example, Fig. 1-1 shows three doublets, the two outside doublets providing proton bucket area while the center doublet provides antiproton bucket area. A simple fanout system is shown to demonstrate that the required phasing can be accomplished using easily available components, quadrature hybrid junctions and π radian splitters. In the array shown, with all gap voltages equal, the proton bucket area will be larger than the antiproton area by a factor 1.414 during beam storage. During acceleration, the bucket-area difference will be slightly larger because the antiprotons will require a larger synchronous phase angle because less voltage is available and consequently the moving-bucket factor reduction will be larger.

The cavity spacing described is essentially a series of cavities (1, 4, and 5) with their gaps spaced an integral number of half-wavelengths apart and another group (2, 3, and 6) with the same relative spacing but all

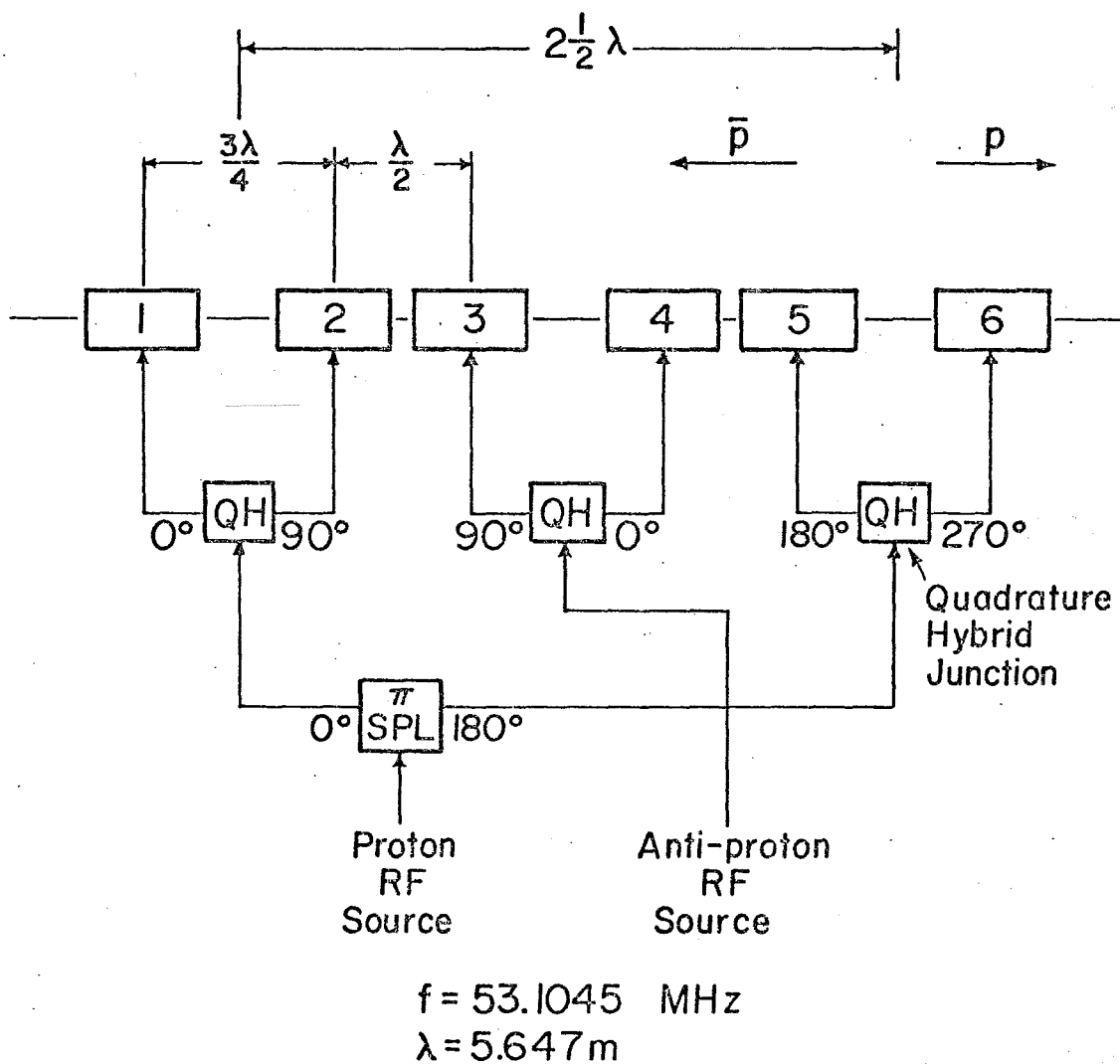


Fig. 1-1. RF cavity spacing and phasing for orthogonal \bar{p} p control.

displaced by $\lambda/4$. Such an array of cavities can be phased in a slightly different manner to provide a greater total bilateral bucket area if requirement (iii) is relinquished. Such a phasing scheme is shown in Fig. 1-2. The proton and antiproton bucket areas are equal and each effective voltage is $0.707 V_{tot}$.

With the phasing shown in Fig. 1-2, the intersection point is $\lambda/8$ to the left of the midpoint of the array. If the voltages of cavities 2, 3, and 6 are reduced to zero, the intersection point will move to the midpoint of the array, with a slight reduction in bucket area, and if cavities 2, 3, and 6 are raised to maximum voltage with opposite phase, the intersection point will move to a point $\lambda/8$ to the right of the midpoint.

It is possible that the phasing of Fig. 1-2 could be used during acceleration and the phasing switched to the phasing of Fig. 1-1 to provide orthogonal control after storage energy is reached. Because of the quite different geometry of the two fan-out systems, this phase switching would be difficult and would require great care to avoid phase-space dilution or loss of particles.

1.3 System Design

A frequency of 53 MHz, the same as the Main Ring, is chosen in order to:

- (i) give high-efficiency transfer of beam from the Main Ring by means of a synchronous bucket-to-bucket scheme;
- (ii) minimize the rf voltage;
- (iii) take advantage of an existing 160-kW power amplifier at this frequency;

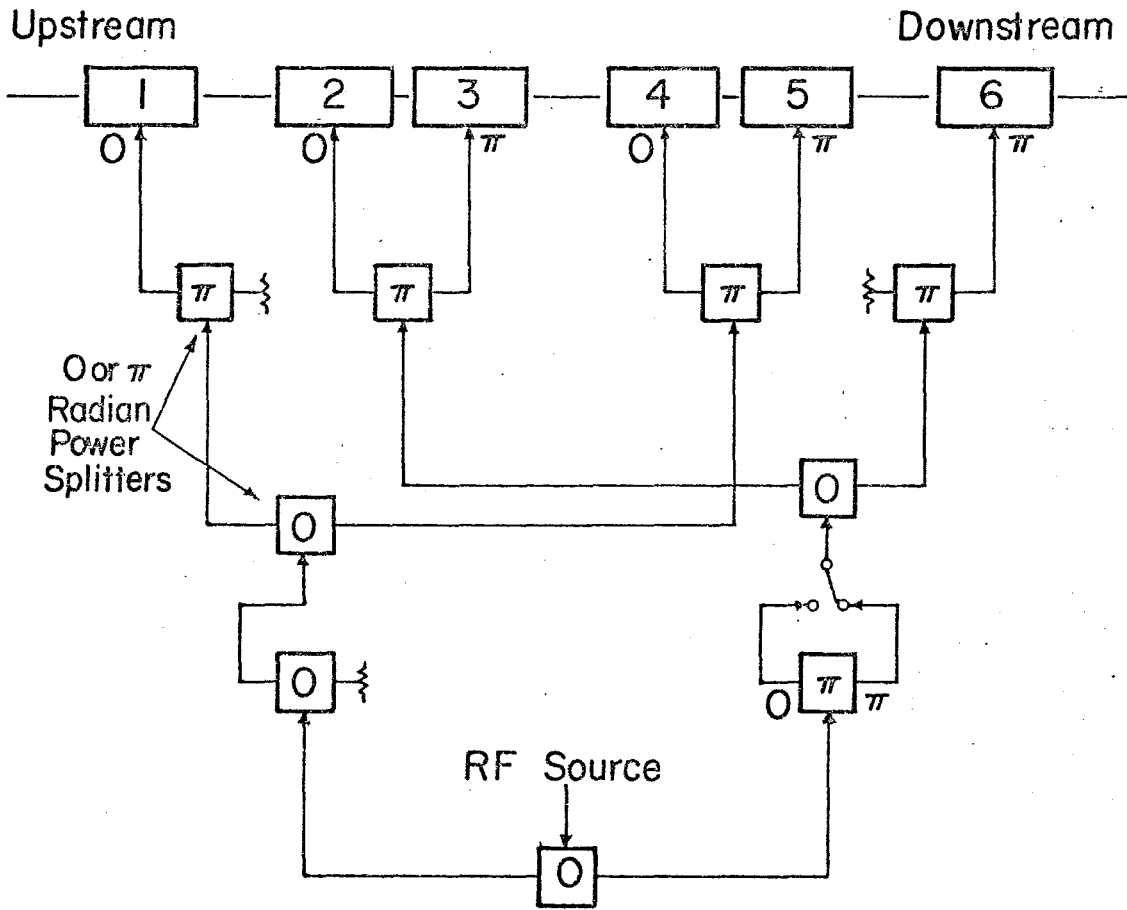


Fig. 1-2. RF cavity spacing and phasing without orthogonal $\bar{p}p$ control.

(iv) have the Main Ring and superconducting ring beams collide in the simplest possible way.

In order to utilize existing facilities and to utilize straight-section space efficiently, it is highly desirable to locate the system in straight-section F. A layout of the six cavities in the straight section is shown in Fig. 1-3. Recent development work has upgraded the voltage and power levels of Main-Ring rf stations. If additional space is needed for the new system, some Main-Ring cavities can be removed without injury to present performance.

The rf power amplifiers will be located in a new ground-level equipment building (65 ft x 28 ft) located directly above the F0 straight section. RF power will be delivered to the cavities by a $3\lambda/2$ long 9-in. coaxial transmission line connecting the equipment room and tunnel. Locating the power amplifiers upstairs has several advantages: less space is required in the tunnel, all the active electronics is directly accessible for repair, and radiation exposure to personnel is reduced. Radiation leakage through the transmission-line penetration should be small.

1.4 RF Station Components

A cross section of an rf station is shown in Fig. 1-4. The components are described below.

1.4.1 Power amplifier. The 160-kW modified Main-Ring power amplifier (PA) is capable of powering a superconducting-ring cavity at levels appropriate for intensities of 2.5×10^{13} ppp (see Table 1-I, column 1) with sufficient power to compensate satisfactorily for beam loading. Above

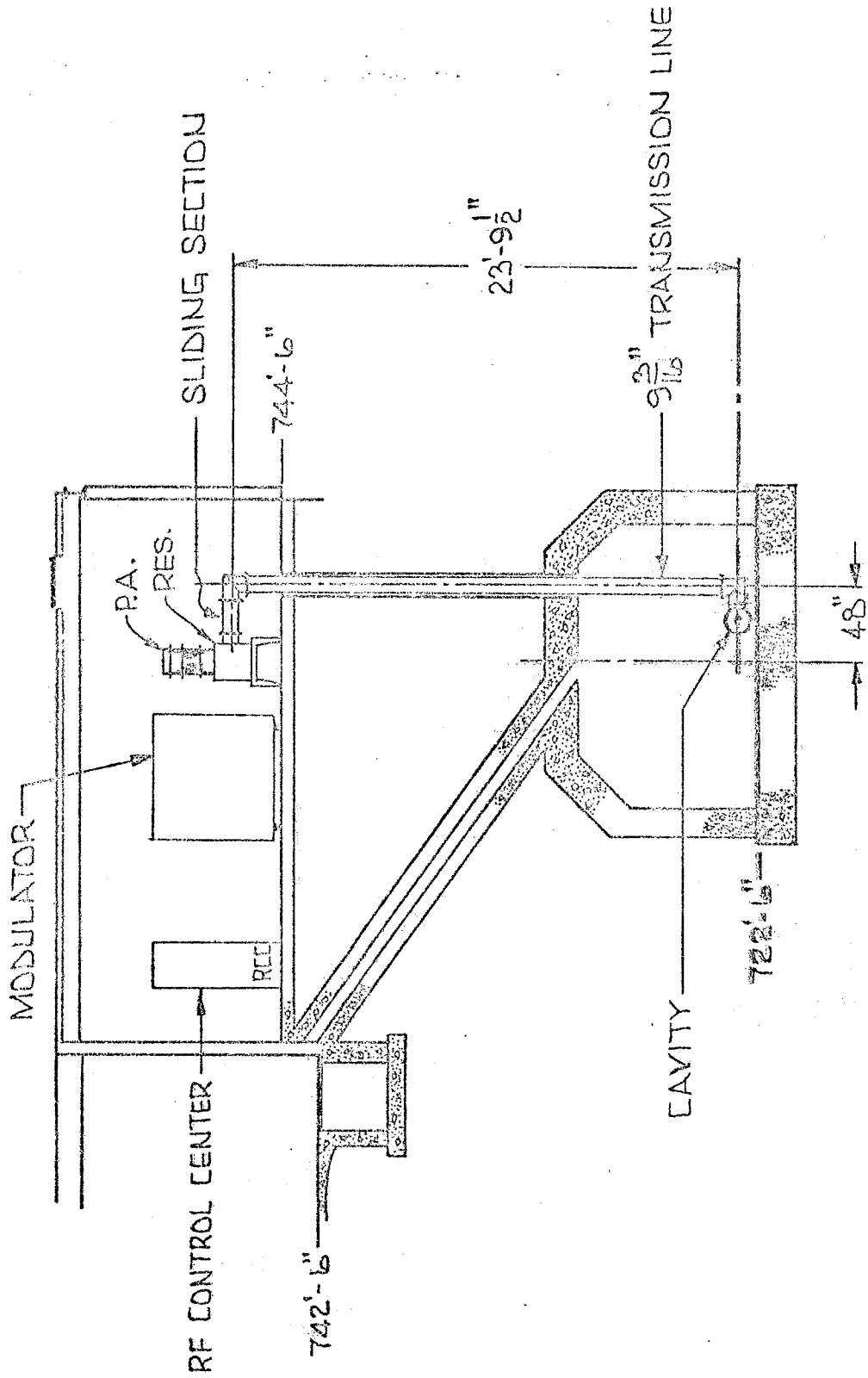


Fig. 1-4. RF station cross section.

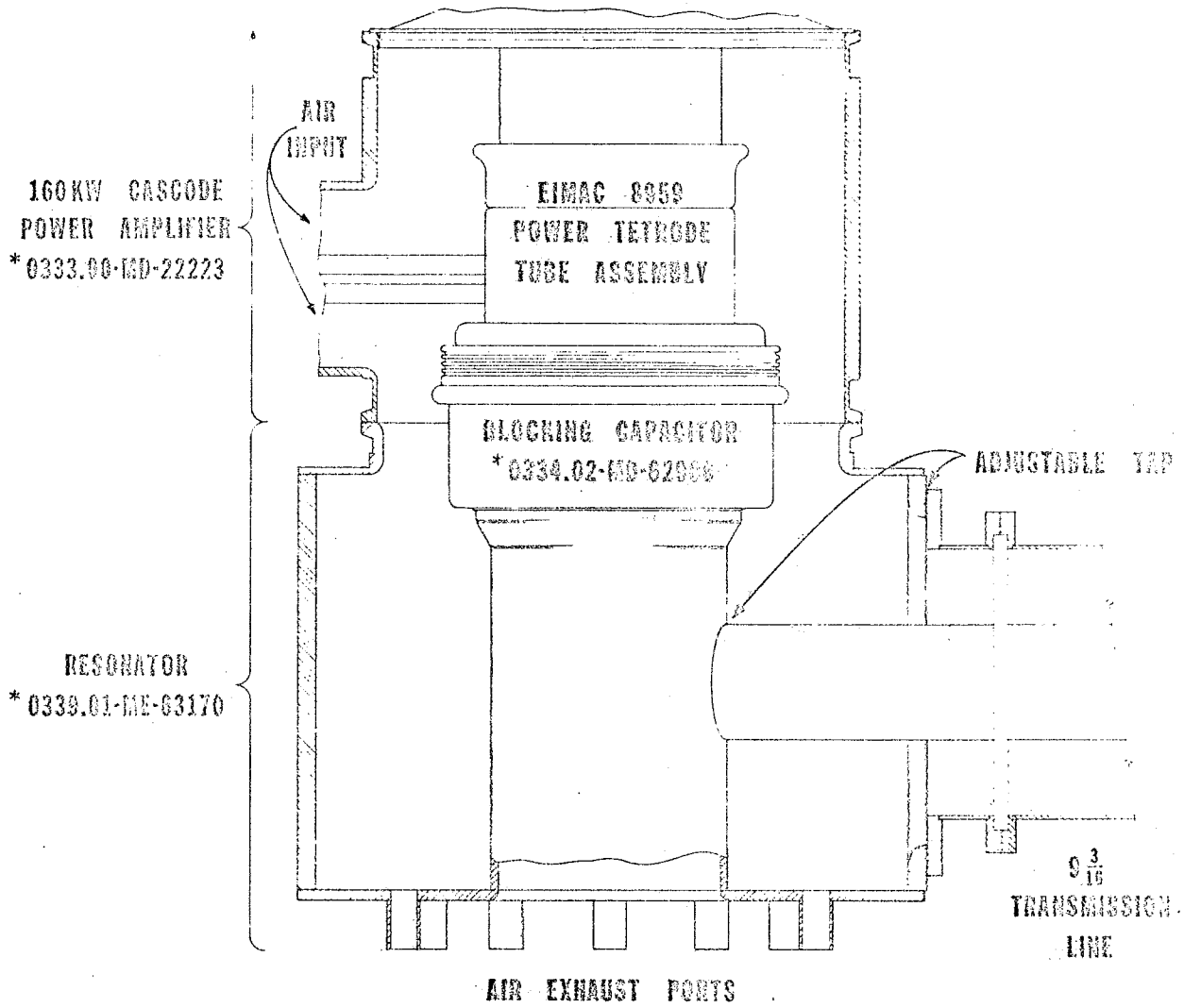
intensities of 2.5×10^{13} ppp, it will be necessary to consider additional rf power for both real and reactive beam loading, for example, two PA's per system or a single higher-power PA. Furthermore, by the time beam intensity necessitates increased power requirements, a new PA design could be available. The parameters in column 2 of Table 1-I (10^{14} ppp) can be met with higher-power amplifiers plus fast beam-loading feedback.

1.4.2 Resonator. A tunable resonator is used to match the PA output impedance into a $50\text{-}\Omega$ transmission line. A newly designed blocking capacitor of the type used in the Fermilab Booster will be used to couple the PA into the resonator. Figure 1-5 shows a cross-section view of the PA, resonator, and impedance-matching tap arrangement.

A prototype resonator has been constructed for testing the 160-kW PA. A means of automatic tuning of the resonator over a frequency range of a few kHz will be worked out to adapt the test resonator to the rf system. Power is coupled out of the resonator into a $3\lambda/2$ transmission line.

1.4.3 Transmission line. The coaxial line will be 9-3/16-in. rigid $50\text{-}\Omega$ line with Rexolite insulators. The average power rating of 9-3/16 in. rigid line at 53 MHz is 600 kW. This average rating is based on an allowable temperature rise (above 40°C ambient) of 23°C for the outer conductor and 62°C for the inner conductor. The maximum peak power for the line is 5.8 MW, which corresponds to a 24-kV peak.

The transmission line will be fixed at the cavity end and have a sliding section at the resonator end. The sliding section will be used to adjust line length.



* REFERS TO FINAL DRAWING NUMBER

Fig. 1-5. RF power amplifier and resonator.

1.4.4 Modulators. Statements about the modulator suitability require some knowledge of the exact rf program intended. The Main-Ring modulators are presently being modified to operate at 30-kV output for operation with the modified cavities. They are capable of a regulated output current of 10 A as presently designed.

At 2.5×10^{13} intensity, the required PA power is 126 kW, with 57% efficiency. The power required from the modulator at (28 kV dc) is therefore 221 kW. The modulator current is 7.75 A, which, with a 5-kV series-tube drop, results in a modulator series-tube power dissipation of 38.8 kW. When power is being delivered to the beam, the rf voltage will remain high, so we will keep the series tube voltage drop near 5 kV. Present modulators are a good match to the 160-kW PA at 2.5×10^{13} ppp. During flat-top, there is no real beam power, but there are reactive beam load and cavity power to be considered. Maximum dissipation occurs when the modulator output is approximately 16.5 kV. By careful programming of the voltage drop across the series tube, we can use the 15 A capability of the series tube.

Main-Ring rf modulators will be used initially as designed and later with modifications to deliver 15 A as beam intensity increases. To achieve 1×10^{14} ppp, a new modulator design will be required. One modulator will then be used to supply plate voltage to a higher-power PA.

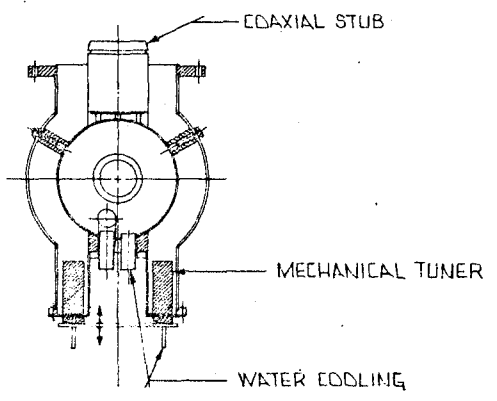
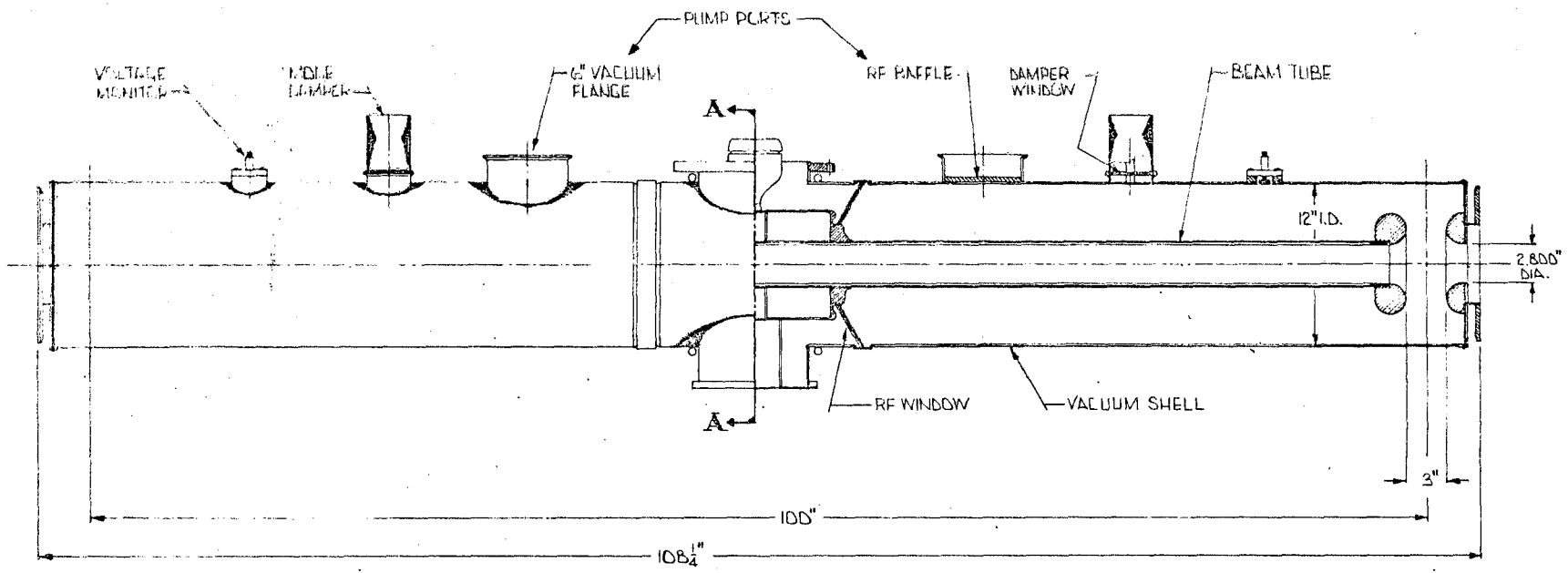
1.4.5 Anode power supplies. Presently two anode power supplies across the road from the F0 RF Building supply dc voltage for Main-Ring modulators. These power supplies are each rated for 33 kV at 48 A average dc load. A series 20- Ω resistor is installed in the dc output of the supply to prevent overstressing the power transformer during crowbar operation.

If we run rf stations with two modulators on each anode supply, the resulting 30-A load current is well below the average rating of the supply. This assumes that we accelerate in the Main Ring only during the fall of the superconducting field. For a cycle requiring acceleration in the Main Ring during superconducting acceleration or flat-top, as will be required for any colliding-beam mode, additional anode power-supply capability will be necessary for intensities greater than 2.5×10^{13} .

1.5 Cavity Design and Operation

1.5.1 Electrical design parameters. The cavity, shown in Fig. 1-6, is a coaxial resonator, 12 in. in diameter and 108-1/4 in. long, formed of copper 102 with ceramic rf windows. The characteristic impedance Z_0 is approximately 70Ω over most of its length, purposely lowered in the center section, and modified at each end by corona rings. Because the required frequency range Δf is a maximum of 2.271 kHz, the cavity is designed as a fixed-tuned two-gap structure of length $l \approx \beta\lambda/2$. The drift tube is actually 160° long electrically rather than 180° , so that $V_{\text{effective}} = V_{\text{gap}} \sin(160^\circ/2) = 0.985 V_{\text{gap}}$ is slightly less than the maximum achievable. The cavities' resultant mechanical length permits mounting them end-to-end at 180° electrical spacing if desirable.

The 160° drift tube is supported by ceramic rf windows and is capped by corona rings dimensioned to minimize the corona-ring gradient. At 200-kV peak gap voltage, the rf gradient is approximately 70 kV/cm. The corona-ring capacitance somewhat increases the skin loss. This design results in the parameters in Table 1-II.



SECTION A-A

FOR FURTHER DETAIL SEE FINAL DRAWINGS

- BEAM TUBE ASSEMBLY ----- 1734.02-ME-63224
- VACUUM SHELL ASSEMBLY---- 1734.02-ME-63225
- CENTER SECTION----- 1734.02-ME-63252

Fig. 1-6. RF cavity.

Table 1-II. RF Cavity Parameters.

Parameter	Unloaded Cavity	Cavity w/Beam Load (2.5×10^{13} ppp)	
Peak voltage	360	360	kV
Frequency	53	53	MHz
Z_0	70	70	Ω
Q	6,500	3,650	
Shunt impedance	1	0.56	M Ω
Time constant	39	22	μ s
RF power required	64	114	kW
0.707 bandwidth	8	14	kHz
Stored energy	1.2	1.2	J

RF power is applied near the center of the cavity at a point tapped down on the drift tube where the 50- Ω drive line is impedance-matched at full load. At less than full load, the $3\lambda/2$ line will operate at the same rf voltage at the voltage maxima as with full load, but instead of operating as a flat line, will contain voltage minima. This scheme was chosen to minimize the possibility of line sparking. There will be spark-protection circuitry that interrupts rf drive and anode supply voltage for either cavity, coax line, or PA sparking.

It is expected that the cooling and spark protection will allow operation at 360-kV peak accelerating voltage per cavity (180-kV peak per gap).

Damping of obnoxious modes will be accomplished by resistors coupled through the side walls of the resonator, comparable to what has been successfully done on the present Main-Ring cavities.¹ At 1×10^{14} ppp, we will need the "stunbox," which sends an antipulse through the PA to arrive at the cavity synchronously with the beam-loading perturbation.² This feed-forward technique is available to us in principle at any time, but we will have to construct additional low-level hardware for its implementation.

1.5.2 Mechanical design. The mechanical design is sketched in Fig. 1-6. The drift tube is cooled by internally circulating water; this cooling is necessary to minimize thermal detuning. The outer copper tank is also water-cooled and temperature-stabilized.

The rf windows are 99% Al_2O_3 ceramic cones, metallized and brazed to OFHC copper rings that are in turn heliarc-welded to the copper inner and outer coaxial conductors. Thus, the entire cavity structure is vacuum-tight with no organic vacuum seals and is completely bakeable to 250°C if needed in order to lower initial outgassing rates.

1.6 Bunch Reconfiguration in the Main Ring

For antiproton-proton colliding beams, it is necessary to rebunch the beam in the Main Ring to approximately 12 bunches, in order to concentrate more protons per bunch to increase luminosity.

The plan is to debunch the beam from the usual harmonic $h = 1113$ by reducing the rf voltage adiabatically, then turning on a low-harmonic cavity to relocate bunches in phase space. After one-fourth of a phase oscillation, the bunches will have roughly clustered in phase at the lower harmonic, with an increase in total energy spread. The bunches are then recaptured in $h = 1113$ buckets by turning on the ordinary rf system.

Recent storage studies in the Main Ring have indicated, at an intensity of 2×10^{13} protons in approximately 1066 of the 1113 buckets, some 90% of the beam is contained within bunches 3 ns long and appear to be matched to stationary buckets of 1.25 MV/turn. This corresponds to a bunch length $\Delta\phi$ of 0.5 radians and a bunch area of 0.19 eV-s per bucket.

If the rf voltage is reduced until the bucket area has shrunk to the bunch area, then turned off, dilution by a factor $\pi/2$ will occur, so that the debunched emittance will be 0.3 eV-s per bunch, corresponding to an energy spread of ± 7.8 MeV or a phase-space density of 5.7×10^{10} protons/eV-s. In order to create bunches containing 10^{11} protons, a charge bunch occupying area 1.75 eV-s must be captured. To compensate for losses in extraction, injection, and acceleration, we take this area to be 2 eV-s.

The voltage to create a 150-GeV 2-eV-s bucket at $h = 1113$ is 226 kV, so that recapture will create no problems. The maximum energy spread corresponding to a 2-eV-s bucket is ± 83 MeV, well within the observed useful momentum aperture at 150 GeV.

The low-harmonic cavity should keep the center of charge stationary with respect to $h = 1113$ buckets while rotating a set of bunches. Its harmonic number must therefore be a factor of 1113. Consider, for example, $h = 21$, corresponding to a frequency of 1.0049 MHz. This bucket covers the azimuthal region occupied by 53 bunches. Approximately 26 bunches can be rotated into a vertical strip 19 ns long using a voltage of 12.7 kV. The synchrotron period is 0.6 s, so rotation will require 150 ms.

If the same exercise is carried out at $h = 53$, $f = 2.53$ MHz, each bucket will encompass 21 of the original bunches. The required voltage is 32 kV, a little high. The problem of aligning the $h = 1113$ bunches vertically in this phase space also appears to be more difficult than at $h = 21$, because of synchrotron tune spread, so the $h = 53$ option looks less favorable.

The question of whether the Main-Ring beam can be debunched at 150 GeV without instability has been investigated in a recent storage study.

Main-Ring beam was debunched at 100 GeV in a manner close to that described above and was observed to have a beam-storage lifetime consistent with that observed for bunched beam. Attempts to measure the momentum spread of the debunched beam by Schottky-scan techniques were not successful, due possibly to insufficient detector sensitivity or magnet ripple. Further attempts to make such measurements are planned.

Actual study and verification of the parameters described above cannot be accomplished at present, because we do not have an rf cavity of sufficiently large voltage that can operate in the Main Ring below 5 MHz. Reconfiguration studies at frequencies that are not integral sub-harmonics of 1113 are nevertheless useful and should be pursued. To this end, a surplus low-frequency cavity from the PPA accelerator has been installed in the Main Ring and various bunch-reconfiguration experiments will be done in coming months to clarify the precise requirements.

The antiproton beam is expected to consist of 12 bunches of 2-ns width, each containing 10^{10} antiprotons with a bunch area of 0.08 eV-s. This will require a stationary bucket of 3.6 eV-s and a voltage of 120 kV/turn at 1000 GeV.

References

- ¹Q. A. Kerns and H. W. Miller, IEEE Trans. Nucl. Sci. NS-24, 1704 (1977).
- ²Q. A. Kerns, Proton-Proton Colliding-Beam Storage Rings for the National Accelerator Laboratory (unpublished).

2. REFRIGERATION

2.1 Description of the Refrigeration System

Refrigeration is provided by a central plant (the CHL) with nitrogen and helium liquefiers and 24 satellite refrigerators in service buildings. This arrangement combines advantages of a single central facility with those of individual stand-alone units stationed around the ring. The central liquefiers have the high efficiency associated with large components, but requirements for distribution of cryogenic liquids and electric power to the service buildings are reduced. The likelihood of continued operation in the event of equipment failure is also significantly improved.

The total power to run the system is 14.33 MW. This provides 2,550 ℓ /h of liquid nitrogen, which in turn is used in the liquefaction of 4,000 ℓ /h of 4.6 K helium. The helium is then used in the 23 kW of 4.6 K refrigeration produced by the satellites.

The nitrogen reliquefier produces liquid into a 14,000-gallon dewar which supplies the needs of the CHL, the satellite system and the magnet shields. It operates in a closed cycle, collecting warm nitrogen gas from the magnet shields, the transfer lines, the helium cold box, purifiers, and satellites. The liquid is transported in vacuum-insulated transfer lines from the dewars to all use points.

Liquid helium from the central liquefier is collected in a 5000-gallon dewar and pumped through the feed line to each of the 24 satellites and subsequently distributed to the ring. Each satellite uses 144 ℓ /h for lead cooling and satellite "boosting." The boosting action results in 966 W of 4.6 K refrigeration being delivered to the magnet string. In this process,

the liquid from the CHL is warmed to ambient temperature and recompressed for delivery back to the CHL and use in the high-pressure stream to the cold box. This system has the advantage of extracting the available refrigeration from the stream at each satellite location, reducing the size and cost of the necessary transfer lines.

Figures 2-1 and 2-2 show schematically the major components of the helium-refrigeration system. Figure 2-1 on page 119 shows the components located at the central helium-liquefaction facility. These are:

- a) Two parallel helium compressors A and B.
- b) A single oil-removal system C serving both compressors.
- c) A medium pressure helium gas storage facility D which removes or adds gas to the system upon demand.
- d) A compressor-seal gas-cleanup system E to repurify helium gas leaking from the compressor piston-rod packings.
- e) The helium-liquefier cold box F.
- f) A liquid-gaseous helium separator G in which the gas of the liquefier JT stream is separated from the liquid and returned to the liquefier.
- g) A 5,000-gallon liquid-helium storage tank H.
- h) A liquid-helium pump I followed by a subcooler to drive liquid helium from the CHL to the distribution system.

Figure 2-2 on page 120 shows the major components of one of the 24 satellite stations along the ring. Liquid helium circulates through the distribution line, which parallels the magnet ring. Excess liquid is returned to the storage dewar H of Fig. 2-1. Each satellite station refrigerator cold box M requires liquid in an amount sufficiently large to cool two strings of magnets. Liquid from M flows to the magnet string through a subcooler L. At the end of each magnet string the pressure of the

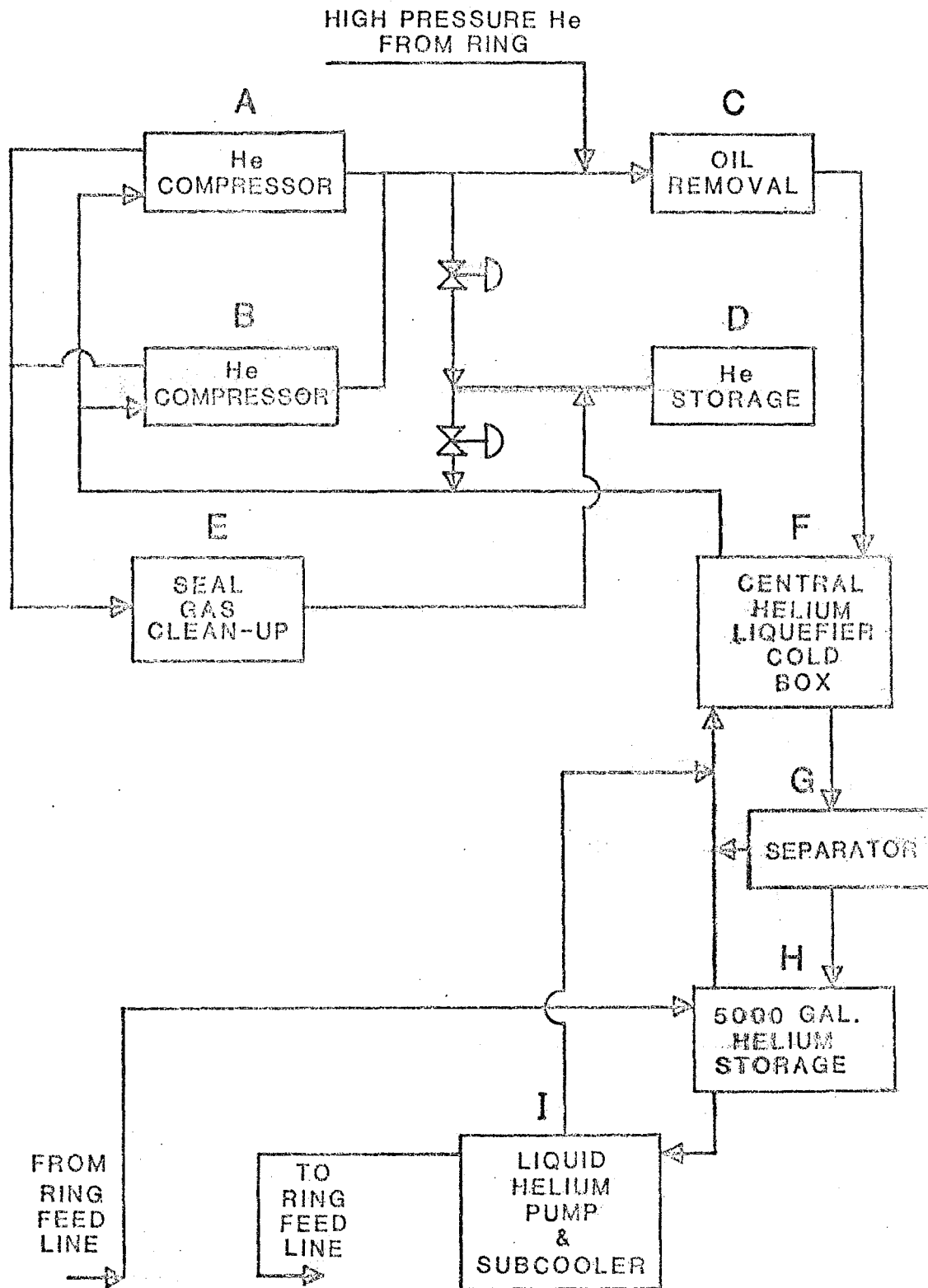


Fig. 2-1. Central helium-liquefier.

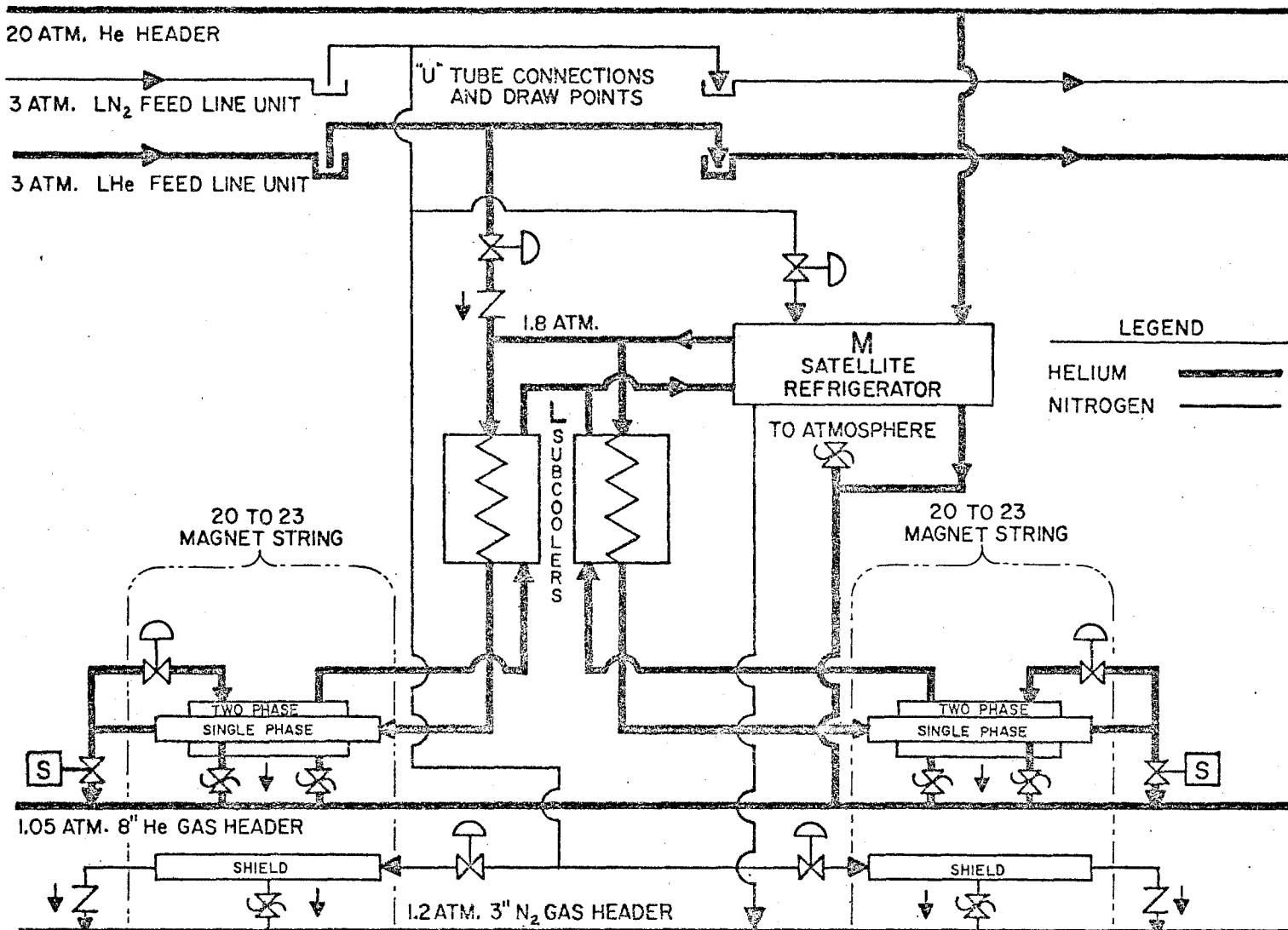


Fig. 2-2. Satellite refrigerator.

single-phase liquid is dropped in a JT valve and it is returned as two-phase liquid. This two-phase fluid cools the magnets and is returned to the satellite-refrigerator cold box M, after passing through the low-pressure side of the subcooler L.

An overall layout of the helium refrigerator system is shown in Fig. 2-3 on page 122, illustrating the relative location of the major refrigeration components, helium-transfer line and warm piping. Compressors of the satellite refrigerator are located in six service buildings along the ring. Low- and high-pressure gas is distributed through 8-in. and 3-in. pipes, respectively. The 8-in. pipe also serves to receive the low-pressure gas flow from the electrical leads and cooldown flow during the time when the ring is cooled from ambient temperature. Helium gas is returned to the CHL after compression by the satellite refrigerator compressors through the 3-in. high-pressure header.

2.2 System Requirements

The static heat load of a dipole magnet has been measured to be approximately 7 W at 4.6 K. AC eddy current and hysteresis losses are approximately 450 J per magnetic cycle. Quadrupole-package heat loads at 4.6 K are estimated to be approximately equal to those of a dipole. Tables 4-I and 4-II list the calculated load for the dipole and quadrupole magnets. The dipole numbers differ slightly from those measured from a string of magnets.

Each of the 24 satellite refrigerators supply subcooled single phase helium to typically 32 dipoles and 8 quadrupoles in the two parallel

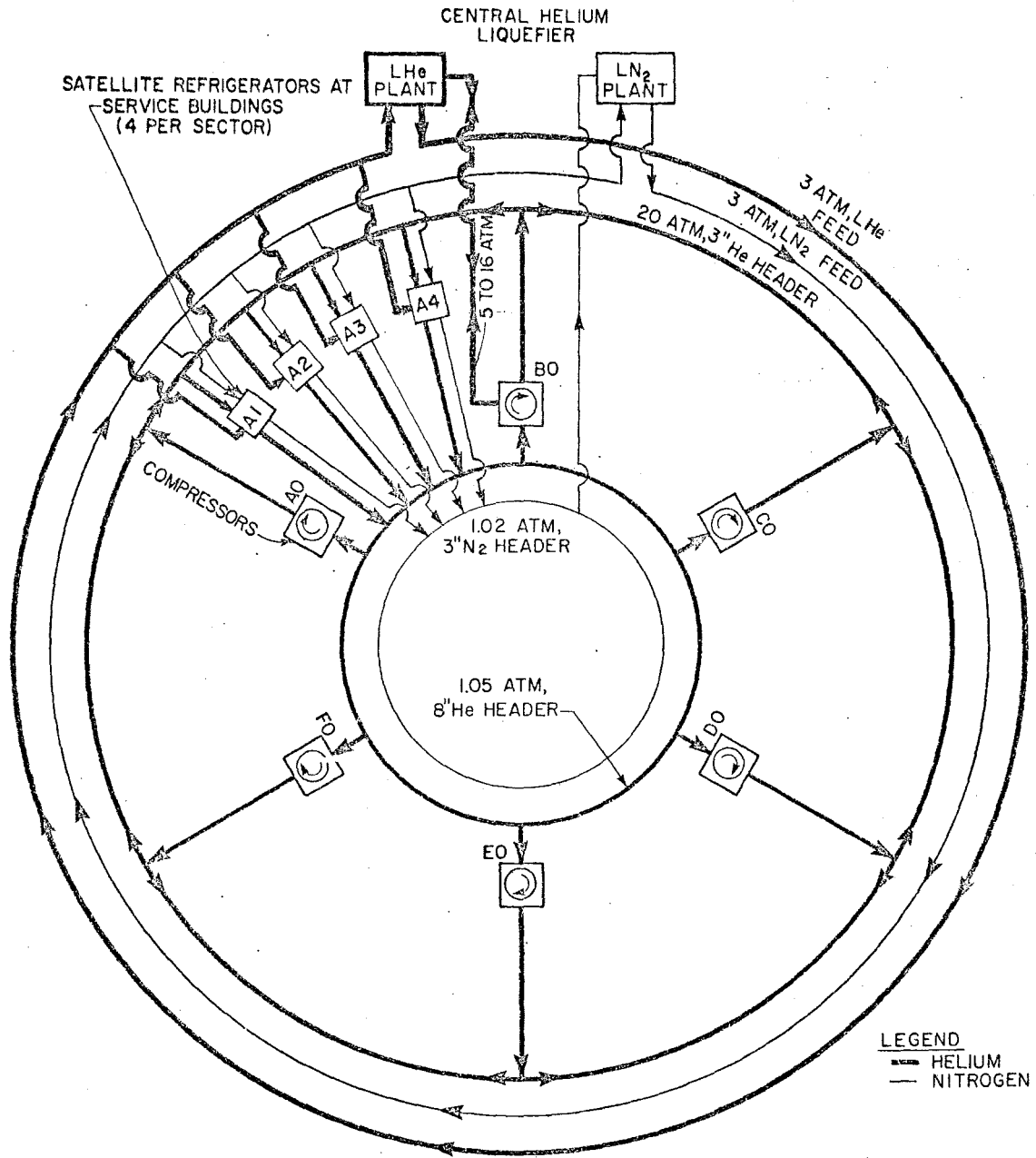


Fig. 2-3. Layout of the refrigeration system.

Table 2-I. Calculated Dipole Heat Loads.

Dipole Model 135 Cryostat	80 K W	4 K W
Infrared (main body)	10.08	0.384
Supports conduction	13.30	3.028
Anchor	1.00	0.164
Vent pipe (Mark 1 Model)	1.66	0.108
Instrumentation leads		0.156
Infrared (junction)	0.38	0.155
4 K cooling	-3.99	
Totals	22.43 W	3.992 W

Table 2-II. Calculated Quadrupole Heat Loads.

Quadrupole	80 K W	4 K W	Evap. ℓ/h
Infrared (main body)	6.41	0.210	
Infrared (junction)	0.19	0.008	
Supports conduction	3.04	0.680	
4 K cooling	-0.90		
Vent pipe for LN ₂	0.27		
Vent pipe for 1∅	1.91	0.496	
Vent pipe for 2∅	1.57	0.325	
1 safety lead (5 kA)		1.000	
5 pairs of correction leads (75 A)		0.75	1.05
Instrumentation leads		0.156	
Totals	12.49 W	3.63 W	1.05 ℓ/h

cryogenic loops. The heat deposited in the liquid is exchanged with the return two-phase counterflow helium. The entire helium system is shielded by a two-phase nitrogen system. Table 2-III gives the distribution of loops in a sector with the location of the feed and turn-around points and the number of magnets per loop. Table 2-IV gives the heat loads and refrigeration and helium requirements of a worst-case

Table 2-III. Magnet Cooling Loops.

Building	Feed Station	Four Satellites per Sector			Quads	Special Quads
		Turn-Around Station	Loop	Dipoles		
1	15	11	1	16	3	3
		21	2	18	5	-
				34	8	3
2	25	21	3	16	4	-
		29	4	16	4	-
				32	8	-
3	35	29	5	16	4	-
		39	6	16	4	-
				32	8	-
4	45	39	7	16	4	-
		49	8	15	2	3
				31	6	3
Totals				129	30	6

Table 2-IVa. 4.6 K Refrigeration Loads (Worst Building).

	Each		1000 GeV DC		1000 GeV	35 s cycle
	W	ℓ/h	W	ℓ/h	W	ℓ/h
34 dipole magnets	7.0	-	238.0	-	238.0	-
34 dipole ac losses ^a	13.0	-	-	-	442.0	-
11 quad magnets	7.0	1.05	77.0	11.55	77.0	11.55
11 quad ac losses ^a	11.0	-	-	-	121.0	-
1 pair 5000-A leads ^b	10.0	14.0	10.0	14.0	10.0	14.0
Set end boxes	20.0	-	20.0	-	20.0	-
Totals			345.0 W	25.55 ℓ/h	908.0 W	25.55 ℓ/h

^a 35-s cycle time
^b 7 out of 24 buildings

Table 2-IVb. 80 K Nitrogen Requirements (Worst Building).

	Each	1000 GeV DC	1000 GeV
	W	W	35-s Cycle W
34 dipole magnets	22.4	762	762
11 quadrupole magnets	13.5	138	138
Totals		900	900

service building. In the standard mode of operation the satellite refrigerator uses liquid helium from the Central Helium Liquefier to produce the necessary refrigeration in a building. In addition, the CHL must supply the liquid for the power leads. Specifications for the satellite are given in Table 2-Va and b and those for the Central Helium Liquefier and Nitrogen Reliquefier in Tables 2-VI and Table 2-VII respectively, shown immediately following.

Table 2-Va. Satellite-Refrigerator Parameters.

Mode	Consumption	Production
Satellite	129 l/h He	966 W
Refrigerator	52 l/h N ₂	623 W
Liquefier	84 l/h N ₂	126 l/h He
Accelerator standby	59 l/h N ₂	490 W + 26.6 l/h He

Table 2-Vb. Mycom Satellite-Compressor Parameters.

Type	Screw
Stages	2
Power	350/261 Bhp/kW
Suction pressure	1.05 atm
Discharge pressure	20 atm
Throughput	57.54 g/s

Table 2-VI. Central Helium Liquefier Specification.

Inlet pressure	1.05 atm
Discharge pressure	12.3 atm
Flow rate (two compressors)	8,573 lb/h
Power required (two compressors)	2,470 kW
Power required (He air cooler)	52 kW
Liquid helium production (9,900 lb/h of He at 11.9 atm to the cold box)	≥ 4,000 l/h at 4.6 K
Liquid nitrogen consumption per liter of liquid He produced	≤ 0.6 l/l

Table 2-VII. Nitrogen Reliquefier Specifications.

Nitrogen reliquefier	2,550 l/h 54 tons/day
Production rate based on a compressor flow rate of suction pressure	37,500 lb/h 1.05 atm
discharge pressure	123.5 atm
power requirement	2,540 kW

A summary of the total system requirements, consumption, and production specifications is given in Table 2-VIII, together with power requirements.

Table 2-VIII. Summary of Refrigeration Requirements and Production Figures.

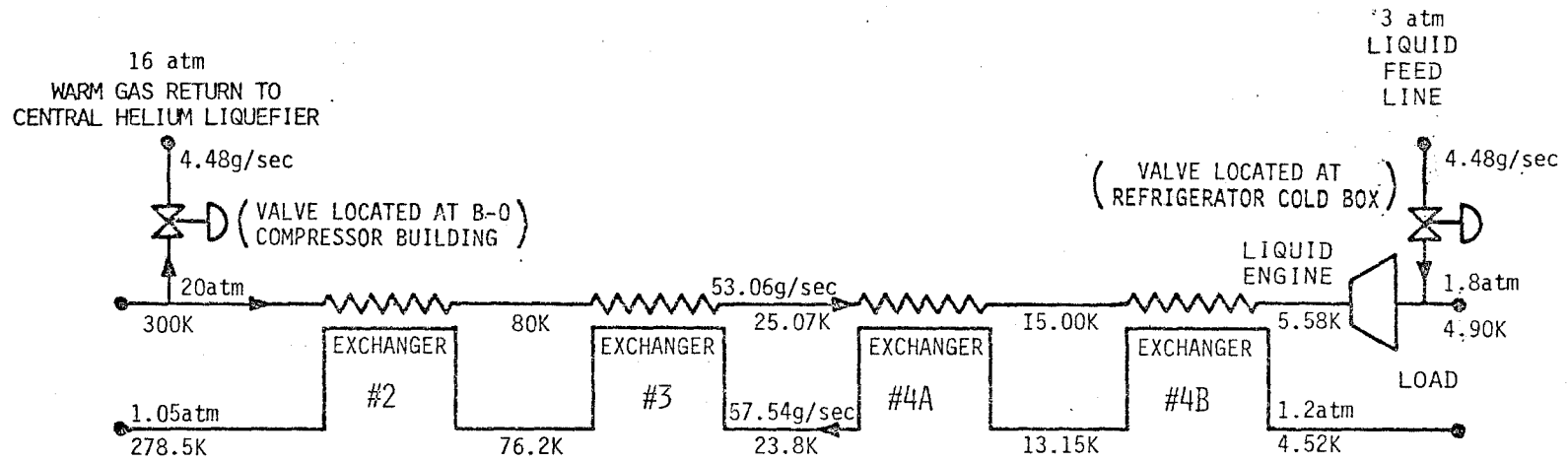
Requirements	1000 GeV, dc		1000 GeV, 35-s cycle	
	W	l/h	W	l/h
<u>Helium</u>				
Magnet system helium, 4.6K	7,480	350	19,918	350
Helium transfer line pump, 4.6 K	200		200	
Satellite consumption		≈1,548		3,096
Total	7,680 W	≈1,898 l/h	20,118 W	3,446 l/h
	W	Equiv. l/h	W	Equiv. l/h
<u>Nitrogen</u>				
Magnet system nitrogen, 80 K	21,600	490	21,600	490
Helium transfer line CHL at 3,446 l/h	4,500	100	4,500	100
Total at 3,446 l/h He				2,658 l/h
Total at max. operation				3,590 l/h
<u>Power</u>				
		kW		
24 satellites		6,270		
Central Helium Liquefier		2,552		
Nitrogen Reliquefier		2,540		
Total		11,332 kW		
Production	W		l/h	
<u>Helium</u>				
Satellite refrigerators	23,000			
Central Helium Liquefier	200		≥4000	
<u>Nitrogen</u>				
Reliquefier (Additional liquid nitrogen can be purchased at approximately \$ 140 for 2400 l)			2,550	

2.3 Central Helium Liquefier

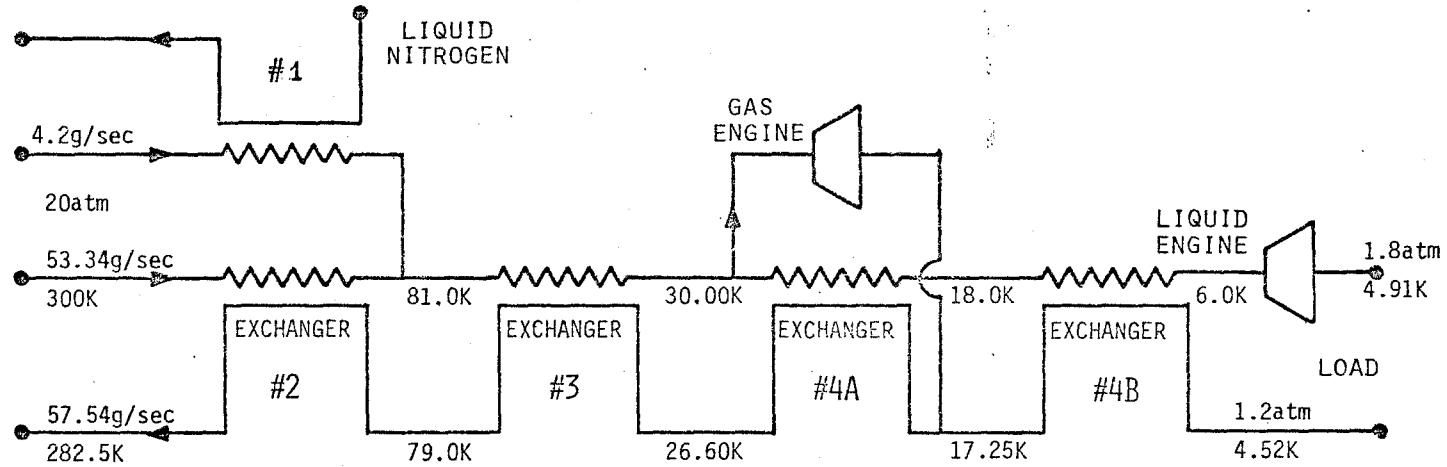
The central liquefier consists of three large compressors, a helium liquefier, nitrogen liquefier, purification equipment, and storage tanks. The compressors are surplus compressors from an air-separation plant. Two of the three have been modified for helium service, while the third will operate for nitrogen service. Nitrogen production is rated at 2550 l/h. The liquid helium is fed from the storage dewar to a pump dewar, where it is compressed from 1.4 to 3.0 atm. The flow is then cooled to 4.65 K by heat exchange with liquid in the pump dewar. The dewar boil-off is returned to the liquefier as 5 K gas. The 4.65 K, 3-atm output of the exchanger feeds the ring transfer line.

2.4 Satellite Refrigerators

Each unit consists of a 35-ft long heat-exchanger column, a liquid expansion engine, two flow-splitting subcoolers, and a stand-by 30 K gas expansion engine. The unit has four modes of operation, as illustrated in Table 2-Va and shown schematically in Fig. 2-4. The primary mode, which will be used for the accelerator operation, is the satellite mode. The unit is continuously supplied 4.48 g/s liquid helium (plus 0.5 g/s power-lead flow) from the CHL. This causes an imbalance in the heat-exchanger flow (53.06 g/s supply vs 57.54 g/s return) giving a double pinch at 25 K and 5 K. The liquid engine expands from 20 atm to 1.8 atm, producing slightly subcooled liquid. The cold-end refrigeration comes from three sources: 44% from the heat exchangers flow imbalance, 48% from the liquid expander, and 8% from the central liquefier flow.



SATELLITE MODE



REFRIGERATOR, LIQUEFIER & E.D. STANDBY MODE
(refrigerator values illustrated)

Fig. 2-4. Satellite refrigerator modes.

In the other three modes, liquid nitrogen is used instead of liquid helium. The stand-by gas engine is now operated at 30 K for these modes, while the liquid engine produces a two-phase liquid-gas mixture. We have tested the cold box and expanders in the first three modes and exceeded design in both the liquefier and refrigerator modes and 90% of design in the first attempt in the satellite mode. The stand-by mode is a mixture of refrigeration modes and liquification with a trade-off ratio of 5.0 W to 1.0 l/h. This mode is designed to cool strings of magnets without the aid of the CHL both during initial construction and later during failures of the CHL. This mode was used for both the 10- and 25-magnet A1 runs. There are many additional mixtures of satellite and refrigeration modes that could be used if the CHL were operating at reduced efficiency.

2.5 Feed System

The liquid He and N₂ will be fed to the ring by a 25-section, 4-mile long vacuum-jacketed loop. The loop runs from the CHL to A4, around the ring in the proton-beam direction to A3 and then back to the CHL. The N₂ that is used to cool the shields of the magnets also provides the shield for the feed line. The sections are coupled by two rigid vacuum-jacketed U-tubes, each with a branch tee to feed the local satellite refrigerator. This will permit us to install, test, and cool down one section at a time without interfering with the operation of the rest of the system. With the connection of the last service building, A3, back to the CHL, we can take any section out of service for repair, if needed, by feeding the return line in reverse. We estimate a maximum 4.6 K heat load of 150 W and maximum 80 K load of 4500 W for the entire line.

The satellite gas piping consists of three gas header loops. On the wall of the tunnel behind the magnet, there is an 8-in. low-pressure He pipe and a 3-in. low-pressure N₂ pipe. The He pipe is the suction line for the compressors, as well as the main magnet relief and manifold for lead and cooldown flow. The N₂ pipe is the collection header for all shield flow, pre-cooler flow, and also N₂ reliefs. The third header is a high-pressure He pipe that is located on the Main Ring road side of the berm. These are shown in plan in Fig. 2-3 and in elevation in Fig. 2-5.

Two 3-in. gas headers which connect to the CHL are located at A4. The first is a 10- to 18-atm bidirectional He gas line. Normally it is used as the gas return for the liquid supplied by the CHL, dumping gas into the discharge of the CHL compressors (13 atm). During startup and in accelerator standby mode, the line can also supply gas to the 8-in. header. The second header is teed into the 3-in. N₂ loop and is the main N₂ return for the N₂ liquefier.

The compressor system is located in the six "zero" buildings, with four compressors per building for maximum capacity. The compressors are connected across the two He headers with all twenty-four in parallel. The grouping of compressors into a header system totally decouples cold boxes from compressor operation; that is, we can shut down all four compressors at B0 without shutting down any cold boxes (but of course we have lost 1/6 of our total capacity).

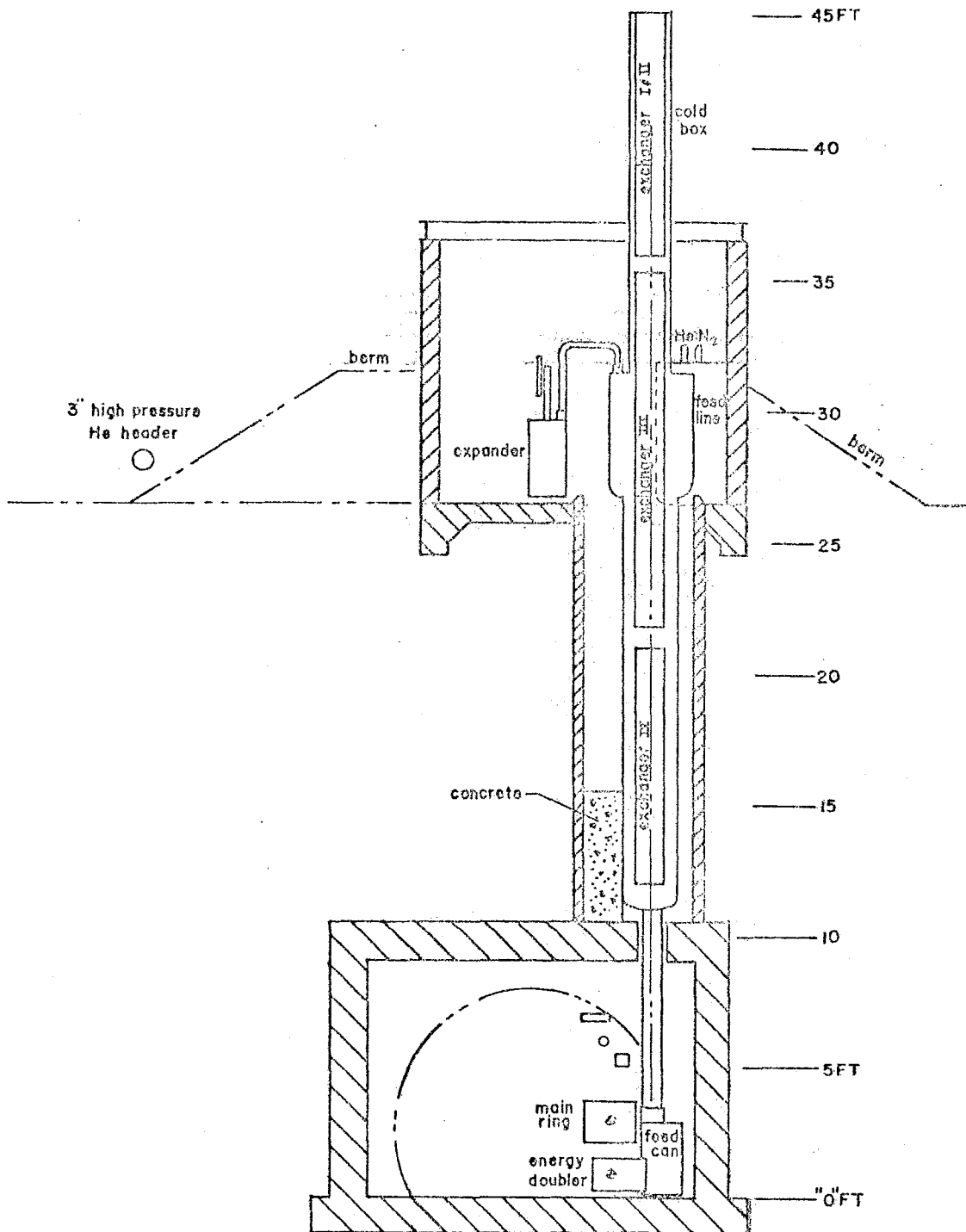


Fig. 2-5. Cross section of satellite refrigerator and cryogenic feed to the superconducting magnets in the tunnel.

2.6 Tunnel Components

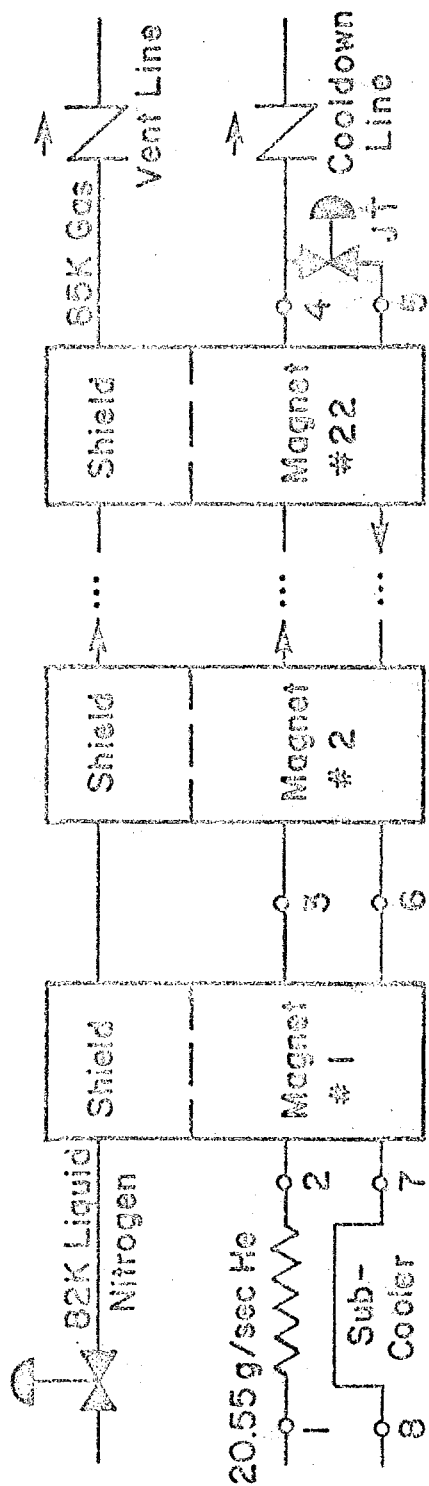
The tunnel cryogenic system consists of 48 cryogenic loops. Figure 2-6 is a block diagram of one loop, giving the temperatures at significant points along the flow. The liquid helium is subcooled by a small heat exchanger in the feed box. It reaches equilibrium after the first magnet, at point 3. There is a small temperature rise, 0.05 K, from point 3 to point 4 because of the two-phase pressure drop from point 5 to point 6. The flow is controlled by the Joule-Thompson valve (JT) to maintain point 8 at 0.4 K of superheat.

The operation of the system at higher capacity is simply a matter of turning on additional compressors, since to first order the ratio of capacity to mass flow rate is constant. It must be noted that the pressure drop in the two-phase cryostat of the magnet plus the shell side of the heat exchanger varies as the square of mass-flow rate, so that the operating temperature of the shell side of the magnets increase with the square of the mass-flow rate.

$$T = T_0 + \alpha \left(\frac{F}{F_0} \right)^2,$$

where $T_0 = 4.277$ K. The parameter α for the shell side of the prototype refrigerator was designed to be as low as possible and was measured to be 0.4 K. We have redesigned the A2 cold box to give a lower value of this parameter.

The extreme importance of α as a design parameter is not generally appreciated. Commercial refrigerators give 0.3 to 0.4 K, but we have been trying to reach less than 0.2 K. Not only does a low α mean that one can



POINT	T(K)	P _{atm}	H _v /g	% LIQUID
1	4.90	1.8	14.22	100.
2	4.50	1.8	11.20	100.
3	4.55	1.8	11.47	100.
4	4.60	1.8	11.75	100.
5	4.47	1.25	11.75	96.
6	4.42	1.2	27.49	13.
7	4.42	1.2	27.99	10.
8	4.52	1.2	31.01	0.1K Super Heat

Fig. 2-6. Details of the cooling loop for a string of cryogenic magnets (1/48 of the ring).

operate at lower temperatures and, conversely, higher capacities in special areas (low beta, extraction, and injection), but also that one can operate at twice nominal capacity during quench recovery, which means a factor of 3 to 5 in recovery time. In addition, with the control system as installed at A2 we can automatically shift refrigeration from one loop to another or from one sector to another on a pulse-to-pulse basis, as the beam scrapes at different locations.

The main magnet cryogenic, vacuum, and electrical components are unavoidably interwoven. The cryogenic system consists of 48 single phase-two phase loops. Each satellite refrigerator feeds two loops and each loop has a JT valve at its far end. The beam-tube vacuum system (discussed in more detail in Section 5) has warm gate valves that isolate sections of each sector at (typically) ten locations. These valves are located between cryo loops and at the two ends of each warm region (the long straight section and the medium straight sections at locations 17 and 48). The electrical circuit (discussed in more detail in Section 6) for the main magnets consists of all coils connected in series along the coil bus and of foldbacks at the two ends of the B0 straight section bringing current back through the magnets along the return bus. Power-supply feed points are located once per sector at the same locations as one of the cryogenic feeds. Thus cryogenic feedthroughs of the two electrical buses are necessary at the end of every cryogenic loop except at B0. The interrelation between the three systems is illustrated for a typical sector in Fig. 2-7.

The feed box contains a pair of power leads where necessary, one or two cryogenic feedthroughs, a pair of subcoolers and instrumentation for

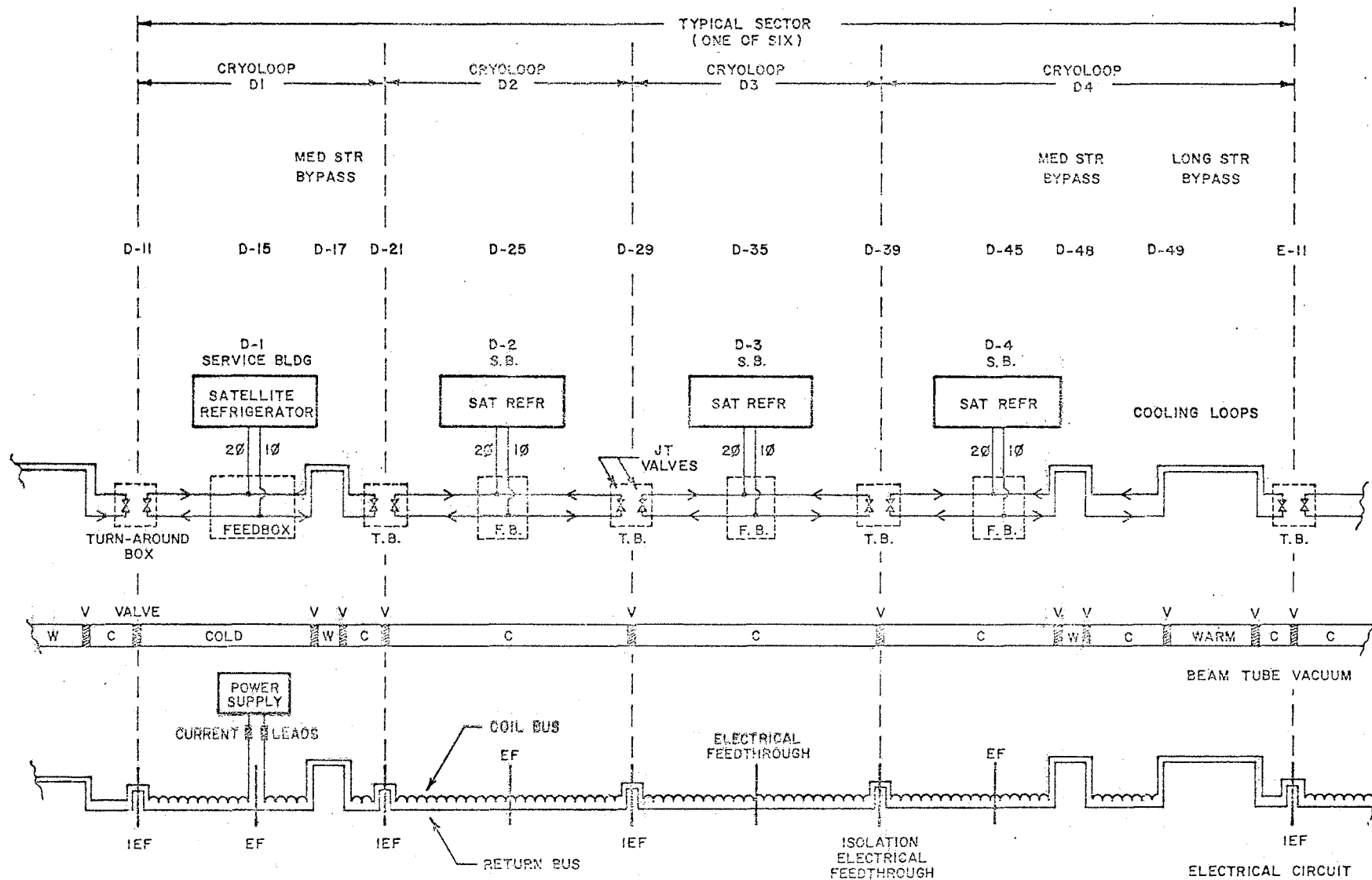


Fig. 2-7. Schematic of cryogenic components in the tunnel for a typical sector.

cryogenic control of the refrigerator and magnets. Figure 2-8 is a simplified engineering drawing of a feed box. These boxes are welded into the downstream ends of normal quadrupole cryostats at locations 15, 25, 35, and 45 and use 20 in. of available mini-straight space.

The turnaround box, shown in Fig. 2-9, has a cold-warm-cold transition for the beam-tube vacuum isolation valve, a pair of JT valves for the turnaround of the two cryogenic loops, a pair of He cooldown vents, a pair of N₂ vents, and instrumentation for the cryogenic control of the refrigerator and magnets. In addition, it contains the special feedthroughs for the electrical circuits, which must be maintained at helium temperatures.

The design requirements on this electrical feedthrough are:

- (i) During normal operation, it must make a 5000-A superconducting connection. Heat load per cryo loop is $\frac{1}{2}$ ℓ /h plus $\frac{1}{2}$ W maximum.
- (ii) When one pair of cryoloops is cold and the adjacent pair is warm:
 - (a) The heat load into the cold loop shall be less than 5 ℓ /h plus 10 W.
 - (b) No surface in the warm loop shall be less than 0° C.
- (iii) During warmup of a pair of cryo loops, the feedthrough must be able to carry current starting at 1000 A, decreasing to 10 A over a 4-h period. During this period, there is no heat-load limit on the cold loops.

The turnaround boxes are also welded into the quadrupole cryostats and use 20 in. of mini-straight space. They occur at locations 11, 21, 29, and 39.

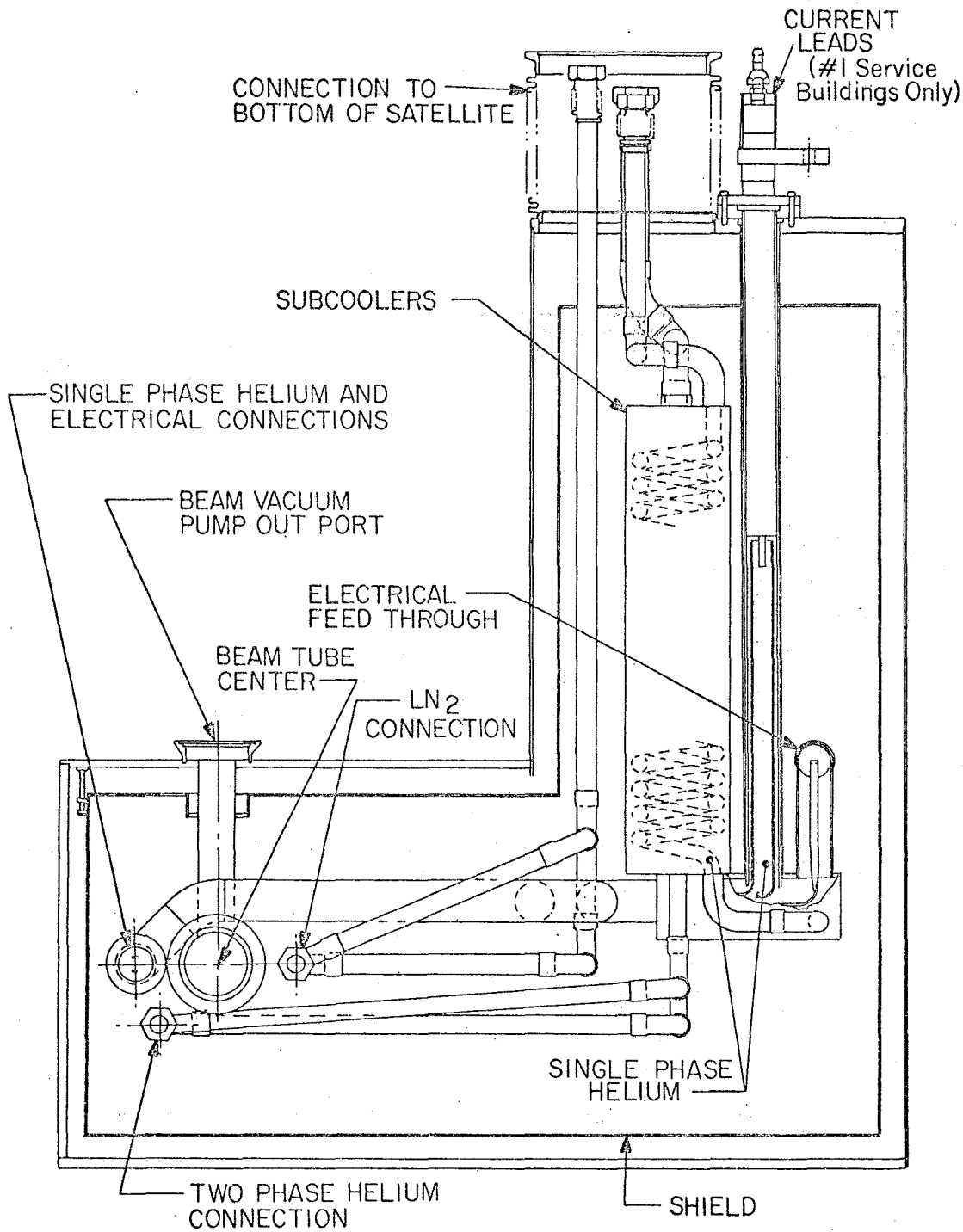


Fig. 2-8. Feed box.

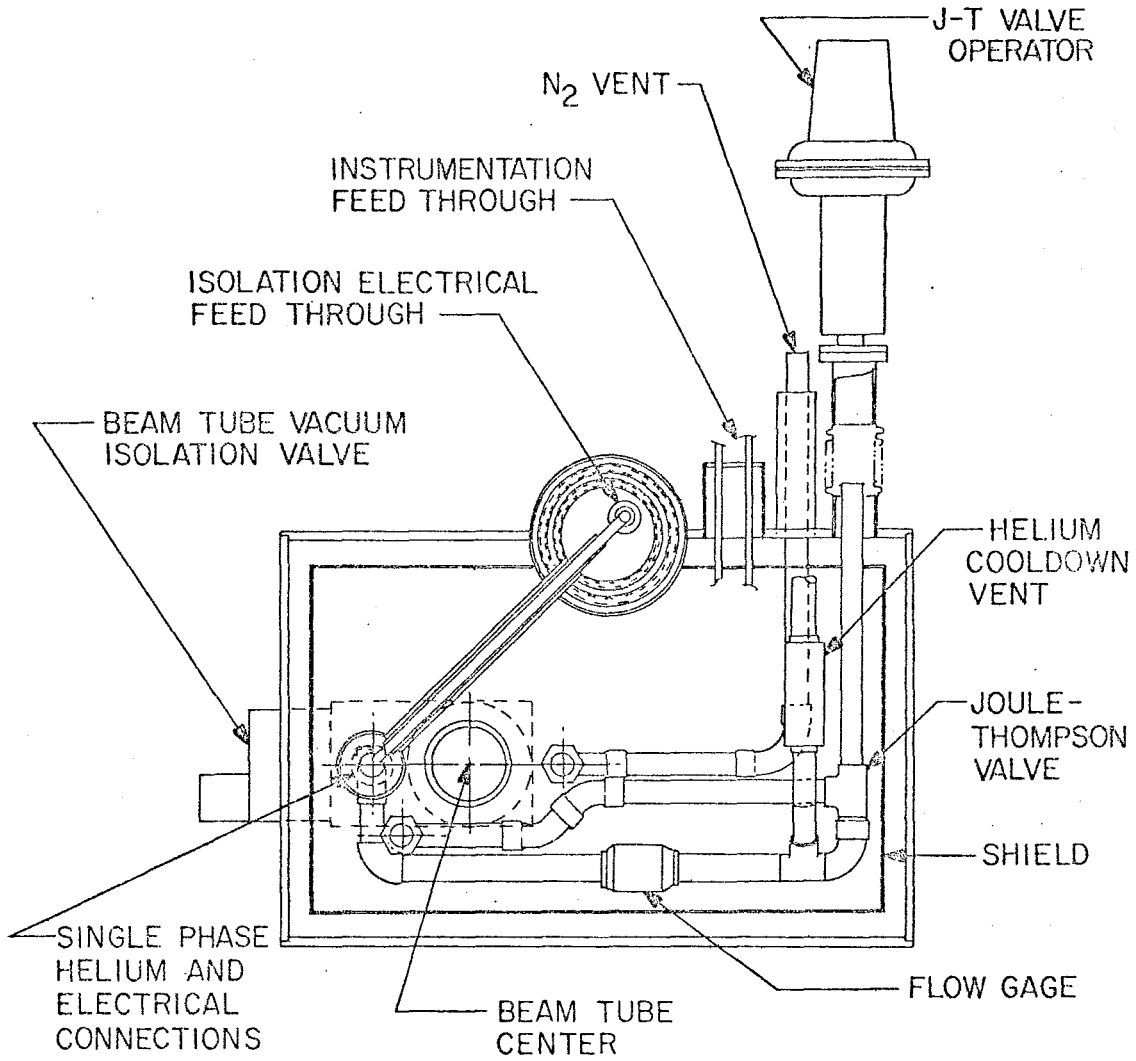


Fig. 2-9. Turnaround box.

The straight section bypasses occur at the long straight sections and at locations 17 and 48. At these locations a helium-transfer line containing the two power leads is brought out parallel to the beam tube for the length of the straight section. Straight-section space required for the bypass and cold-warm transitions is a total maximum of 25 in. for both ends. Isolation vacuum valves and sublimation pumps will require an additional 24 in. of straight-section space at each end. Figure 4-10 illustrates a typical bypass.

2.7 Cooldown and Warmup

If one attempted to cool down long strings of magnets in the normal operating mode, it would take several months or might be altogether impossible, because the magnets are heat exchangers and therefore most of the refrigeration that is supplied is heat exchanged with the return line and then vented. We therefore use single-pass cooling of the single-phase rather than loop flow, with the two-phase deadheaded. The wave front is very steep and travels through the magnet string much like a step function through a transmission line; the discharge remains at room temperature during almost the entire cooldown cycle.

Cooldown with the CHL operational is very straightforward. The satellite is tuned up in the liquefier mode, producing 126 l/h, which is added to the 200 l/h from the central (if one is cooling only one service building this might be as high as 2000 l/h, stress, pressure drops, and thermo-acoustic oscillations permitting). This helium is run through the single phase of the magnets, returning to compressor suction by way of the cooldown lines, where it recompresses to 20 atm. The excess gas is then

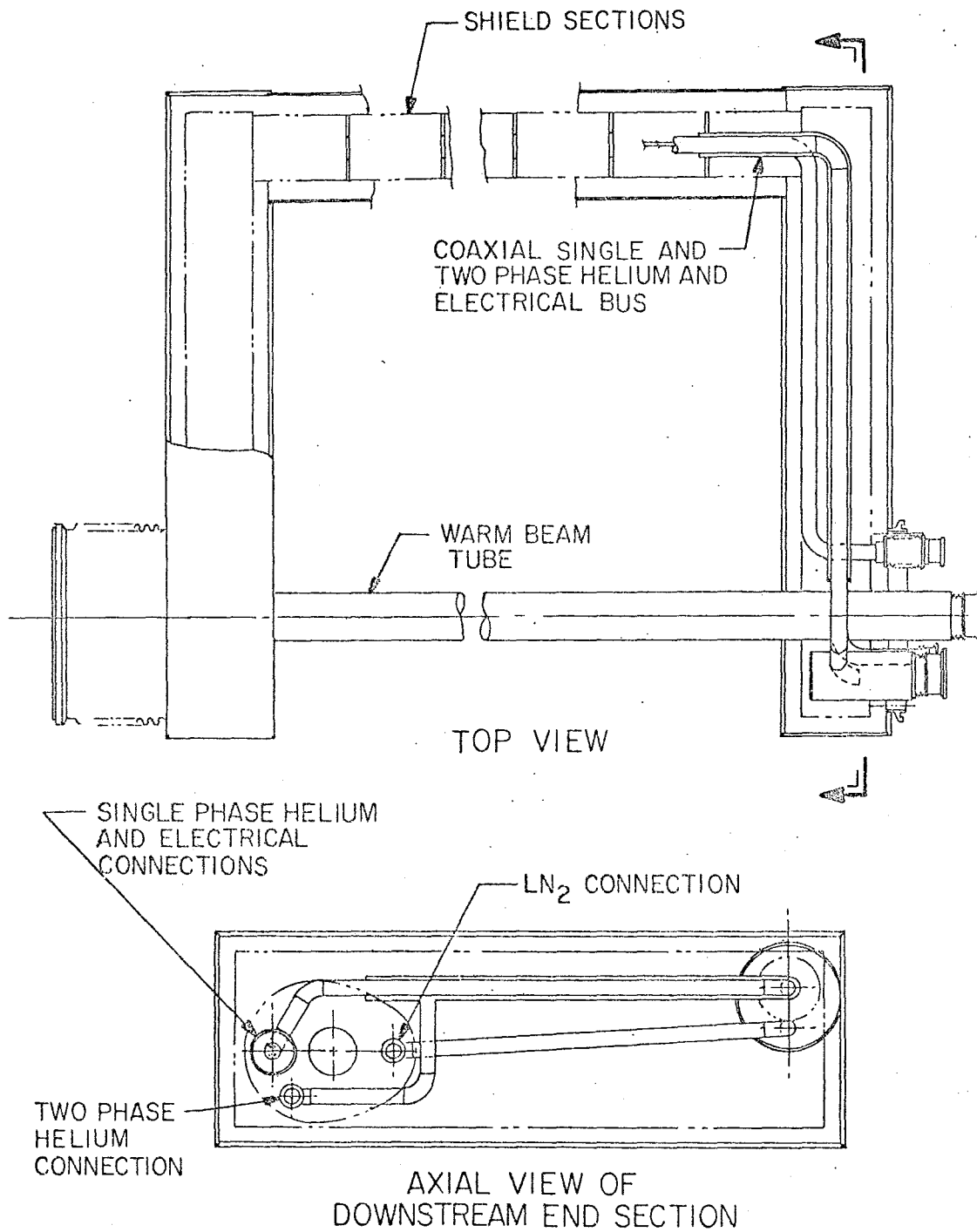


Fig. 2-10. Bypass.

returned to the discharge of the CHL compressor (13 atm), where it is reliquified. When the wavefront reaches one of the cool-down lines, it is shut off and the magnet JT is opened. When it reaches the second one, the same is repeated, 1000 ℓ are transferred from the central to fill the magnets, the dry engine is turned off and the satellite is tuned for the satellite mode.

If the CHL is not operational, cooldown is slightly more complicated, but can be carried out using the liquefier mode followed by the standby mode of the satellites. Since the CHL was not complete, this mode was used to cool the 25-magnet string in the A1 tests.

Cool down after a quench is a function of the energy dissipated in the magnet. For a quench during injection, recovery time should be less than 100 s. During the 25-magnet A1 test, the system recovered much faster than the length of time it took to turn on the power supply.

For fast recovery at high power levels we require a fast electronic valve control circuit which does the following:

- (i) Fire relief or auxiliary cool-down valves at both ends of quenched half-cell in a time $\Delta t < 50$ ms.
- (ii) Close JT valve in $\Delta t < 2$ s.
- (iii) After 5 seconds, close valve on quad closer to refrigerator.
- (iv) Run in cool-down mode, venting into suction header at the quad further from refrigerator until T_{out} equals 10 K.
- (v) Close second quad valve and open JT valve.
- (vi) Refrigerate and fill.

Warmup is a function of the electrical status of the magnets. If there is continuity in the electrical circuit, the string can be warmed up in 4 hours using either the main power supply or a special warmup supply.

If electrical continuity is lost, several heater supplies can be installed across the safety leads so that, combined with hot gas from the compressor, a heating rate of 50 kW can be achieved (10-20 h warmup).

If both electrical continuity is lost and there are large holes in the single-phase He cryostats, hot N₂ at 3 atm is connected and warmup takes several days.

2.8 Failure Modes

Because of the complexity of the system, it is highly probable that at any one time, one component may be down and several may be operating at reduced efficiency. The system must be designed to continue to cool the magnets with at most a reduced ramp rate. Table 2-IX gives projected replacement and beam-off times for various component failures. Times do not include an allowance for troubleshooting the system and travel time for the repair crew; troubleshooting in many cases can be longer than replacement times. The extremely rapid replacement time is possible because of our concept of separate cryostats and quick-disconnect vacuum U-tubes.

Table 2-IX. Operation in Failure Modes.

Defective Component	Consumption Times		Beam Off (h)	Replace-ment (h)	Ramp Rate (min)	Action Taken	Comments
	Replacement (l/h) He	N ₂					
Normal operation	144	20	-	-	1		
Central Helium Liquefier	0	79	-	as needed	5	start gas engines	
Central Nitrogen Liquefier	144	20	-	as needed	1	buy N ₂	\$105/h for total ring
Feed line	144	20	1.0	168-336	1	reverse flow	
Magnet	-	-	48	48	beam off		
Satellite Cold Box	-	-	48	48	beam off		
Satellite Compressor	144	20	-	as needed	1	turn on standby compressor	each comp. is 4% of total re- frigeration
Satellite Wet Expander	400	20	2×0.1	2	1	sat. JT valve	
Satellite U-Tube	as needed	20	0.1	0.1	beam off		
Feed U-Tube	as needed	-	0.5	0.5	beam off		

3. SPECIAL DEVICES

3.1 Additional Correction Elements

We believe that additional correction elements beyond those outlined in the Energy Saver and Superconducting Accelerator Design Reports will be needed. It is planned that these will be constructed following the designs of the presently planned correction elements.

3.2 Low-Beta Long Straight Section¹

By replacing the two inner pairs of quadrupoles in the normal long straight section with considerably longer, independently powered, three-shell quadrupoles, as shown in sketch (b) in Fig. 3-1, a pp colliding insertion can be produced. With the four outer quadrupoles running normally and the inner ones set at rather weak values, the lattice functions across this insertion can essentially duplicate those of the normal straight sections. By leaving quads #1 and #12 connected in series with the regular magnets, turning off quads #2 and #11, and repowering the inner quads, a β^* of approximately 10 m can be obtained. Quadrupole settings for these cases are listed in Table 3-I and some dynamic parameters are listed in Table 3-II. Figure 3-2 illustrates the Type I interaction region. By adding additional power supplies to the other two pairs of quadrupoles, one can obtain lower values of β^* , although β_{\max} starts to increase rapidly.

With the insertion of four more long, strong, and independently powered quadrupoles, one can produce a β^* of the order of 1 m. This is the Type II low- β shown in Fig. 3-1 and Fig. 3-3. Table 3-I lists quadrupole settings for minimum beta values of 1 and 2 m. Parameters for these

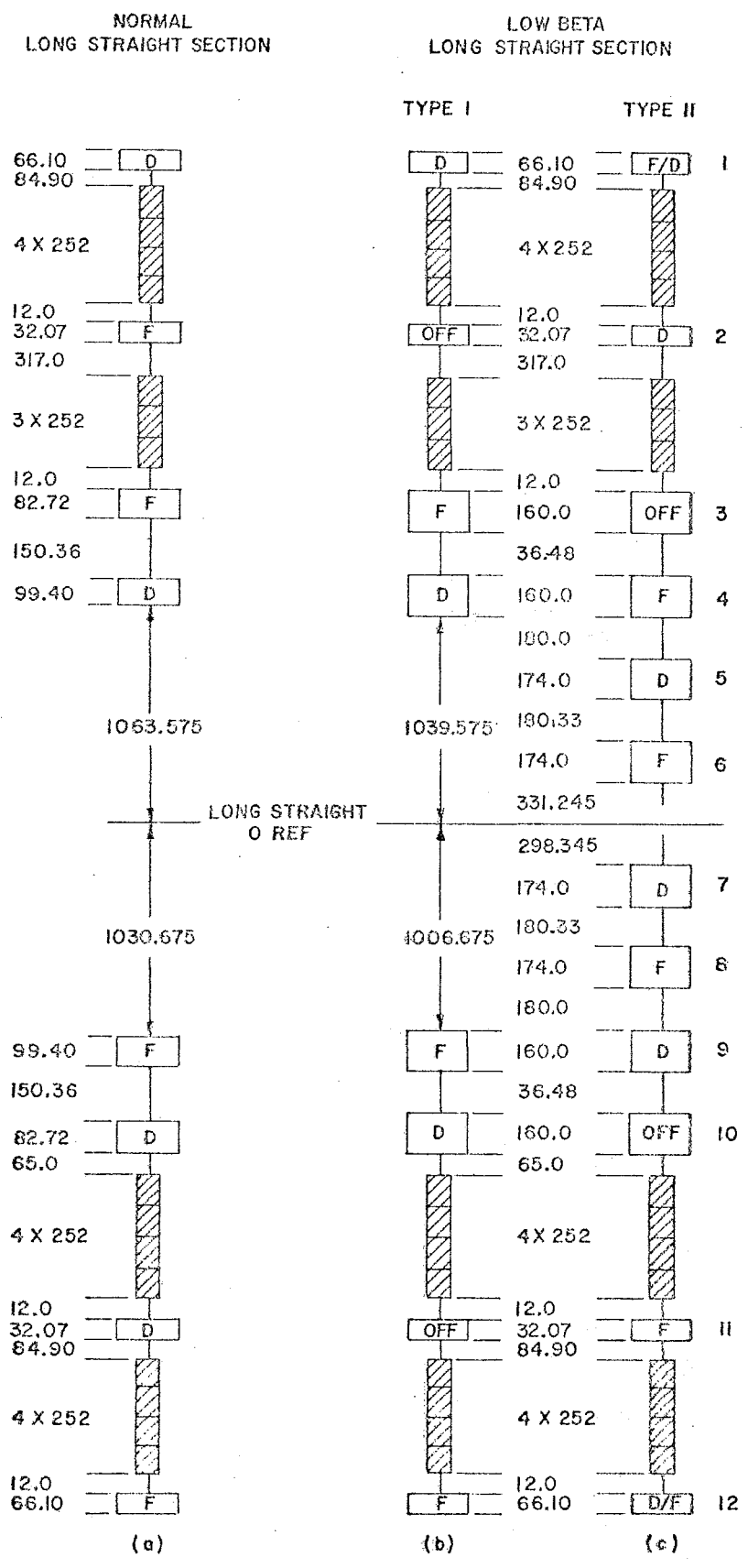
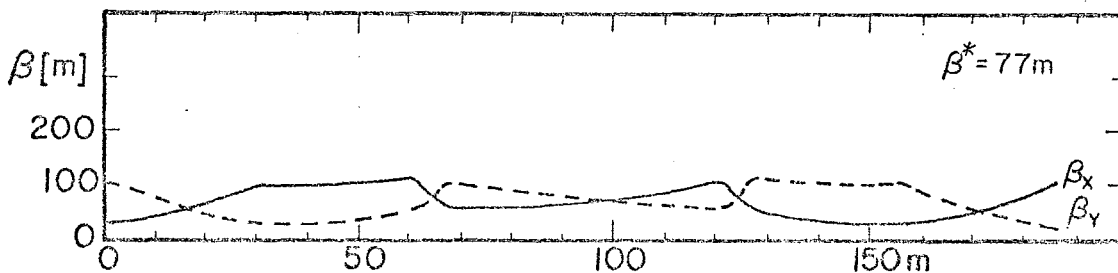
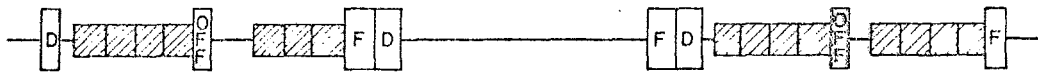
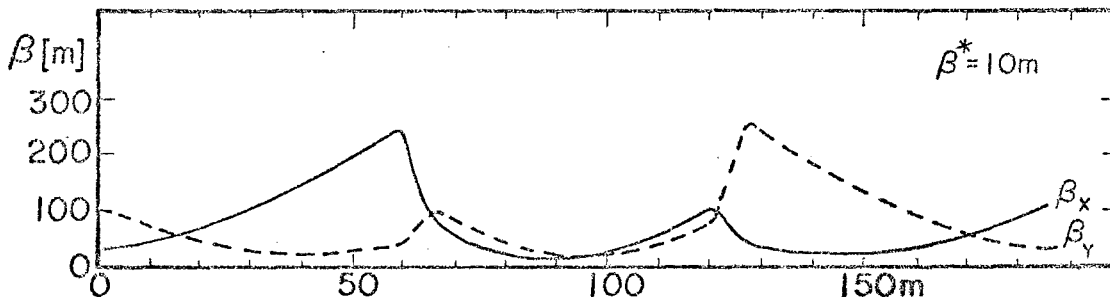


Fig. 3-1. Layout of normal and two types of low-beta long straight section.

cases are again listed in Table 3-II. A few arbitrary decisions have been made at this point and should be mentioned.



NORMAL LONG STRAIGHT SECTION



LOW BETA LONG STRAIGHT SECTION
TYPE I

Fig. 3-2.. Lattice functions for normal and for type I low-beta long straight sections.

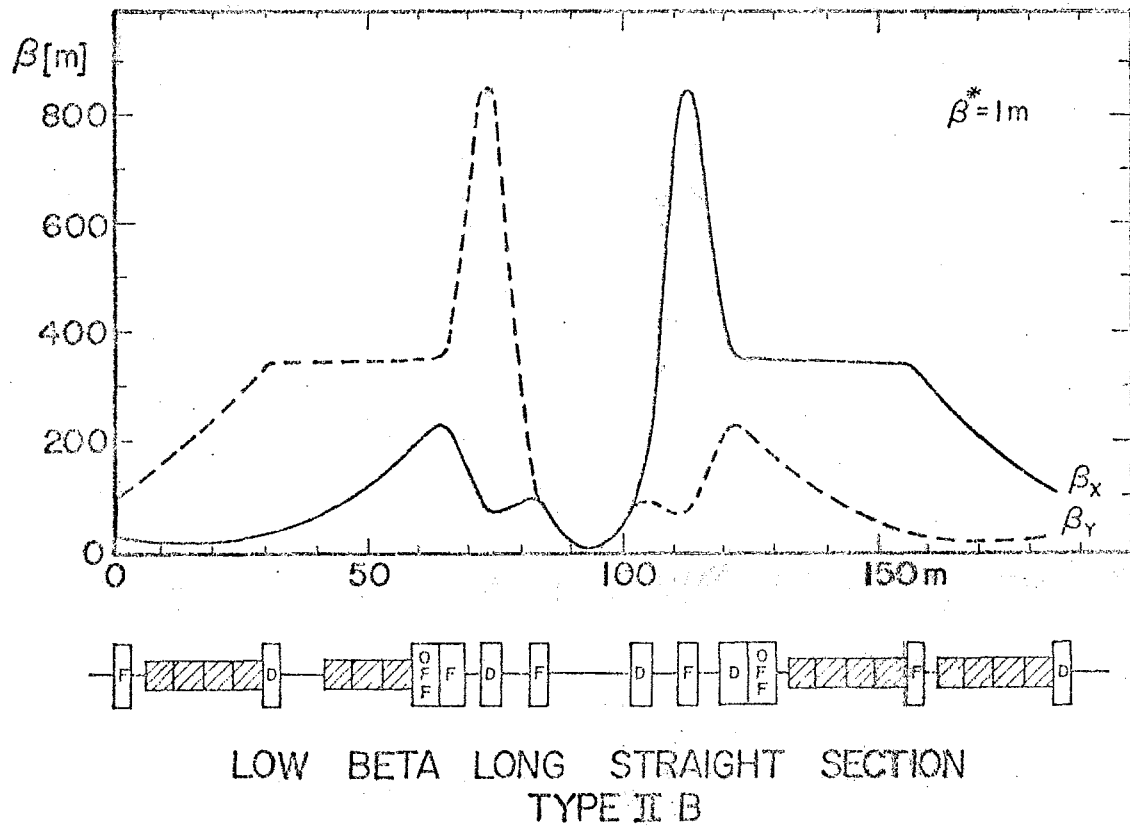
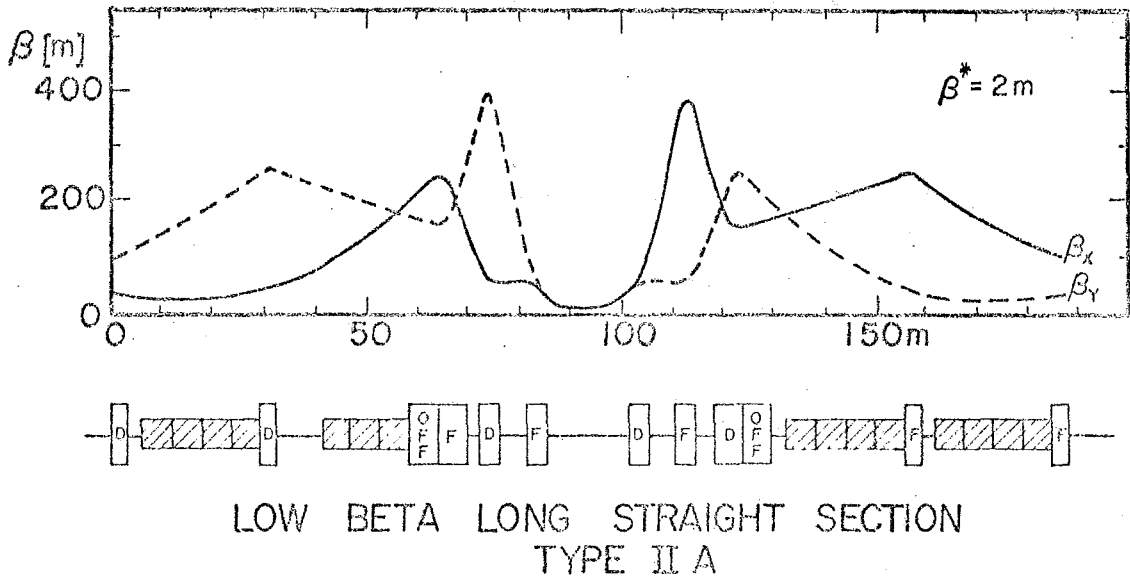


Fig. 3-3. Lattice functions for type II low-beta long straight sections.

Table 3- I : Quadrupole Settings (Values in kG/m for 1 TeV).

Quad #	Type I			Type II	
	Case A	Case B	Case C	Case D	Case E
	"normal"	$\beta^* = 10$ m	$\beta^* = 2$ m	$\beta^* = 1$ m	$\beta^* = 2$ m, $r_i^* = 0$
1	-760.3206	-760.3206	-159.4277	195.9240	-326.7387
2	760.3206	0	-530.2842	-690.3435	181.1120
3	481.9685	931.4100	0	0	-302.2334
4	-561.0630	-1023.1598	696.6825	677.6592	908.8754
5	-	-	-1032.4382	-1056.4156	-1039.4206
6	-	-	885.3317	1040.3000	932.9205
7	-	-	-885.3317	-1040.3000	-466.9477
8	-	-	1032.4382	1056.4156	1038.6460
9	561.0630	1023.1598	-696.6825	-677.6592	-654.7409
10	-481.9685	-931.4100	0	0	-75.5129
11	-760.3206	0	530.2842	690.3435	346.6425
12	760.3206	760.3206	159.4277	-195.9240	812.9308
13	normal	normal	normal	normal	-634.0335
14					702.6145
Correct. Quads	0	± 28.3963	± 25.3289	± 29.9300	± 29.9300

1. Quadrupoles #3 and #10 are turned off. These could be missing, but it seemed easier to leave them and add new ones. They are useful to return to normal, fixed-target operation, and, at least in the 1-m case, are not long enough to serve as one of the inner quads.
2. The lengths of the strong quadrupoles may have to increase slightly depending on the maximum gradient obtainable. A maximum value of approximately 26.8 kG/in. at 1 TeV has been used. Slight differences could be accommodated, perhaps down to around 25 kG/m, but certainly not as much as if one went to two-shell quadrupoles.

Table 3 - II. Lattice Functions.

	Normal lattice	Case A	Case B	Case C	Case D	Case E
Free Space (m)	53.194	51.974	51.974	15.992	15.992	15.992
β_x^* (m)	72.7	73.9	10.3	2.0	1.0	2.0
η^* (m)	2.24	2.26	0.21	0.40	0.48	-0.08
$\eta^{*'} (mrad)$	18.1	18.2	-6.4	144	298	4.7
$\beta_{x \max}$ (m)	243	243	247	378	851	240
$\beta_{y \max}$ (m)	243	243	252	380	868	618
η_{\max} (m)	6.0	6.0	8.6	9.5	10.5	7.5
η_{\min} (m)	1.1	1.1	-0.5	-3.3	-5.2	-0.1
Q_x	19.395	19.393	19.394	19.393	19.400	19.632
Q_y	19.434	19.432	19.434	19.432	19.441	19.205
ξ_x	-22.5	-22.5	-23.2	-25.2	-29.1	-24.6
ΔQ of cor- rection used	-	-	-0.317	-0.283	-0.334	-

Most of the objections raised with the previous low- β designs have been overcome in these designs. The maximum values of beta and dispersion have been brought down to believable sizes, and the dispersion mismatch throughout the ring is also relatively small. Further investigations of these designs show them to be quite reasonable. The tune corrections needed, from 30 correcting quads per sector, are easily handled, and the chromaticity corrections are also rather simple. Table 3-III lists the effect of momentum on various machine parameters for the low- β cases. The one parameter that could present a problem is the change in β_{\max} . The percentage change of β_{\max} as a function of $\Delta p/p$ is plotted in Fig. 3-4. Although this change in β_{\max} is rather large, the correction system is the simplest possible, two independent sextupole families. By going to a larger

Table 3-III. Accelerator Parameters vs $\Delta p/p$.

$\beta^* = 2 \text{ m,}$		$(B''l)_F = 429 \text{ kG/m,}$		$(B''l)_D = -733 \text{ kG/m}$	
$\Delta p/p (\%)$	$\beta^* (\text{m})$	$\eta^* (\text{m})$	$\eta_{\text{max}} (\text{m})$	Q_x	Q_y
-0.375	1.76	0.36	9.3	19.394	19.434
-0.250	1.84	0.37	9.4	19.393	19.433
-0.125	1.92	0.39	9.5	19.393	19.433
0	2.01	0.40	9.5	19.393	19.432
0.125	2.10	0.42	9.6	19.393	19.433
0.250	2.20	0.43	9.7	19.393	19.433
0.375	2.30	0.44	9.7	19.394	19.434

$\beta^* = 1 \text{ m,}$		$(B''l)_F = 492 \text{ kG/m,}$		$(B''l)_D = -842 \text{ kG/m}$	
$\Delta p/p (\%)$	$\beta^* (\text{m})$	$\eta^* (\text{m})$	$\eta_{\text{max}} (\text{m})$	Q_x	Q_y
-0.375	0.77	0.40	10.5	19.405	19.449
-0.250	0.84	0.43	10.4	19.402	19.444
-0.125	0.92	0.46	10.2	19.401	19.442
0	1.01	0.48	10.5	19.400	19.441
0.125	1.11	0.51	10.8	19.401	19.442
0.250	1.24	0.53	11.0	19.402	19.444
0.375	1.38	0.55	11.2	19.405	19.449

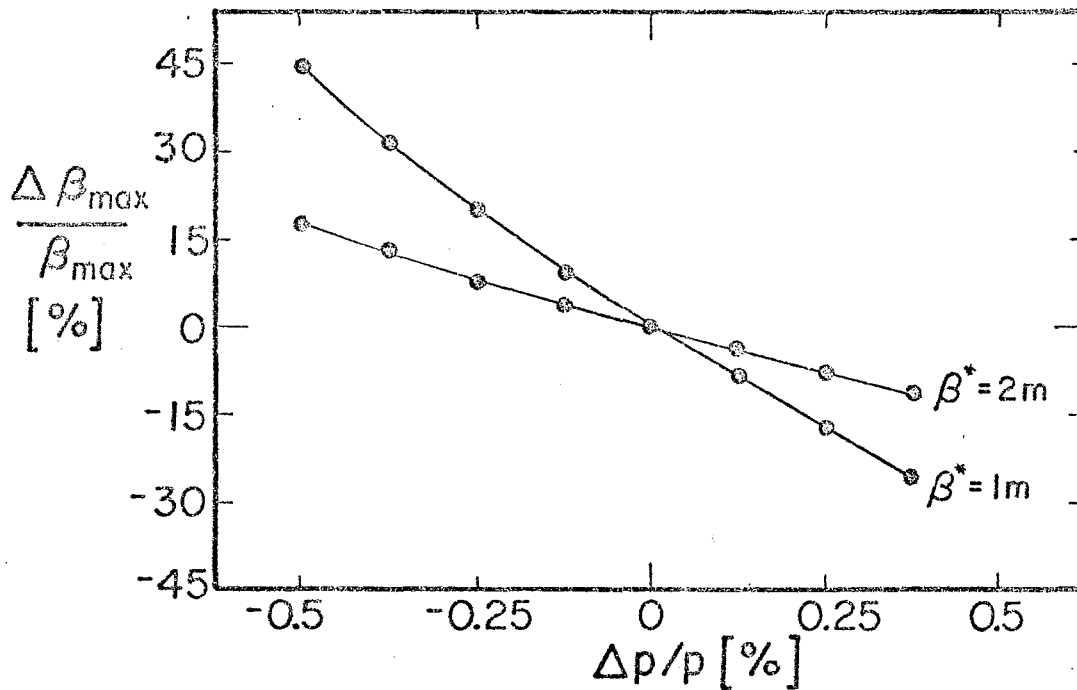


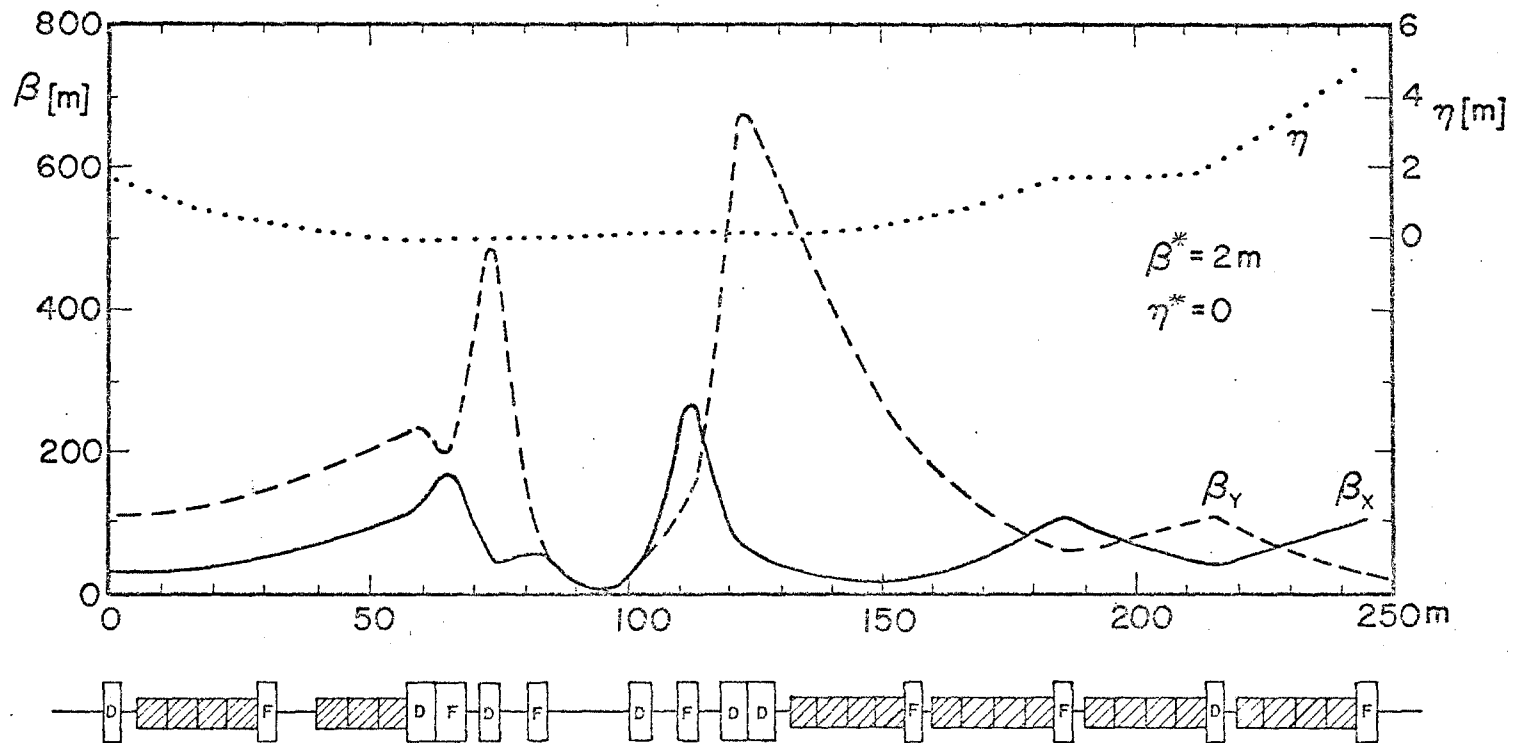
Fig. 3-4. Change in β_{max} as a function of $\Delta p/p$ for $\beta^* = 1\text{m}$ and $\beta^* = 2\text{m}$.

number of circuits, a much smaller variation could be obtained. It should be noted that the momentum aperture discussed herein is for perfect magnets. Putting in design field distributions shrinks the available aperture considerably.

Finally, the question of non-zero dispersion at the collision point has been considered and a solution to overcome this problem has been found. This has not yet been studied in depth, but rather is presented as an existence proof. It consists of separately powering 14 quadrupoles, the 12 of Type II plus the next two downstream of the straight section, that is, those at stations 14 and 15. A plot of lattice functions for this case is shown in Fig. 3-5, and this is described in Tables 3-I and 3-III. There are several points to be noted:

1. This was done for a 2-m β^* . An initial attempt to do it for 1 m failed.
2. The quadrupole at station 15 is definitely needed. Perhaps the one at station 14 could be run normally.
3. Quadrupole #12 is running too hard for a two-shell quad.
4. The tunes have not been properly rematched to 19.4. Completely making the dispersion zero is an extremely difficult process and may not be possible for other tunes.
5. The dispersion at the crossing point is shown as 8 cm. It can be made to be zero.

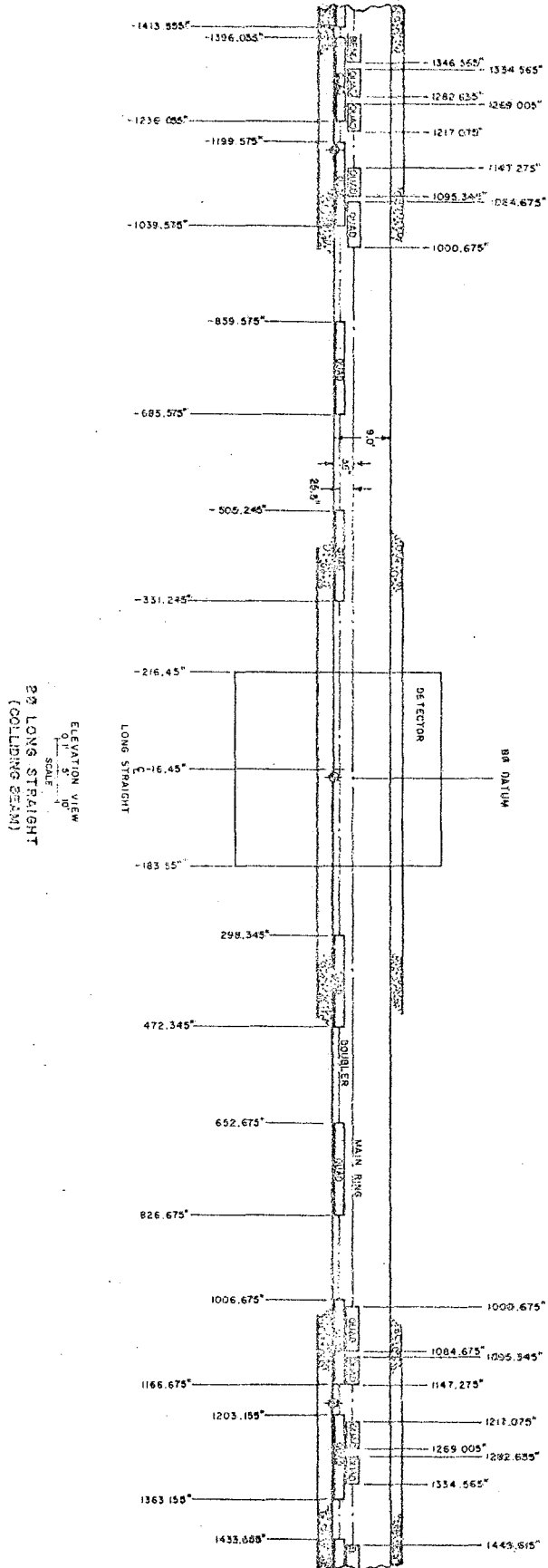
Finally, Fig. 3-6 is a layout of the interaction region at E_0 .



LOW BETA LONG STRAIGHT SECTION
TYPE II C

Fig. 3-5. Lattice functions for type IIC low-beta long straight section.

Fig. 3-6. Layout of the B0 long straight section.



3.3 Electrostatic Beam Separators

Measurement of collision parameters and luminosity calibration can be achieved by an electrostatic system to separate the beams at the collision point. This is most easily done by placing deflection plates at quadrature points of betatron phase from the intersection point, at, for example, approximately 7 m from the center of adjacent long straight sections. In order to reduce the interaction rate to about 1% of the undeflected rate (for Gaussian profiles), an electric field-length product of approximately 20 MV is required at each quadrature point ($\beta \approx 68$ m). If a 5-MV/m field can be sustained over the 2-cm aperture, 4 m of electrode is required. In principle systems should exist for separating both the horizontal and vertical directions.

A discussion of antiproton production is given in Ref. 2. A discussion of proton-proton collisions is given in Ref. 3.

3.4 Beam Detectors

Several new beam detectors will be needed. These include:

- (i) Unidirectional position detectors to separate effects of the proton and antiproton beams.
- (ii) Profile monitors.
- (iii) Super-high-frequency pickup.

There are several research and development projects already underway on these topics.

References

- ¹D. E. Johnson, High Luminosity pp and $\bar{p}p$ Colliding Beam Straight Section Designs, Fermi National Accelerator Laboratory Internal Report TM-876, April 1979.
- ²F. E. Mills and D. E. Young, A Scenario to Achieve a Luminosity of Approximately $5 \times 10^{29} \text{ cm}^{-2} \text{ s}^{-1}$ for $\bar{p}p$ Collisions in the Fermilab Energy Doubler, Fermilab report UPC-73 (unpublished) November 11, 1978.
- ³D. Ayres et al., Kissing Magnet Design for the pp Collider, Fermilab report UPC-76 (unpublished) November 8, 1978, revised December 21, 1978.

E. EXPERIMENTAL AREAS

The conceptual design of the B0 detector is far more advanced than that of the D0 detector, and, as a consequence, the design of the conventional facilities to house the detector is far more advanced in the B0 case than in the D0 case.

The B0 area has been designed to incorporate the following features: a) space around the $p\bar{p}$ intersection region to accommodate a large magnetic detector; b) access up and downstream around the beam pipe adequate for small-angle detectors; c) rapid removal of the entire detector system from the beam tunnel for repairs; and d) a work area outside the ring with enough space to allow the detector to be serviced and with enough shielding to permit operation of the accelerator while the work area is occupied.

The working detector size used in the area design was a 30-ft cube weighing 2000 tons. The design of the Fermilab magnetic detector is still being refined, but it fits within these specifications. The magnet-yoke assembly is to be a cube of steel with end plates forming the pole tips of the solenoidal field (axis coincident with the beam axis), and with return iron in four heavy corner pieces, which leaves the four sides of the magnet outside the coil accessible. The iron yoke must be assembled in the pit using cranes brought in for that purpose. After assembly, the magnet will roll in and out of the intersection region on steel rails that are supported by caissons to bed rock--about 30 ft below the rails. The rest of the detector can be assembled in the work area using a 20-ton overhead crane and various special rigs that are attached to the magnet yoke. Space to one side of the

detector is provided to remove the magnet coil along its axis should this prove necessary. The floor in the work area has been set at several levels to minimize the square footage required 40 ft below grade, and yet provide adequate access to a very large detector.

An integral part of the plan is to have the detector, the shield door, the electronics house, and all the correcting cabling move in and out of the intersection region as a unit. The electronics house will sit up at the top, near grade level. This way none of the cabling need be disturbed when the detector is shifted. An auxiliary shield door, stored on the inside of the collider area when the detector is in the beam line, is moved across to shield the work area from the circulating beam when the detector is out. This requires a duplication of the shielding, but eliminates the time-consuming task of unstacking and restacking 1500 tons of concrete blocks when the detector is moved. Concrete and earth shielding will be used over the roof of the collision area. There will be no heavy overhead crane in the collision area.

The D0 area will be similar in size to the one at B0, and will also employ the moving-detector concept. The collision area will have to be enlarged on the away side to accommodate the fixed-target extraction apparatus when it is removed from the ring for colliding-beam running.

In Figs. 1-1 and 1-2, the B0 collider area is shown with the detector in the beam region. Elevations above sea level are given in feet. Eighty ft of Main-Ring tunnel will be cut away to construct the enlarged collision room with a floor 40 ft below grade level. The various elevation steps are

designed to give access to the detector and minimize the floor area required at $706\frac{1}{2}$ feet. In the assembly area, shown in Figs. 1-1 and 1-2, a 20-ton overhead crane is available for lifting parts to trucks, which enter just below grade level. The solenoid can be removed from the detector in the assembly area. The electronics trailer, shield, cables, and detector all move in and out of the beam as a unit. The D0 area is similar in design, with a somewhat smaller assembly area and room in the collision region for the fixed-target extraction apparatus.

Building 90' x 90' .16 ft above crane rail
Detector 30' x 30' x 30' overall
Interaction Region 96' x 32' x 33'

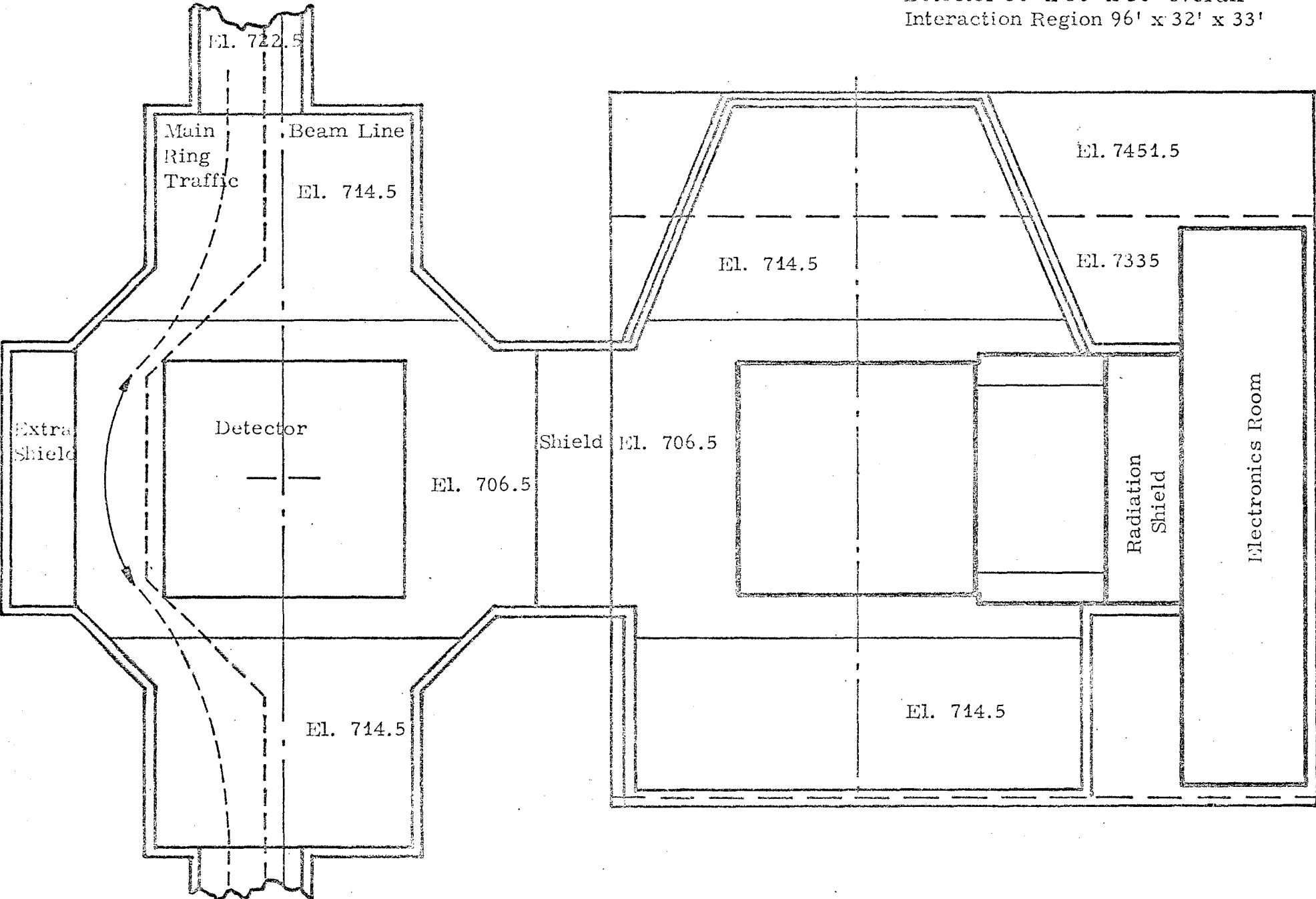


Fig. 1-1. Plan view of Experimental Area.

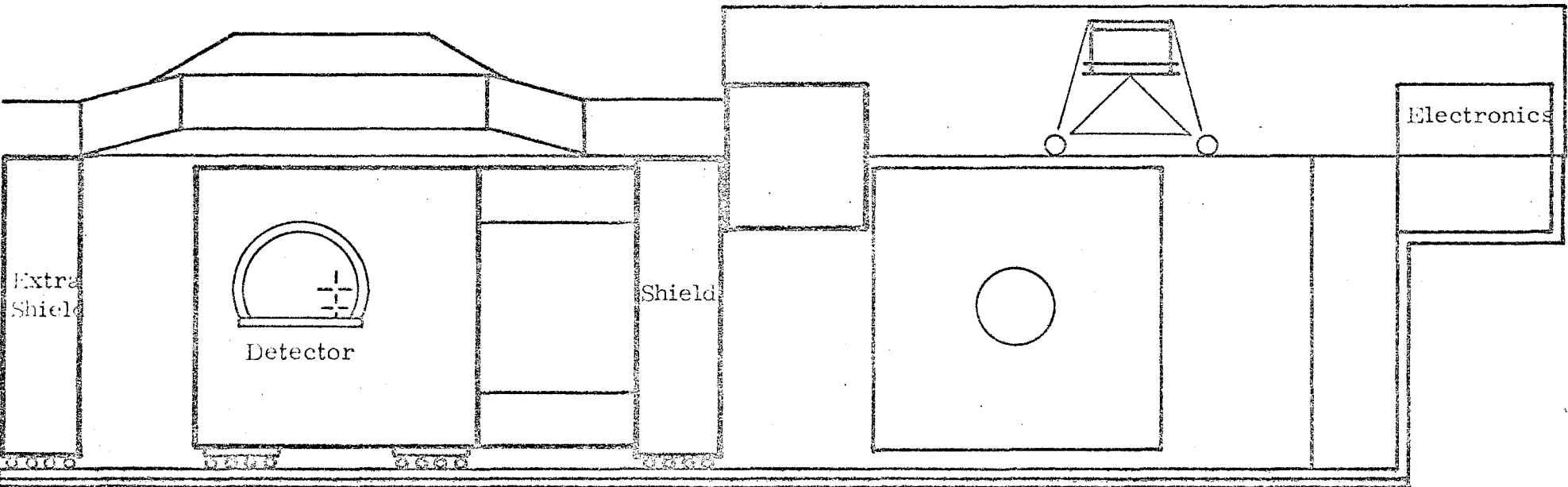


Fig. 1-2. Elevation view of Experimental Area.

F. COSTS AND SCHEDULES

1. Total Funding for Accelerator

Colliding Beams Project

(Initial Detectors Not Included)

The Fermilab Colliding Beams project will provide a facility for studying 1-TeV protons interacting with 1-TeV antiprotons at a luminosity of $10^{30} \text{ cm}^{-2} \text{ sec}^{-1}$. The project includes a \bar{p} source, two experimental areas, and accelerator components to convert the Energy Saver into a 1-TeV storage ring for protons and antiprotons.

A program of R & D is underway to study electron and stochastic cooling of particles, rf manipulation of beams in the Main Ring, antiproton production, and to develop magnets and power supplies for low β^* .

The funding pattern for the total project is given in the tables below.

Table 1-I Total Colliding Beams Budgets by Year

(Initial Detectors Not Included)

(Millions of Dollars)

OPERATING R&D (COSTS)

	<u>Prior Years</u>	<u>1980</u>	<u>1981</u>	<u>1982</u>	<u>1983</u>
Cooling Ring	1.800	0.200	0.200		
Operation (M&S, Sal.)	1.100	1.100	1.600	1.800	
Studies (rf, targeting, etc.)		0.500	0.500	0.500	
Transport Lines		0.300	0.200		
P Source (magnets, kickers, etc.)		0.300	1.000	0.200	
Low β			<u>0.500</u>	<u>0.500</u>	
	<u>2.900</u>	<u>2.400</u>	<u>4.000</u>	<u>3.000</u>	

	<u>Prior Years</u>	<u>1980</u>	<u>1981</u>	<u>1982</u>	<u>1983</u>
<u>EQUIPMENT (OBLIG.)</u>					
General	0.900	0.250	0.600	1.000	
Magnets & P.S. (Rev. line, \bar{p} target, C.R.-Booster)		0.500	0.300		
Low β			<u>0.500</u>		
	<u>0.900</u>	<u>0.750</u>	1.400	1.000	
<u>AIP (OBLIG.)</u>					
Rev. Inj.- Abort			0.600		
Rev. Line Target	0.470				
Refr.	<u>0.500</u>				
	0.970		0.600		
<u>GPP (OBLIG.)</u>					
Cooling Ring	<u>0.125</u>				
	0.125				
<u>CONSTRUCTION (OBLIG.)</u>					
Areas			2.300	5.700	0.700
\bar{p} Source			0.200	12.000	4.800
Accelerator			<u>5.000</u>	<u>1.500</u>	<u>1.500</u>
			7.500	19.200	7.000

Table 1-II summarizes estimated construction costs broken down by project element.

Table 1-II Estimated Construction Costs

TEVATRON, PHASE I

\bar{p} Source

Conventional facilities	2.7	
Technical components	8.4	
	<u>11.1</u>	
Escalation	<u>2.0</u>	13.1
EDIA	1.6	
Escalation	<u>0.3</u>	
		1.9
Contingency		2.0

Accelerator Components

Satellite refrigerators	12 x .3	3.6	
RF	3 x .3	0.9	
Special devices		<u>1.1</u>	
		5.6	
Escalation		<u>1.0</u>	6.6
EDIA		0.3	
Escalation		<u>0.1</u>	
			0.4
Contingency			1.0

Areas

Facility #1		3.3	
Facility #2		<u>2.6</u>	
		5.9	
Escalation		<u>1.1</u>	7.0
EDIA		0.6	
Escalation		<u>0.1</u>	
			0.7
Contingency			1.0

TOTAL

EDIA			3.0
Construction			26.7
P Source	13.1		
Accelerator Components	6.6		
Areas	7.0		
Contingency			<u>4.0</u>
	TOTAL		33.7

2. Details of Construction Cost Estimates

The tables below give details of the estimated costs of construction of the project.

Table 2-I Summary of Technical Components

and Conventional Facilities

(Millions of Dollars)

		<u>FY 80 Dollars</u>
A.	P Source	\$ 11.1M
B.	Accelerator Components	5.6
C.	Areas	5.9

Tables 2-II and 2-III give details of the estimated \bar{p} source construction costs.

Table 2-II Summary Estimated \bar{P} Source Costs

(Millions of Dollars)

A. \bar{P} Source		\$11.1M
Conv. Fac.	2.70	
Magnets & P.S.	2.67	
Injection, ext., etc.	0.34	
rf	0.71	
Vacuum	0.83	
Cooling	0.79	
Controls & Diagnostics	0.99	
Transport Lines	1.11	
Electron Cooling	0.96	
	TOTAL	\$11.1M

Table 2-III Detailed \bar{P} Source Cost Estimate

(Thousands of Dollars)

I. Conventional Facilities		2,690
1. Ring Building		
(excavation concrete, drains, backfill)	928	
2. Service Buildings (3 ea.)	64	
3. Beam Transfer Building	367	
4. Power Supply Building	200	
5. Electrical Service	468	
6. Water and Utilities	118	
7. Beam Transport Enclosures	495	
8. Site Development	50	
II. Technical Components		
A. Magnets and Power Supplies		2,677
1. Total Bending Magnet related cost (128)	742	
2. Quadrupoles Magnet related costs (80)	370	
3. Straight Section Quads (16)	120	
4. Trim Quads	80	
5. Sextupoles	70	
6. Other Correction Elements; Trim Dipoles	45	
7. Water and Power Distribution	150	
8. Magnet Power Supplies	750	
9. Miscellaneous; Supports, etc.	125	
10. Installation Labor	225	
B. Injection, Extraction, Septums & Kickers and Power Supplies		341

P Source Costs (cont'd)

C. RF System		709
Decelerating System:		589
1. Ferrite		164
2. Power Tubes		25
3. Power Supplies		70
4. Cavities, Assembly & Cooling		180
5. Low Level System		50
6. Construction Labor		100
Accelerating System:		120
7. Cavities Modifications		10
8. Power Supplies		30
9. Controls		20
10. Construction Labor		40
11. Miscellaneous		20
D. Vacuum System		828.
1. Pumps, Power Supplies & Cables (200 - 60 l/s)		444
2. Vacuum Chamber, Bellows & Parts		156
3. Valves		42
4. Heaters & Insulation		60
5. High Temperature Degasing		36
6. Instrumentation		24
7. Roughing Stations		36
8. Miscellaneous, Stands, Ceramic Insulators, parts		30
E. Stochastic Cooling System		794
1. Ferrite Rings & Mountings		140
2. Tank housings, Feed thrus, Connectors		66
3. Power Amplifiers		300
4. Low Level Systems		42
5. Filter Lines		46
6. Shorting Hardware		20
7. Miscellaneous Hardware		30
8. Diagnostics & Instrumentation		50
9. Construction Labor		100
F. Controls, Diagnostics and Safety		985
1. Local Control Stations, 35 at 10K/Station		350
2. Central Control Consoles, 3 at 50K/ea.		150
3. Beam Diagnostic Equip. & Instru- mentation		150
4. Safety and Security Systems		90
5. Miscellaneous; cables, relay racks		45
6. Fabrication and Installation Labor		200

P Source Costs (cont'd)

G.	Transport Line; Target to Precooler		756
1.	Dipoles (20)	116	
2.	Quadrupoles (30)	196	
3.	Power Supplies	244	
4.	Utilities	50	
5.	Miscellaneous	50	
6.	Installation Labor	100	
H.	Transport Line; Precooler to ECR		350
I.	Improve Electron Cooling Ring		960
1.	New Enclosure w/shielding	190	
2.	Power Supply Building	100	
3.	New Electron Cooling System	425	
4.	New Power Supplies	80	
5.	Injection System Magnet w/P.S. and Kickers	45	
6.	Installation Labor	120	
	TOTAL II		<u>8,400</u>
	TOTAL I and II		11,090

Tables 2-IV and 2-V give summaries and details of accelerator construction cost estimates.

Table 2-IV Summary Accelerator

Construction - Cost Estimates

(Millions of Dollars)

B. Accelerator Components \$5.6M

Refr. 12 x .3 = 3.6

rf 3 x 0.3 = 0.9

Special devices =1.1

Table 2-V Detailed Accelerator

Construction - Cost Estimates

(Thousands of Dollars)

Refrigerators (12 units)

a.	Compressors	1,080
b.	Expansion Engines	840
c.	Transfer Lines & Valves	720
d.	U-tubes	144
e.	Instrumentation & Controls	480
f.	Installation Manpower	300
	TOTAL	<u>3,564</u>

Accelerator Costs (cont'd)

Accelerator System (3 cavities)

a. Cavities	140
b. Power Amplifiers	292
c. Modulators	255
d. Anode Supply	68
e. Low-level rf	34
f. Controls	39
g. Cooling	28
h. Power and Water Distr.	45
TOTAL	<u>901</u>

Tables 2-VI and 2-VII give summaries and details of experimental area construction cost estimates.

Table 2-VI Summary Experimental

Area Estimated Costs

(Millions of Dollars)

C. Areas	\$5.9M
Fac. #1	3.3
Fac. #2	2.6

Table 2-VII Details of Experimental

Area Construction - Cost Estimate

(Thousands of Dollars)

Assembly Area	<u>Facility 1</u>	<u>Facility 2</u>
a. Excavation and Backfill	150	123
b. Caissons and Steel Rails	309	309
c. Sheet Piling	69	69
d. Concrete Footings, Walls, Floors, etc.	579	393
e. Underdrains, sumps, damp proofing, dewatering	51	51
f. Steel Building, Counting House	294	116
g. Crane (20-ton, 50 ft. span)	170	20
h. Crane for steel install.	30	30
i. Utilities, HVAC	240	193
j. Contingency	189	130
TOTAL	<u>2,081</u>	<u>1,434</u>

P Source Costs (cont'd)

G.	Transport Line; Target to Precooler		756
	1. Dipoles (20)	116	
	2. Quadrupoles (30)	196	
	3. Power Supplies	244	
	4. Utilities	50	
	5. Miscellaneous	50	
	6. Installation Labor	100	
H.	Transport Line; Precooler to ECR		350
I.	Improve Electron Cooling Ring		960
	1. New Enclosure w/shielding	190	
	2. Power Supply Building	100	
	3. New Electron Cooling System	425	
	4. New Power Supplies	80	
	5. Injection System Magnet w/P.S. and Kickers	45	
	6. Installation Labor	120	
			<hr/>
		TOTAL II	<u>8,400</u>
		TOTAL I and II	11,090

Tables 2-IV and 2-V give summaries and details of accelerator construction cost estimates.

Table 2-IV Summary Accelerator

Construction - Cost Estimates

(Millions of Dollars)

B. Accelerator Components \$5.6M

Refr. 12 x .3 = 3.6

rf 3 x 0.3 = 0.9

Special devices =1.1

Table 2-V Detailed Accelerator

Construction - Cost Estimates

(Thousands of Dollars)

Refrigerators (12 units)

a.	Compressors	1,080
b.	Expansion Engines	840
c.	Transfer Lines & Valves	720
d.	U-tubes	144
e.	Instrumentation & Controls	480
f.	Installation Manpower	300
	TOTAL	<u>3,564</u>

Accelerator Costs (cont'd)

Accelerator System (3 cavities)

a. Cavities	140
b. Power Amplifiers	292
c. Modulators	255
d. Anode Supply	68
e. Low-level rf	34
f. Controls	39
g. Cooling	28
h. Power and Water Distr.	45
TOTAL	<u>901</u>

Tables 2-VI and 2-VII give summaries and details of experimental area construction cost estimates.

Table 2-VI Summary Experimental

Area Estimated Costs

(Millions of Dollars)

C. Areas	\$5.9M
Fac. #1	3.3
Fac. #2	2.6

Table 2-VII Details of Experimental

Area Construction - Cost Estimate

(Thousands of Dollars)

Assembly Area	<u>Facility 1</u>	<u>Facility 2</u>
a. Excavation and Backfill	150	123
b. Caissons and Steel Rails	309	309
c. Sheet Piling	69	69
d. Concrete Footings, Walls, Floors, etc.	579	393
e. Underdrains, sumps, damp proofing, dewatering	51	51
f. Steel Building, Counting House	294	116
g. Crane (20-ton, 50 ft.span)	170	20
h. Crane for steel install.	30	30
i. Utilities, HVAC	240	193
j. Contingency	189	130
TOTAL	<u>2,081</u>	<u>1,434</u>

Experimental Costs (cont'd)

Tunnel Section	<u>Facility 1</u>	<u>Facility 2</u>
a. Excavation and Backfill	126	136
b. Breakout of Existing Structures	132	132
c. Caisons and Steel Rails	136	136
d. Concrete Footings, Walls, Floors, etc.	449	491
e. Underdrains, sumps, damp- proofing, dewatering	88	88
f. Utilities, HVAC	77	77
g. Overtime Wages (10%)	101	
h. Contingency	<u>111</u>	<u>106</u>
	TOTAL	<u>1,220</u>
	TOTAL	<u>1,166</u>
	TOTAL	3,301
		2,600

EDIA

The breakdown in manyears for the EDIA is given in the next section. Also included is all other manpower associated with Colliding Beams.

Escalation

As per the letter Tuszka, OB to Secretarial Officers Headquarters, we have used 7% per year.

Contingency

Contingency has been taken as 15% of construction costs throughout.

Table 2-VIII summarizes these cost elements.

Table 2-VIII Summary of EDIA,

Escalation and Contingency

(Millions of Dollars)

EDIA	3.0
Escalation	4.0
Contingency	4.0

3. Manpower Requirements

Table 3-I gives estimated manpower needs of the project.

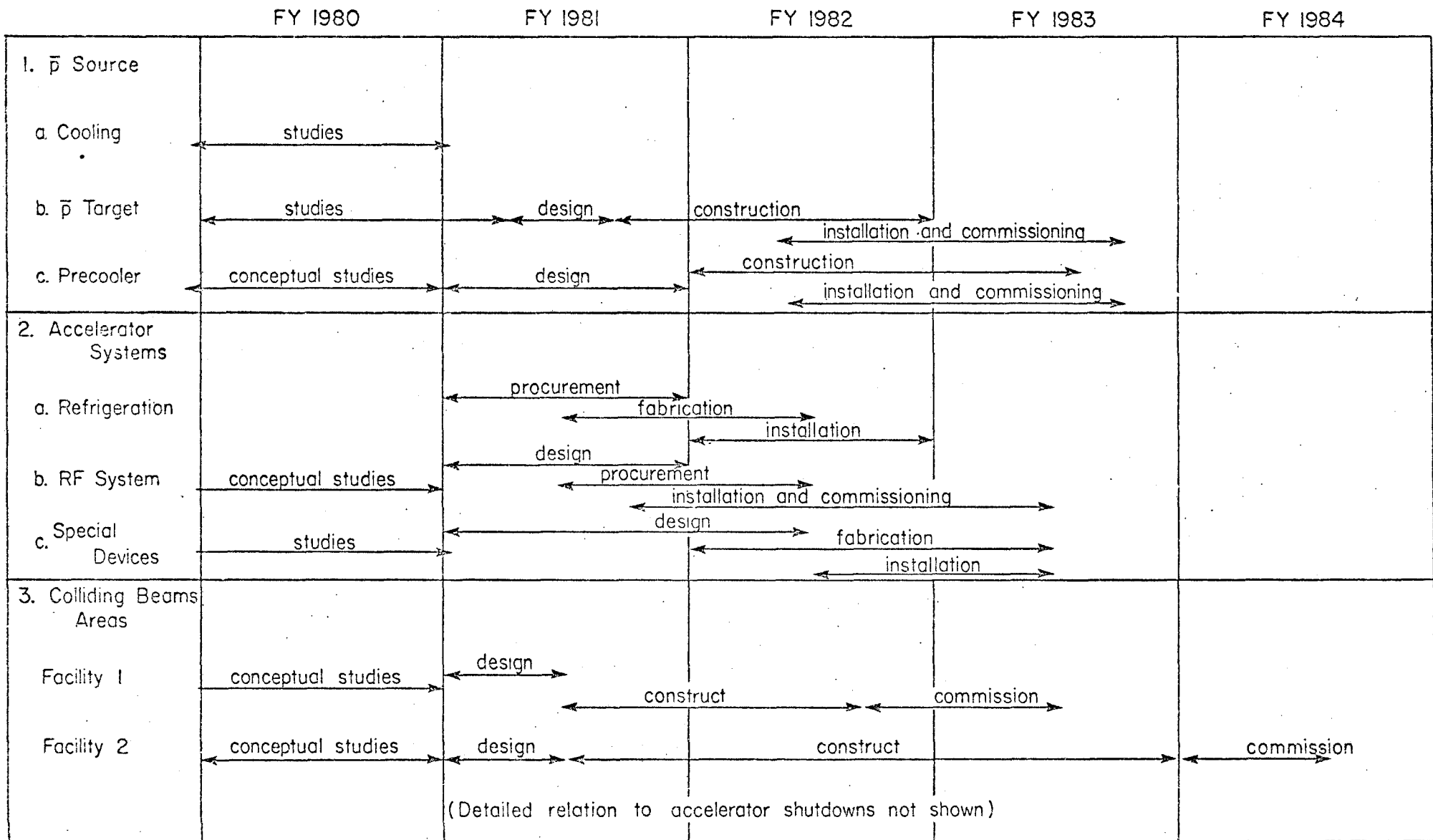
Table 3-I Manpower (Manyears)

	<u>1980</u>	<u>1981</u>	<u>1982</u>	<u>1983</u>
Source				
R & D	26	30	30	
Equip.	5	8	5	
EDIA		7	30	23
Const.			10	20
AIP		4		
	<u>31</u>	<u>49</u>	<u>75</u>	<u>43</u>
Acc.				
R & D		5	5	
EDIA		4	4	3
Const.		9	3	
		<u>18</u>	<u>12</u>	<u>3</u>
Areas				
EDIA		11	8	3

4. Schedules

The attached schedules show the time sequence of the complete Tevatron Phase I project and in more detail of the \bar{p} source part of the project.

TEVATRON PHASE I SCHEDULE



PRECOOLER DESIGN & CONSTRUCTION SCHEDULE

ITEM	DESCRIPTION	FY. 1980									FY. 1981									FY. 1982									FY. 1983																										
		10	11	12	1	2	3	4	5	6	7	8	9	10	11	12	1	2	3	4	5	6	7	8	9	10	11	12	1	2	3	4	5	6	7	8	9	10	11	12	1	2	3	4	5	6	7	8	9						
1	ENCLOSURE a) BEAM TRANSFER BUILDING (PHASE 1) b) RING BUILDING (PHASE 2)	DESIGN									BID									CONSTRUCTION																																			
											DESIGN									BID									AWARDS CONSTRUCTION																										
2	MAGNETS	DESIGN . PROTOTYPE TEST									CORRECTION & FINAL DESIGN									PROCUREMENT									FABRICATE									INSTALL COMMISSION																	
3	INJECTION EXTRACTION SEPTA & P.S. SEPTA POWER SUPPLY	DESIGN PROTOTYPE									MODIFICATIONS									PROCURE FABRICATE									INSTALL COMMISSION																										
		DESIGN									BID									AWARD PROCURE									INSTALL									COMMISSION																	
4	R.F. SYSTEMS	DESIGN & PROTOTYPE																		PROCURE & FABRICATE									INSTALL									COMMISSION																	
5	VACUUM SYSTEMS	DESIGN									PROTOTYPE FINAL-DESIGN									PROCURE & FABRICATE									INSTALL									COMMISSION																	
6	STOCHASTIC COOLING SYSTEMS	DESIGN									PROTOTYPE CORREC. FINAL-DESIGN									PROCURE FABRICATE									INSTALL									COMMISSION																	
7	CONTROLS DIAGNOSTICS & SAFETY	DESIGN																		BID									PROCURE & FABRICATE									INSTALL									COMMISSION								
8	TRANSPORT LINES	DESIGN																		BID									PROCURE & FABRICATE									INSTALL									COMMISSION								
9	ELECTRON COOLING RING IMPROVEMENTS										DESIGN									BID									PROCURE & CONSTRUCT									INSTALL									COMMISSION								

APPENDIX
SCHEDULE 44

DEPARTMENT OF ENERGY
 ENERGY, SCIENCE, DEFENSE ACTIVITIES - PLANT AND CAPITAL EQUIPMENT
 FY 1981 BUDGET REQUEST
 (TABULAR DOLLARS IN THOUSANDS; NARRATIVE MATERIAL IN WHOLE DOLLARS)
 CONSTRUCTION PROJECT DATA SHEET

CHICAGO OPERATIONS OFFICE
 Field Office

BASIC SCIENCE
 MULTI RESOURCE
 HIGH ENERGY PHYSICS
 FERMI NATIONAL ACCELERATOR

1. Title and location of project:
 TEVATRON, Phase I, Fermi National Accelerator
 Laboratory, Batavia, Illinois

2. Project No.
 81-CH-097

3. Date A-E work initiated: 1st Qtr. FY 1981

5. Previous cost estimate: (\$26,000)
 Date: 8/27/79

3a. Date physical construction starts: 2nd Qtr. FY 1981

6. Current cost estimate: \$33,700
 Less amount for PE&D: \$"0"

4. Date construction ends: 3rd Qtr. FY 1983

Net cost estimate: \$33,700
 Date: 12/11/79

7. Financial Schedule

<u>Fiscal Year</u>	<u>Authorization</u>	<u>Appropriations</u>	<u>Obligations</u>	<u>Costs</u>
1981	\$33,700	\$ 7,500	\$ 7,500	\$ 6,500
1982	0	19,200	19,200	19,000
1983	0	7,000	7,000	8,200

8. Brief Description of Project:

This project provides for:

1. the construction of an antiproton collection system;
2. the modification of the Energy Saver superconducting accelerator ring so that it can be used as a 1-TeV proton on 1-TeV antiproton colliding-beam storage ring; and
3. conventional construction to provide facilities for more than one simultaneous high-energy physics experiment.

DEPARTMENT OF ENERGY
ENERGY, SCIENCE, DEFENSE ACTIVITIES - PLANT AND CAPITAL EQUIPMENT
FY 1981 BUDGET REQUEST
(TABULAR DOLLARS IN THOUSANDS; NARRATIVE MATERIAL IN WHOLE DOLLARS)
CONSTRUCTION PROJECT DATA SHEET

CHICAGO OPERATIONS OFFICE
Field Office

BASIC SCIENCE
MULTI RESOURCE
HIGH ENERGY PHYSICS
FERMI NATIONAL ACCELERATOR

1. Title and location of project:

TEVATRON, Phase I, Fermi National Accelerator
Laboratory, Batavia, Illinois

2. Project No.
81-CH-097

The Fermilab scheme for collection of antiprotons uses the present accelerators plus two additional rings. The first is the precooling ring operating at about 5-GeV energy, which will have a large phase-space acceptance for antiprotons and will be used to pre-cool the antiproton beam as it comes from the antiproton production target. The term "cooling of a particle beam" means reducing the transverse and/or longitudinal momentum spread of the beam. This cooling is particularly important for producing accelerator-type beams with the secondary particles from a target. Particles coming from a target have a large spread of momenta. Cooling is required to make beams with momentum spreads of about a few tenths of a percent so that some reasonable fraction (several percent) of the particles produced at the target can be utilized.

A second approximately 200-MeV ring will be used for final cooling of the antiproton beam after it emerges from the pre-cooler and for accumulating antiprotons from successive cycles of targeting and pre-cooling in the first ring. The cooling at this stage of the collection scheme is required not only to reduce the momentum spread of the particles but also to stack the particles produced in each cycle. The project will provide for the construction of the pre-cooler, its enclosure, and the conversion of the R&D electron-cooling experiment to an operating device.

To operate the superconducting Energy Saver ring near the full energy of 1 TeV requires additional satellite refrigerators or their equivalent. The additional refrigeration is needed because superconductors near full field will make the transition from the superconducting to normal state with only small amounts of energy deposited in them. Thus, extra cooling will help prevent quenches of the superconducting ring. To accelerate and store protons in one direction and antiprotons in the opposite direction requires additional rf cavities and other special devices.

The conventional construction for high-energy physics experiments will be an integral part of the Main Ring tunnel. Important considerations that will be incorporated into the design are: the rapid and efficient introduction of detectors into the beam and a detector assembly area. These detectors will weigh thousands of tons.

DEPARTMENT OF ENERGY
 ENERGY, SCIENCE, DEFENSE ACTIVITIES - PLANT AND CAPITAL EQUIPMENT
 FY 1981 BUDGET REQUEST
 (TABULAR DOLLARS IN THOUSANDS; NARRATIVE MATERIAL IN WHOLE DOLLARS)
 CONSTRUCTION PROJECT DATA SHEET

CHICAGO OPERATIONS OFFICE
 Field Office

BASIC SCIENCE
 MULTI RESOURCE
 HIGH ENERGY PHYSICS
 FERMI NATIONAL ACCELERATOR

1. Title and location of project:

TEVATRON, Phase I, Fermi National Accelerator
 Laboratory, Batavia, Illinois

2. Project No.

81-CH-097

9. Purpose, Justification of Need for, and Scope of Project

When protons and antiprotons are stored in the superconducting ring and brought into collision, the energy available for particle production would be ~ 2000 GeV. This is about 65 times greater than the 31 GeV of cm energy which is available now at Fermilab when 500-GeV protons strike a fixed target.

The proposed energy is expected to be sufficiently high to produce the conjectured, but as yet unobserved, intermediate vector mesons. This family of particles is presumed to be the source of the weak forces responsible for nuclear beta decay. A phenomenological description of these forces was first made by Enrico Fermi, after whom Fermilab was named, nearly fifty years ago. Attempts to put this description on a more fundamental basis led to the postulation of the existence of these particles.

The data from experiments done at Fermilab and at other high-energy accelerators has shown that the proton behaves as though it were made up of constituent particles called quarks. The energies available in $\bar{p}p$ collisions will further enhance our understanding of the quark model and may even produce free quarks.

There are suggestions that there are new phenomena at cosmic-ray energies corresponding to about 0.5 TeV colliding-beam energy. At present these suggestions emerge from the observation of the handful of unusual events which have been accumulated during years of intensive work. The frequency of collisions of colliding beams could duplicate these results in a matter of seconds.

These are some of the many compelling reasons why extending particle physics to still higher-collision energies is of immense scientific value. The most compelling reason, however, is the anticipation of totally unexpected phenomena in this enormous extension of collision energy. The creation of ultra-high energy collisions of particles with modest expenditure of funds has always been a central goal of Fermilab. The flexibility of the set of accelerators at Fermilab was purposely planned so that a continuing evolution would be possible.

DEPARTMENT OF ENERGY
ENERGY, SCIENCE, DEFENSE ACTIVITIES - PLANT AND CAPITAL EQUIPMENT
FY 1981 BUDGET REQUEST
(TABULAR DOLLARS IN THOUSANDS; NARRATIVE MATERIAL IN WHOLE DOLLARS)
CONSTRUCTION PROJECT DATA SHEET

CHICAGO OPERATIONS OFFICE
Field Office

BASIC SCIENCE
MULTI RESOURCE
HIGH ENERGY PHYSICS
FERMI NATIONAL ACCELERATOR

1. Title and location of project;

TEVATRON, Phase I, Fermi National Accelerator
Laboratory, Batavia, Illinois

2. Project No.

81-CH-097

10. Details of Cost Estimate*

	<u>Item Cost</u>	<u>Total Cost</u>
a. Engineering, design and inspection ~ 11% of construction costs		\$ 3,000
b. Construction costs		26,700
1. Antiproton source	\$13,100	
2. Accelerator modification	6,600	
3. Conventional construction for experiments	7,000	
c. Contingency about 15% of construction costs		<u>4,000</u>
Total		\$33,700†

*Based on completed conceptual design

†Escalation included at 7% per year (ref. 3/28/79 ltr. Tuszka, OB, to
Secretarial Officers Hq.)

11. Method of Performance

Design of facilities will be by the operating contractor and subcontractor as appropriate. To the extent feasible, construction and procurement will be fixed-price contracts awarded on the basis of competitive bids.

12. Incorporation of Fallout Shelters in Future Federal Buildings

Efforts will be made to slant the design of any suitable buildings to incorporate shelters at no additional cost to the project.

DEPARTMENT OF ENERGY
 ENERGY, SCIENCE, DEFENSE ACTIVITIES - PLANT AND CAPITAL EQUIPMENT
 FY 1981 BUDGET REQUEST
 (TABULAR DOLLARS IN THOUSANDS; NARRATIVE MATERIAL IN WHOLE DOLLARS)
 CONSTRUCTION PROJECT DATA SHEET

CHICAGO OPERATIONS OFFICE
 Field Office

BASIC SCIENCE
 MULTI RESOURCE
 HIGH ENERGY PHYSICS
 FERMI NATIONAL ACCELERATOR

1. Title and location of project:
 TEVATRON, Phase I, Fermi National
 Accelerator Laboratory, Batavia, Illinois

2. Project No.
 81-CH-097

13. Incorporation of Measures for the Prevention, Control, and Abatement of Air and Water Pollution at Federal Facilities

The total estimated cost of this project includes the cost of those measures necessary to assure the facility will comply with Executive Order 11752. Sanitary waste will be discharged into existing sewers. As presently conceived, operation of this project will not generate any other environmental pollutants; therefore the requirements of Executive Order 11752 are not applicable and an environmental impact statement will not be required.

14. Evaluation of Flood Hazards

These projects will be located in an area not subject to flooding as determined in accordance with the requirements of Executive Order 11296.

15. Funding Schedule of Project Funding and Other Related Funding Requirements

	<u>Prior Years</u>	<u>FY 1981</u>	<u>FY 1982</u>	<u>FY 1983</u>	<u>Total</u>
a. Total project funding					
1. Total facility costs					
(a) Construction line item	\$ 0	\$ 6,500	\$19,000	\$ 8,200	\$33,700
(b) PE&D	0	0	0	0	0
(c) Expense funded equipment	0	0	0	0	0
(d) Inventories	0	1,200	0	0	1,200
Total facility costs	\$ 0	\$ 7,700	\$19,000	\$ 8,200	\$34,900

DEPARTMENT OF ENERGY
 ENERGY, SCIENCE, DEFENSE ACTIVITIES - PLANT AND CAPITAL EQUIPMENT
 FY 1981 BUDGET REQUEST
 (TABULAR DOLLARS IN THOUSANDS; NARRATIVE MATERIAL IN WHOLE DOLLARS)
 CONSTRUCTION PROJECT DATA SHEET

CHICAGO OPERATIONS OFFICE
 Field Office

BASIC SCIENCE
 MULTI RESOURCE
 HIGH ENERGY PHYSICS
 FERMI NATIONAL ACCELERATOR

1. Title and location of project:
 TEVATRON, Phase I, Fermi National
 Accelerator Laboratory, Batavia, Illinois

2. Project No.
 81-CH-097

	<u>Prior Years</u>	<u>FY 1981</u>	<u>FY 1982</u>	<u>FY 1983</u>	<u>Total</u>
2. Other project funding					
(a) Direct R&D operating costs necessary to complete construction	\$ 5,300	\$ 4,000	\$ 3,000	\$ 500	\$12,800
(b) Other project-related costs	<u>1,900</u>	<u>1,400</u>	<u>1,000</u>	<u>500</u>	<u>4,800</u>
Total Other Project Funding	<u>\$ 7,200</u>	<u>\$ 5,400</u>	<u>\$ 4,000</u>	<u>\$ 1,000</u>	<u>\$17,600</u>
Total Project Funding (Items 1 and 2)	\$ 7,200	\$13,100	\$23,000	\$ 9,200	\$52,500
b. Total related annual funding requirement (estimated life of project: 20 years)					
1. Facility operating costs				\$ (300)	
2. Programmatic operating expenses directly related to the facility				2,000	
3. Programmatic equipment costs				3,000	
4. GPP, AIP programmatic costs				<u>200</u>	
Total				<u>\$ 4,900</u>	

DEPARTMENT OF ENERGY
ENERGY, SCIENCE, DEFENSE ACTIVITIES - PLANT AND CAPITAL EQUIPMENT
FY 1981 BUDGET REQUEST
(TABULAR DOLLARS IN THOUSANDS; NARRATIVE MATERIAL IN WHOLE DOLLARS)
CONSTRUCTION PROJECT DATA SHEET

CHICAGO OPERATIONS OFFICE
Field Office

BASIC SCIENCE
MULTI RESOURCE
HIGH ENERGY PHYSICS
FERMI NATIONAL ACCELERATOR

1. Title and location of project:

TEVATRON, Phase I, Fermi National Accelerator
Laboratory, Batavia, Illinois

2. Project No.

81-CH-097

16. Narrative Explanation of Total Project Funding and other Related Funding Requirements

a. Total project funding

1. Total facility

(d) Inventories

In FY 1981 it will be necessary to provide inventories to put the facility into use. These inventories will include spare parts for refrigerators, rf stations, magnets and power supplies.

2. Other project funding

(a) Direct R&D operating costs

A 200-MeV electron-cooling ring has been constructed and operated. Electron and stochastic cooling studies will begin in FY 1980. The \bar{p} target facility will be completed and tested in 1980. Research and development for the pre-cooler ring will begin in 1980. A low-beta system will be installed and tested in one of the Main Ring straight sections. Reverse injection and abort will be partially assembled from existing equipment.

(b) Other project-related costs

The items included in these costs are magnets, power supplies and electronics which are general equipment to support a.2.(a) above.

DEPARTMENT OF ENERGY
ENERGY, SCIENCE, DEFENSE ACTIVITIES - PLANT AND CAPITAL EQUIPMENT
FY 1981 BUDGET REQUEST
(TABULAR DOLLARS IN THOUSANDS; NARRATIVE MATERIAL IN WHOLE DOLLARS)
CONSTRUCTION PROJECT DATA SHEET

CHICAGO OPERATIONS OFFICE
Field Office

BASIC SCIENCE
MULTI RESOURCE
HIGH ENERGY PHYSICS
FERMI NATIONAL ACCELERATOR

1. Title and location of project;

TEVATRON, Phase I, Fermi National
Accelerator Laboratory, Batavia, Illinois

2. Project No.

81-CH-097

16. Narrative Explanation of Total Project Funded and Other Related Funding Requirements (continued)

b. Total related annual funding requirement:

It is assumed that approximately one-third of the accelerator operation will be for colliding beams. This means that the other experimental areas (Meson, Neutrino, and Proton) will not be operating one-third of each year. During the colliding beam operating period, it is anticipated that there will be a net reduction of power consumption of 5 MW. The programmatic effort in the facility will require approximately 30 additional people and the material and supplies required to effectively support these people. It is anticipated that a new experiment will be mounted every three years at an estimated equipment cost of \$9,000,000 per experiment. GPP and AIP funds will be required as experience in running the new facility points out specific areas where improvements are desirable.

